TRACKING STELLAR ACTIVITY ENHANCEMENTS DUE TO A CLOSE-IN GIANT PLANET IN THE HD 179949 SYSTEM

by

LEVENT GURDEMIR

Presented to the Faculty of the Graduate School of

The University of Texas at Arlington in Partial Fulfillment

of the Requirements

for the Degree of

MASTER OF SCIENCE IN PHYSICS

THE UNIVERSITY OF TEXAS AT ARLINGTON

MAY 2010

ACKNOWLEDGEMENTS

This thesis reflects an accomplishment of almost four years of diligent study. In the scope of this research, I had great opportunities such as utilizing McDonald Observatory's research telescopes. I frequently visited the Astronomy Department of the University of Texas at Austin to learn how to use data reduction and analysis software. As the first thesis in the field of Observational Astronomy at the University of Texas at Arlington, this thesis provides important data points and perspectives on the verge of understanding of true nature of star-planet interactions.

First of all, I would like to record my gratitude to my research advisor, Dr. Manfred Cuntz, for his guidance, supervision, encouragement and great support from the very early stage of my carrier at UT Arlington. I also would like to extend my appreciation to the other members of my M. Sc. Committee, Drs. Zdzislaw Musielak and Yue Deng.

I gratefully acknowledge Dr. Seth Redfield for his great support and efforts who advised me on the operation of telescopes and use of software. Dr. Redfield was very generous about donating his precious time to discuss the progress on every stages of this research and provide guidance.

I also gratefully acknowledge the Dr. James Horwitz, the former chairman of the Physics Department, for his great support and administrative help. He had a special interest in this project. Unfortunately, he didn't see the accomplishment because of his unexpected passing.

Finally, I would like to thank to my wife Atika for her support, patience and motivation at every stage of this research from the beginning. This thesis would not have been possible without her.

March 10, 2010

ABSTRACT

TRACKING STELLAR ACTIVITY ENHANCEMENTS

DUE TO A CLOSE-IN GIANT PLANET

IN THE HD 179949 SYSTEM

Levent Gurdemir, M.S.

The University of Texas at Arlington, 2010

Supervising Professor: Manfred Cuntz

We monitored CaII H and K lines (3933Å and 3968Å) of the HD 179949 system to study Planet Induced Emission (PIE) as an effect of star-planet interaction. We obtained high resolution spectra (R > 50,000) with high signal-to-noise ratio (S/N > 50 in the Ca II H and K cores) during 10 nights of observation at the McDonald Observatory. Wide band Echelle spectra covering full optical bandwidth (3,400-10,900Å) were obtained using 2.7 m Harlan J. Smith Telescope located at Mt. Locke. Detailed statistical analyses performed both for H and K cores of calcium to reveal the nature of the fluctuation in the cores as due to planet induced emission. The results are consistent with the previous studies by Shkolink et al (2003, 2008), including the proposed on/off nature of the star-planet interaction. The conclusions of the analysis also include new updates on the time evolution of the HD 179949 star-planet system.

TABLE OF CONTENTS

LIST OF ILLUSTRATIONS

Figure Page

LIST OF TABLES

CHAPTER 1

INTRODUCTION

1.1 Discovery of Extrasolar Planets

An extrasolar planet is a planet orbiting around a star other than the Sun. The existence of extrasolar planets was not known until October 1995; however, the possibility was highly considered by many astronomers. Relative size difference of stars and planets doesn't allow optical observations for most extrasolar planets with current telescopes. As an astronomy laboratory practice, in order to detect a Jupiter size planet around the closest star, Alpha Centauri, the required telescope must be at least 30 meters in diameter. Currently, the world's largest telescope is the Gran Telescopio Canarias (GTC) in Canary Islands, Spain which has 10.4 meters (34-feet) mirror. The world's 3rd largest telescope, the Hobby Eberly Telescope with a 9.2 meters mirror, is located at Mt. Fowlkes, TX and operated by the University of Texas at Austin. A 30 meters (90-feet) telescope's construction is started at Hawaii, and a 42-meters (138-feet) telescope is under construction by European Space Agency.

The distance of planets to their host stars are typically much smaller relative to their distance to Earth, therefore their angular separation is very small. Moreover, large stellar images of stars saturate the faint planetary images. Because of the aforementioned difficulties in direct optical observations, almost all extrasolar planets are observed indirectly. There are only a few cases where planets can be directly observed.

There are four prominent methods to discover extrasolar planets. Those are:

- Astrometry
- Radial Velocity (RV) Measurements
- Transit Photometry
- Gravitational Microlensing

Astrometry utilizes the motion of the star around the center of mass of the star system. Figure 1.1 shows the simulated motion of the Sun around the center of mass as seen from 30 light years away from the Solar system, counting Jupiter as the only planet. The size of the Sun is demonstrated with dashed lines. As can be seen from the figure, the motion of the Sun is very small. With application of Newton's laws of motion and law of gravity, the following equation can be derived:

$$\beta = [\frac{G}{4\pi^2}]^{1/3}[\frac{P}{M}]^{2/3}m/d$$

where β is the angular size of the planet's orbit (in radians), P is the orbital period of the planet, M is the mass of the star, m is the mass of the planet, and d is the distance of the star from Earth. Because d is so large, β is extremely small angle therefore very difficult to observe.

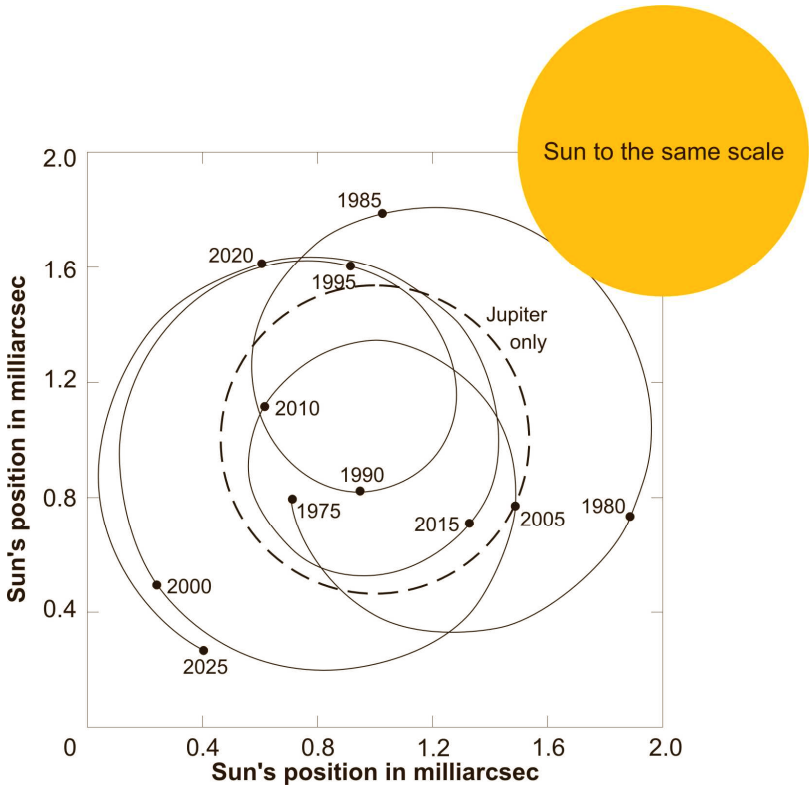

Figure 1.1 Simulated motion of the center of mass of the Sun as seen from 30 light-years away, considering Jupiter is the only planet in the Solar System. The size of the Sun is shown by dashed lines. *Figure credit: B.W. Jones (2008)*

RV measurements are currently the most common method used to detect extrasolar planets. This method utilizes the Doppler Effect phenomena. If a star is moving around the center of mass, its motion will seem like a periodic back-and-fort motion from a fixed point of view. This motion will cause cyclic Dopler shifts (periodic shifts to shorter and longer wavelengths) in its spectra. With current telescopes and accurate data recording devices (such as CCD cameras), even tiny amounts of shifts can be detected today. With circular orbit assumption, planet's mass can be deduced with

$$msin(i) = v_r(P^{1/3}M^{2/3})/(2\pi G)^{1/3}$$

Here, the angle i is the angle between the orbital plane and the line of sight of the observer. In case i = 90˚, planet's mass cannot be deduced (radial velocity = 0). Often times we don't know the angle i.

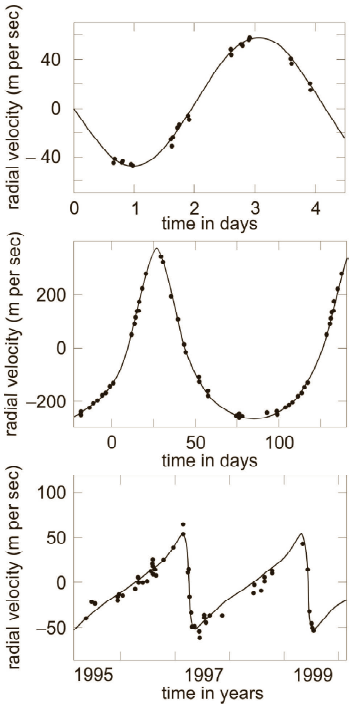

Figure 1.2 Radial Velocity (RV) curves of three different stars hosting planet(s): 51 Peg (upper figure), 70 Vir (middle figure), and 16 Cyg B (lower figure). *Figure credit: B.W. Jones (2008)*

The Figure 1.2 shows acquired RV measurements of three different star-planet systems. Upper curve belongs to 51 Peg system where the planet's orbit is almost circular. 70 Vir (middle curve), and 16 Cyg B (lower curve) systems have planets in eccentric orbits as can be noted from the shape of the curves. The sinus wave implies no speed change for circular orbit case. Planets move at different speeds (by Kepler's second law) on eccentric orbits. The maximum negative point of the curve implies the position of the planet when it is closest to Earth.

In Transit Photometry method, diminish of the star light as planet transits by is used. If the surface brightness of a star was uniform, then the fractional decrease would be ($\pi r^2/\pi R^2$). However, due to limb darkening effect, the ratio of fractional decrease changes during transit. A Jupiter size planet orbiting around a nearby star would cause about 1% fractional decrease. This is detectable by ground based telescopes equipped with modern data recording devices. However, fractional decrease of 0.01%, which would be caused by an Earth size planet, is not yet detectable due to atmospheric limitations of ground based observations. NASA has launched a photometer carrying satellite, Kepler, in March 2009. The Kepler mission will search for Earth-size planets by utilizing transit photometry method. At the time of this thesis written, there were 5 successful discoveries by Kepler.

Finally, the Gravitational Lensing method utilizes Einstein's famous General Relativity theory. If a foreground star comes to an alignment with background star, foreground star's gravitational field bends background star's light (lensing effect). Rather hiding behind the foreground star, the background star appears in the image as a ring (Einstein Ring). In case of a planet transiting in front of a star, the planet appears in the light curve as an upward spike when alignment of star, planet, and Earth occurs. Planet's gravitational field bends the starlight, and focuses towards Earth. Focused light appears brighter, therefore appear as an upward spike in the light curve. Due to momentary nature of this effect, and the requirement of perfect alignment, the Gravitational Lensing cannot be used as a practical method to discover extrasolar planets. There are very few planets have been discoevered by this method.

First evidence for the existence of an extrasolar planet came on October 6, 1995, concerning the star 51 Pegasi. As of today, more than 400 planets are discovered around nearby stars. Detected stars are cataloged at the Extrasolar Planets Encyclopedia, which is maintained by the Paris Observatory in France. The encyclopedia is accessible via internet at http://www.exoplanet.eu.

Naming discovered extrasolar planets is very similar to naming binary stars. Lower case letter “b” is used after star’s name for the first discovered planet in a star system, which is similar to the binary star systems with exception of capital letters. The first discovered planet gets the name “b” (i.e. 51 Peg b). The second discovered planet gets the name “c”, and so on. Thus, further planet discoveries in the same star system do not affect the names of previously discovered planets. With other words, planet with letter b is not necessarily the closest planet to the star.

The definition of an extrasolar planet is established by the International Astronomical Union (IAU) in 2001*. According to the definition, an extrasolar planet must meet with the following criteria:

**IAU General Assembly: Definition of Planet debate". Retrieved 2006-09-24*

1. *Objects with true masses below the limiting mass for thermonuclear fusion of deuterium (currently calculated to be 13 Jupiter masses for objects of solar metallicity) that orbit stars or stellar remnants are "planets" (no matter how they formed). The minimum mass/size required*
2. *for an extrasolar object to be considered a planet should be the same as that used in our solar system.*
3. *Substellar objects with true masses above the limiting mass for thermonuclear fusion of deuterium are "brown dwarfs", no matter how they formed nor where they are located.*
4. *Free-floating objects in young star clusters with masses below the limiting mass for thermonuclear fusion of deuterium are not "planets", but are "sub-brown dwarfs" (or whatever name is most appropriate).*

The first discovered planets were larger than Jupiter, and unlike Jupiter, their calculated orbits were very close to their host star. They were later called Hot Jupiters if similar in size to Jupiter, and orbiting within about 0.05 AU to their host star. To compare: Mercury orbits 0.4 AU, Jupiter orbits 5 AU from the Sun. Hot Jupiters thought to be formed far away from their host star, and later migrated inwards in the star system. Hot Jupiters were also observed around stars those posses unusual stellar properties such as rapid rotation rate and high chromospheric activity (i.e. superflares). If there is a connection between Hot Jupiters and high chromospheric activity, this would explain why we do not observe superflare phenomena at the Sun.

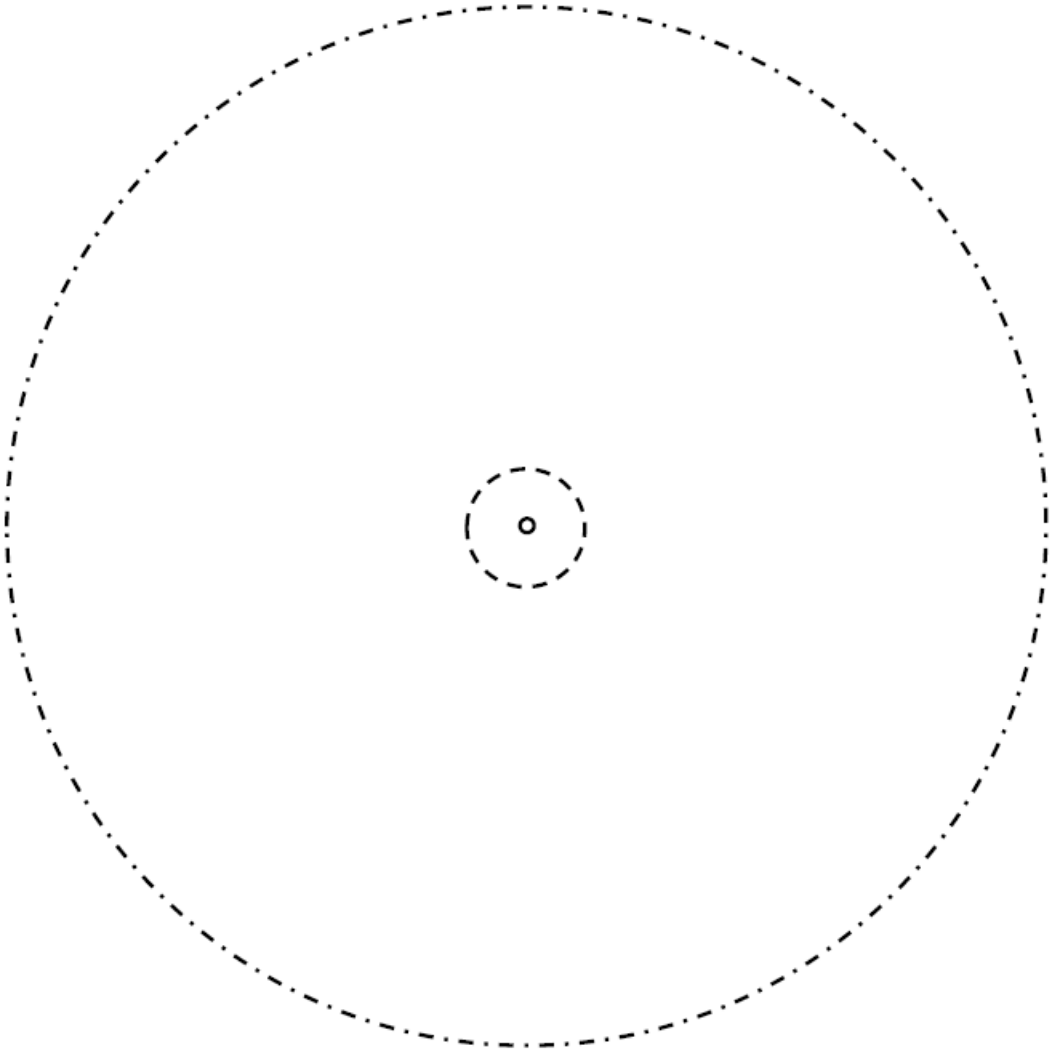

Figure 1.3 Scaled size of orbit of HD 179949b (dashed lines) relative to the size of the host star (solid line). To compare, size of Mercury's orbit is shown with dashed-dot line style.

1.2 Previous Work on Planet Induced Stellar Emission (PIE) and Chromospheric Activity

Stars are known to have strong magnetic fields. Larger planets have stronger magnetic fields as the magnetic field strength is related to the size of the planet size (dynamo activity). This assumption can be tested in the Solar System as Jupiter's magnetic field is stronger than Saturn's, which is stronger than Neptune's and Uranus's. If a planet is Close-In Extrasolar Giant Planet (CEGP), in other words - a Hot Jupiter (at least Jupiter size and closer than 0.05 AU to a star), then its magnetic field may interact with the host star's magnetic field. This interaction may increase the star's chromospheric activity that may result in superflares. This possibility was first suggested by Rubenstein and Schaefer (2000) after studying 9 solar analog stars with rapid rotation and high chromospheric activity.

According to Cuntz et al. (2000), if such interaction exists, it can be either or both tidal or magnetic. If the orbital period of the planet is not equal to the rotational period of the planet (in other words - the orbit is not synchronized), the planet should initiate stellar tidal bulges. Tidal and magnetic interaction will result enhanced Turbulent (ν_t) and flow (ν_f) velocities. Musielak et al. (1994, 1998) showed the dependency of acoustic and magnetic energy to be ν_t^8 and ν_f^6 respectively. Therefore, even a small production of non-radiative energy will result in a significant increase in turbulent and flow velocities that will lead to enhanced heating and activity.

Cuntz, Saar and Musielak (2000) suggested that if the planet induced heating is confined in a narrow stellar longitude (narrow band) due to increased turbulence velocities, the heated regions on the stellar surface should track the planet. In this case, any observed activity should be correlated with the orbital period of the planet (P_{orb}) such that tidal activity has a period of $P_{orb}/2$, and magnetic activity has a period of P_{orb}. In 2001, Cuntz and Saar also suggested that the dynamo action may be confined under the convection zone; therefore, the effect may be spread out over large range of stellar longitude. In this case, the enhanced activity due to excess heat would not demonstrate strong periodic variation.

Previously, three different attempts have been made by Bastian et al. (2000), Saar & Cuntz (2001) and Shkolnik et al. (2001, 2003) to identify planet induced emission. Bastian et al. used the VLA to monitor 74,333 MHz and 1465 MHz frequencies on selected stars, no detections were made however. The authors listed possible reasons for this result including mismatches of the monitored frequencies to the sources, insensitivity of observations, lack of KeV electrons from the sources, and bad timing (no activity during observations). In 2001, it was suggested by Zarka et al. that planet induced radio emission should nevertheless exist.

Saar & Cuntz (2001) used the Lick Planet Search database (with R ~ 50,000, continuum S/N ~ 100) to study variations in the CaII IR triplet. They searched for periodicities at P_{orb} and $P_{orb}/2$ as well as statistical flux enhancements at sub-planetary points. No identifications were made, but this result was no surprise due to insufficient resolution and poor temporal spacing of the data.

Shkolnik et al. (2003) used the Canada-France-Hawaii Telescope (CFHT) with the fiber-fed coudé spectrograph to obtain high-resolution (R ≈ 110,000) and high Signal-to-Noise (S/N ≈ 500pixel^{-1}) spectra. They monitored CaII H and K lines by centering their 60 Å spanning spectrograph at 3947Å. They reported all the spectra were reduced by IRAF's standard routines. Their representative flat-fielded spectrum of HD 179949 is shown in Figure 1.4.

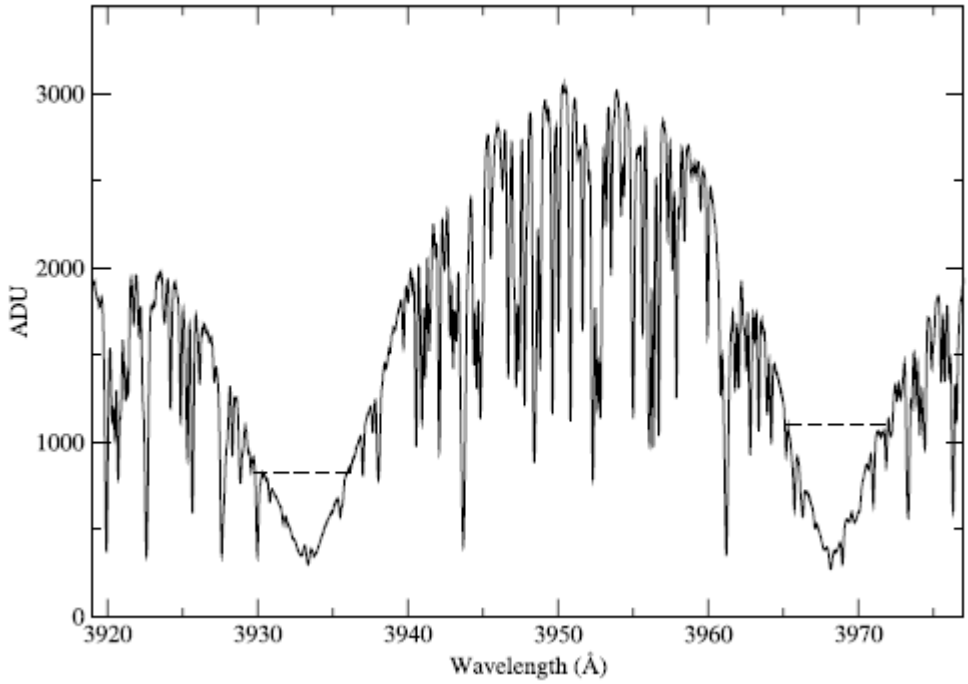

Figure 1.4 Spectrum of CaII centering 3947Å represented by Shkolnik et al (2003). Dashed lines represent the normalization levels. *Figure credit: Shkolnik et al. (2003)*

Shkonik measured differential radial velocities to calculate orbital ephemerides. Calculated ephemerides are given in Table 1.1.

Table 1.1 Ephemerides of Shkolnik's program stars as represented in Shkolnik (2005). *Figure credit: Shkolnik et al. (2003)*

2003 SEPTEMBER EPHEMERIDES

Star	$\sigma_{\Delta RV}$ (m s^{-1})	HJD at $\phi = 0$ (days)	δ(HJD)[a] (days)	Revised P_{orb} (days)	$\delta(P_{orb})$[a] (days)
τ Boo	33	2452892.864	0.066	3.31250	0.00026
HD 179949	19	2452894.114	0.062	3.09246	0.00031
HD 209458	17	2452893.653	0.070	3.52490	0.00020
51 Peg	15	2452895.868	0.085	4.23092	0.00014
υ And	9	2452892.615	0.092	4.61750	0.00052

[a] Uncertainties in the respective measurements.

Since it is not possible to estimate the stellar continuum in the calcium region of the spectra, Shkolnik extracted 7Å portions of each spectrum centering at the H and K lines. To normalize the spectra, the end points of each extracted spectra set to 1 and fitted with a straight line. The normalized spectra for τ Boo and HD 179949 is shown in Figure 1.3.

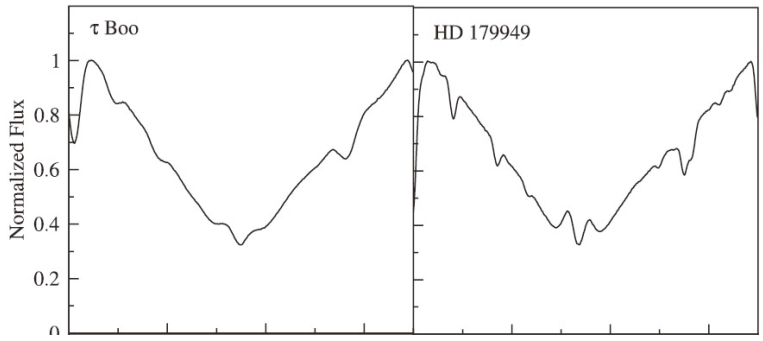

Figure 1.5 Normalized Spectra of t Boo and HD 179949. 7Å chunks centering CaII K line cut and normalized to 1. *Figure credit: Shkolnik et al. (2005)*

Shkolnik grouped all the normalized spectra by date, and computed the nightly mean by co-adding nightly spectra. Shkolnik also computed the overall average to calculate the nightly residuals. Nightly means and average mean were also calculated for AlI (3944Å) line, in 7Å and 2Å windows, to calculate the RMS value. RMS value can be used as an indicator for the data resolution and quality. Computed nightly residuals were smoothened over 21 pixels. Mean

Absolute Deviation was also calculated from the nightly residuals ($MAD = N^{-1} \sum|data_i - mean|$ for N spectra). Plotted MAD and over-plotted overall spectrum of CaII K core, and nightly residuals are shown in Figure 1.6.

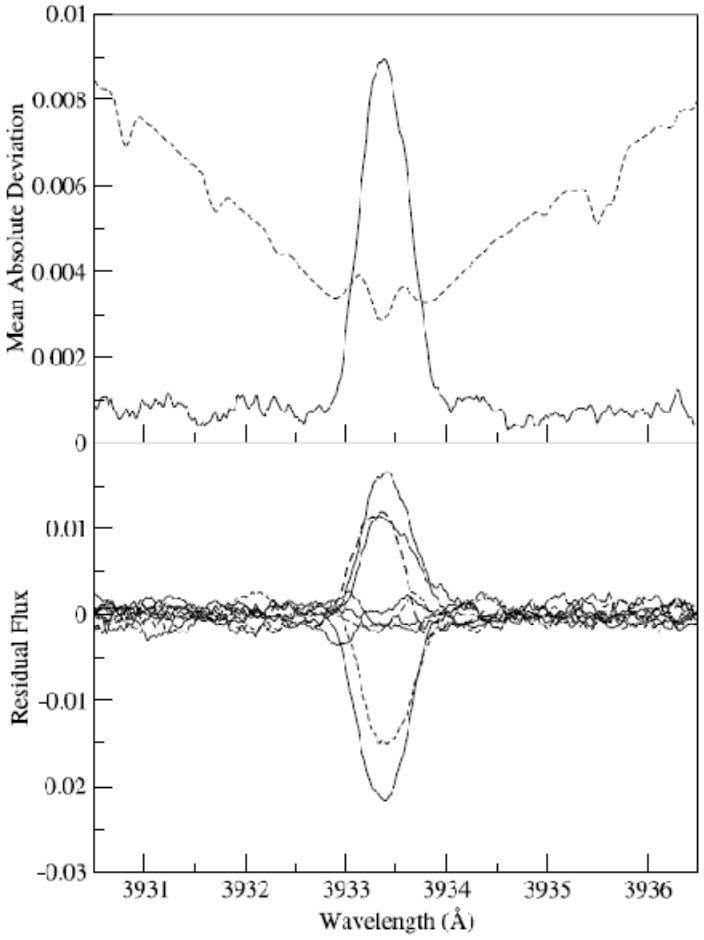

Figure 1.6 Results by Shkolnik et al. (2003). Top figure is the Mean Absolute Deviation of K core computed from the residuals. Overall mean is vertically scaled and shown in the same figure to show that the activity is confined in the Calcium line core. Bottom figure is the nightly residuals of the K core computed from overall spectrum. *Figure credit: Shkolnik et al. (2003)*

Shkonik et al.'s other program stars showed similar variations, called Ca II reversals. Especially in the HD 179949 case, the period of activity was found to be synchronized with the orbital period of the planet. During observations, they also monitored the Sun that showed very steady Ca II emission. Shkolnik et al.'s results were the first confirmation of the magnetic star-

planet interaction; however, various reasons indicated in their previous publications point to the necessity of further observations to understand the nature of interaction.

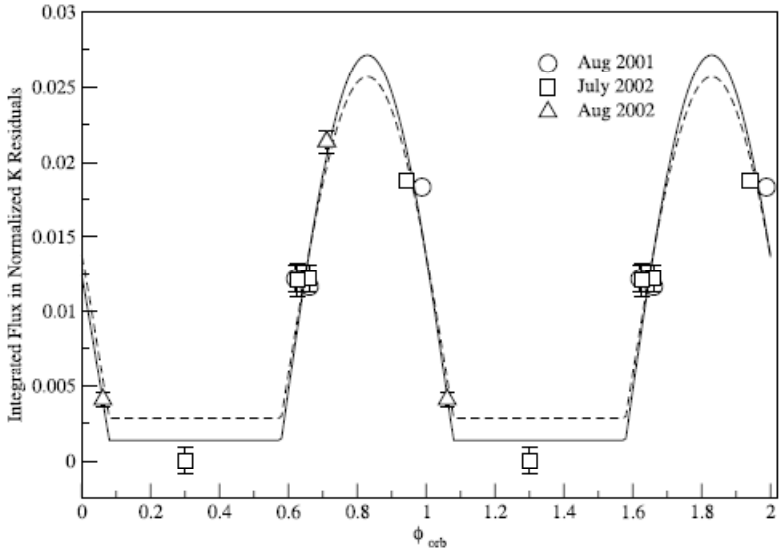

Figure 1.7 Results by Shkolnik (2003). Integrated K residuals as function of phase. The figure indicates that the activity is modulated with orbital period of the planet. The activity peaks when the planet is at $\emptyset = 0.8$. *Figure credit: Shkolnik et al. (2003)*

Cuntz & Saar (2005) proposed further observations of CEGP's to explain the nature of the observed PIE effect. This is needed to test various models suggested to date, such as flare-like interaction of stellar and planetary magnetic fields (Saar et al. 2004), wave-like magnetic interaction (Shkolnik et al. 2005), enhanced dynamo activity due to tidal interactions (Moss et al. 2002), purely wind-driven interaction on non-magnetic planets (Zarka et al. 2001). The scope of the proposed study included seeking answer for the following two questions:

1. What is the dependency of PIE amplitude to:
    a. Star-planet separation (a)
    b. Stellar Activity Level (B_*)
    c. Planet Mass (B_p)
    d. Star-planet shear $\langle {}^{1}/_{P_{rot}} - {}^{1}/_{P_{orb}} \rangle$

e. Planet radius (r_{planet})

f. Stellar wind speed

2. What is the dependency of PIE peak shift to the above parameters?

Shkolnik et al. suggested that the shift is due to differing wave velocities. According to Saar et al., it is due to the spiral of the stellar magnetic field lines in the expanding stellar wind.

Detection of further PIE's and understanding the nature of the effect will ultimately appeal two important astrophysical quantities for the first time:

1. The magnetic fields of exoplanets
2. The close-in properties of solar-like stellar winds

Cuntz and Saar obtained 9 days of observation time from the McDonald Observatory's 2.7-m (107-inch) telescope located on Mt. Locke. 9 target stars are carefully selected among the stars known to have CEGP's. The target stars included HD179949 whose PIE effect is previously confirmed by Shkolnik et al. Observations are performed between April 5, 2006 and April 13, 2006 by Seth Redfield and me. It was my second observation run at the McDonald observatory.

CHAPTER 2

OBSERVATIONS AT THE MCDONALD OBSERVATORY

McDonald Observatory is located 6,791 feet above sea level atop Mt. Locke nearby Fort Davis, TX. The observatory, operated by The University of Texas at Austin, is housing a wide range of state-of-the-art spectroscopy and imaging instruments. The observatory currently operates four research grade telescopes at their facility, which are 9.2, 2.7, 2.1 and 0.8 m in sizes.

Figure 2.1 McDonald Observatory's 2.7-m and 2.1-m telescopes located atop Mt. Locke, Fort Davis, TX. *Image credit: McDonald Observatory*

The 9.2 m telescope (also known as the Hobby-Eberly Telescope (HET)) has the largest yet constructed mirror; however, only 9.2 m portion of the mirror can be utilized at any given moment that makes the HET the fourth largest telescope of the world.

The 2.7 m telescope (also known as the Harlan J. Smith telescope), which is shown in the Figure 2.2, is constructed by Westinghouse between 1966 and 1968. It was the world's third largest telescope when it was built. A 5-story building is housing the telescope and it has been well maintained and upgraded over the years.

Figure 2.2 The 2.7-meter telescope at the McDonald Observatory
Image credit: McDonald Observatory

The telescope has both Cassegrain and Coudè focuses to allow mounting variety of instruments. The Cassegrain focus is located behind the primary mirror and used for CCD imaging in astrometry studies. The Coudè focus is located one story below from the telescope room. When the Coudè focus is in use, the light travels in the mount of telescope to the Coudè room located at the fourth floor. The light is then diverted into the slit room by a flat mirror and ends up focused in the slit. The light that doesn't make it to the spectrograph due to reflection from the slit is captured by a TV camera for guiding. The spectrograph occupies a very large room where the light passes through various lenses, mirrors, a pair of prisms and a diffraction grating, before arriving to the detector. The CCD camera is a nitrogen cooled detector with a very low read-out noise. A hollow-cathode Thorium-Argon lamp is employed on the light path to be used for wavelength calibration during reduction of data. The spectrum of the hollow-cathode lamp is taken frequently during observations. Previously created Thorium-Argon atlas helps identifying Thorium-Argon (ThAr) emission lines and their corresponding wavelengths. Identified wavelengths later correlated with the CCD chip's pixel numbers to provide accurate wavelength readings of the star spectrum.

The focal length of the 2.7-m telescope (when the coudè focus in use) is 88.43 meters. In order to obtain large range of spectrum in a single CCD exposure, the light is cross-dispersed between the slit and the CCD camera by an optic system called Echelle Cross-Disperser. Echelle Cross-Disperser allows CCD chip's rectangular surface be utilized entirely by light. Spectral ranges, almost from the atmospheric UV limit to CCD's infrared limit, can be taken into 2048 x 2048 pixels CCD chip with single exposure. Echelle Cross-Disperser is also called 2D Spectrograph given to its multi-dimensional dispersing function.

The Figure 2.3 illustrates the cross-section of cross-dispersed echelle spectrum. As can be seen from the figure, the Echelle spectrum consists of parallel spectra bracketing slightly different wavelengths. Each parallel spectrum is called order. Bracketing wavelengths in each order are often not consecutive. There are gaps and overlaps in wavelengths between orders. The illustration shows full-optical bandwidth coverage (~300 nm – 1000 nm) in 67 orders.

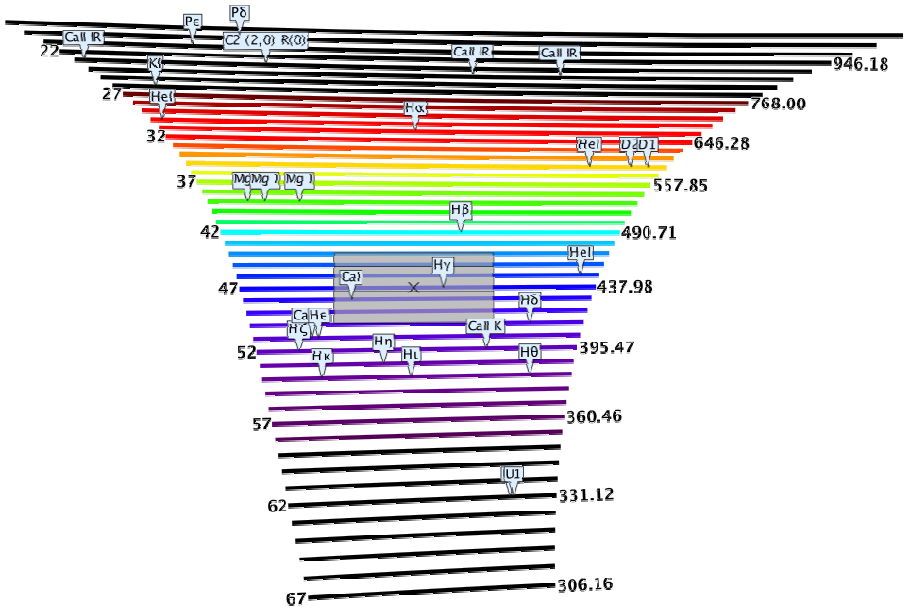

Figure 2.3 Illustration of Cross-dispersed Echelle Spectrum
Image credit: Gemini Observatory

The 2.7 m telescope's Coudè focus is equipped with a thin, grade 1, Tektronix 2048 x 2048 pixels CCD camera. With the echelle gratings, full bandwidth of 3,400-10,900 Å can be collected with single exposure.

This telescope is selected to monitor the chromospheric activity of target stars because of its capability of taking high resolution (R ≈ 50,000) full bandwidth spectra, which allows studying other spectroscopic features beyond Ca lines, as needed. Another reason is the necessity of dedicating such a long telescope time for this study because of days long orbital periods of program stars. In order to obtain full-orbital coverage of program stars, 10 days of uninterrupted observation time of 2.7 m telescope requested from the McDonald Observatory. For larger telescopes, obtaining such a long dedicated telescope time is relatively difficult. Moreover, the 2.7 m telescope is operated by the investigating team rather than a staff member of the McDonald Observatory, which allows observer tweak the observation program according to weather conditions, etc.

The McDonald Observatory is located at about 9 hours driving distance from Arlington, TX. Temperature and air pressure is far different from urban areas of Texas. Observers arrive to the mountain usually a day in advance to adjust the sleeping schedule and get adapted to the environmental conditions. Observers' duty starts in the late afternoon. Telescope motors are started, appropriate diffraction grating is setup into the slit, computer communications are established, and flat-field exposures are taken. A flat-field exposure is an image that is taken when the slit is uniformly illuminated by a hollow-cathode lamp (not ThAr). These flat-field exposures are used to measure the response of individual pixels of the CCD chip and are later used as normalization function during data reduction. A solar spectrum is also taken before sunset to keep record of telluric lines specific to the observation night.

With sunset, the telescope is typically first pointed to a bright star near zenith and then focused. The telescope is then pointed to the first program star of the night. Exposures are started taken approximately an hour after sunset (Astronomical Twilight).

Especially for dim targets, exposure times can be quite long (30-40 mins). CCD camera and telescope are controlled by computers running UNIX operating systems. CCD exposures are started from a terminal with specific commands. Telescope can either be pointed from the control computer, or manually with remote controls. Dome automation is perfectly integrated into the telescope control computer so the dome opening automatically positions itself to avoid blocking the telescope view. An additional monitor shows data from the weather station of the observatory, and advises the observers to close their domes in the event of high humidity, excess wind speeds or particle counts. Luckily, the weather conditions allowed data taken all nights during the observation run. When the telescope is pointed to a target star, the acquisition of spectra is started by a given command from the CCD control computer. After the given exposure time is reached, the CCD camera transfers the captured image of the spectrum to the CCD control computer. Obtained images are saved in FITS files, which are similar to JPG or GIF graphic files.

The observation log from the observation run in April 2006 is given in Table 2.1. Seeing values which represents air (or weather) quality is indicated in the first row of the table. The unit for “seeing” is arc seconds, and indicates the minimum separation angle that can be observed for that particular night. Therefore, seeing improves at smaller values. The numbers in parenthesis indicate the number of exposures taken. Repeating exposures of the same target are usually consecutive. More detailed observation log is included in Appendix A.

Table 2.1 Observation Log of the Observation Run on April 2006

5-Apr	6-Apr	7-Apr	8-Apr	9-Apr	10-Apr	11-Apr	12-Apr	13-Apr
HD187123 (3)	HD73256 (3)	HD73256 (3)	HD73256 (3)	HD73256 (3)	HD49674 (5)	HD49674(3)	tau boo(6)	HD49674(1)
HD179949 (2)	HD49674 (3)	HD49674 (3)	HD49674 (3)	tau boo (12)	tau boo (7)	tau boo(11)	HD49674(1)	
	tau boo(7)	tau boo (6)	tau boo (6)	HD49674 (3)	HD102195 (4)	HD149026 (3)	HD149026(4)	
	HD102195 (3)	HD179949 (2)	HD102195 (3)	HD102195 (3)	HD149026 (5)	HD189733 (4)	HD179949(2)	
	rho crb(2)		HD149143 (3)	HD149143 (3)	HD179949 (3)	HD179949 (3)		
	HD149026 (6)		HD149026 (3)	HD149026 (3)				
	HD189733 (2)		HD187123 (2)	HD187123 (2)				
	HD179949 (3)		HD179949 (3)	HD179949 (2)				

After an observation run, spectra contained in FITS files must be processed and corrected before taking them for further analysis. This intermediate step is called “data reduction” and performed due to following reasons:

- The spectra contain noise from CCD’s electronics and optic system
- CCD’s are not uniform detectors. Pixels sensitivity varies through the surface of the light collecting chip.
- CCD’s may also have defective pixels/sections
- Spectra contains wavelength shifts due to rotation and orbital velocity of Earth
- CCD chip has no information about the wavelength of collected spectra

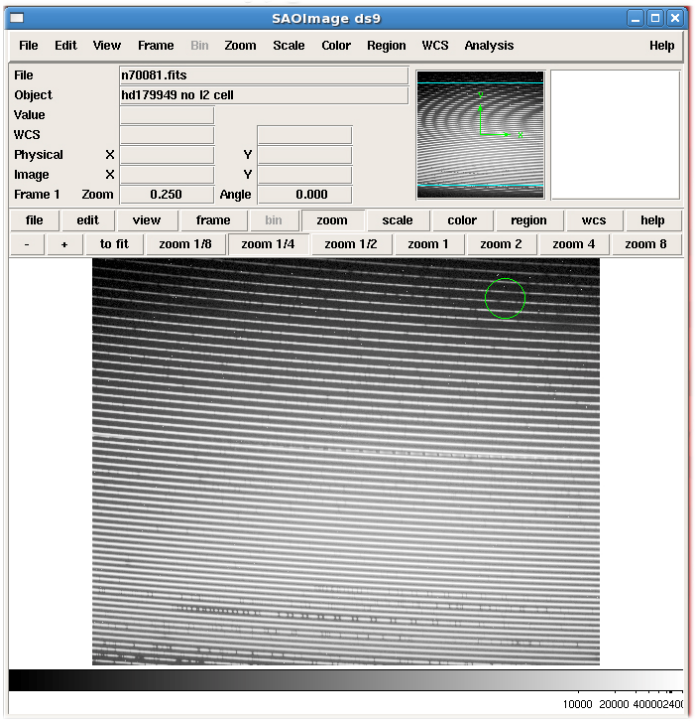

Figure 2.4 An example FITS file that is viewed by SAOImage DS9.

CHAPTER 3

REDUCTION OF ECHELLE SPECTRA USING IRAF

As indicated in the previous chapter, a stellar light is cross-dispersed in the slit of the spectrograph and an image of the spectrum is captured by a CCD camera, these are the steps also pursued in the observation run of 2006. However, the spectra contain several artificial effects that are eliminated by a process called data reduction. These artificial effects include, but are not limited to, sensitivity difference of pixels on the CCD chip, background noise in the CCD electronics, and slight wavelength shifts due to the rotation and orbital velocity of the earth. Moreover, conditions such as cloud coverage, temperature and humidity changes may also significantly affect the obtained spectra. All necessary software tools, including most commonly used data reduction software - IRAF, are introduced below.

3.1 Necessary Tools for Reduction of Observational Data

*3.1.1 IRAF – **I**mage **R**eduction and **A**nalysis **F**acility*

IRAF is an Image Reduction and Analysis Facility that is widely used by scientists in the field of observational astronomy. It was developed by astronomers at the National Optical Astronomy Observatory (NOAO). IRAF is an extensive and powerful software package used to extract and process CCD images. IRAF is developed for 'UNIX – like' operating systems, commonly used on IBM-Unix, SUN-Solaris, Mac OSX and Linux distributions.

IRAF* is obtained from IRAF's official web site http://iraf.noao.edu

**IRAF is distributed by the National Optical Astronomy Observatories, which are operated by the Association of Universities for Research in Astronomy, Inc., under cooperative agreement with the National Science Foundation.*

*3.1.2 IDL – **I**nteractive **D**ata **L**anguage*

IDL is a popular data analysis software package widely used by scientists. IDL was developed at the Laboratory for Atmospheric and Space Physics at the University of Colorado at Boulder to be used at NASA's Goddard Space Flight Center to interpret data from Mars orbiters; Mariner 7 and Mariner 9 spacecrafts.

IDL is currently distributed by ITT Visual Information Solutions (http://www.ittvis.com). It is commonly used by scientists to interpret data. IDL has a powerful plot engine widely used to produce graphs in scientific publications. Unfortunately, IDL is not free.

3.1.3 SAOImage DS9: Astronomical Data Visualization Application

DS9 is a data visualization application developed by Smithsonian Astrophysical Observatory. DS9 is used as a picture viewer for specific file format such as "FITS". FITS file format is introduced under "Pre-Reduction Procedures" in this chapter.

DS9* is obtained from http://hea-www.harvard.edu/RD/ds9/

**This research has made use of SAOImage DS9, developed by Smithsonian Astrophysical Observatory", 2003adass..12..489*

3.2 Data Reduction – Using IRAF

In general, the data reduction process consists of three phases. They are: pre-reduction, reduction and post-reduction. Although the reduction pipe-line is quite standard, different observatories may have unique file naming conventions and directory structure.

3.2.1 Pre-reduction procedures

Pre-reduction procedures introduced here are performed to check the quality of observation files and to eliminate possible corrupted ones.

3.2.1.1 FITS files

As indicated in the previous chapter, star light is cross-dispersed in the optical setup of the telescope, and stellar spectra are captured by a CCD camera. An obtained picture is transferred into a file by the CCD camera control computer, and encapsulated in a file with FITS extension. All FITS (Flexible Image Transport System) files consist of 2 sections: header and picture. The header is the specific information (text) about the payload (picture of spectrum), such as the date and time stamp, given exposure time, type of the CCD used, etc.

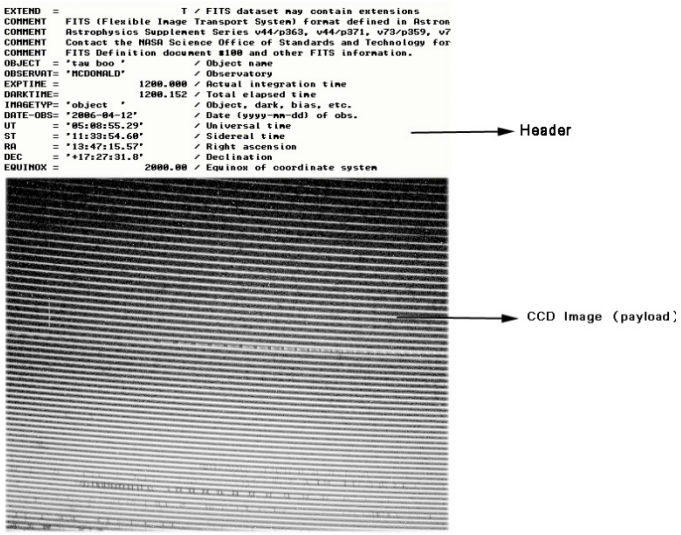

Figure 3.1 The FITS file figure. A FITS file is consist of two parts; header (text) and spectrum (image)

Below is an example of a sample FITS header of McDonald Observatory's 2.7 m telescope's TK3 CCD detector.

```
n70061.fits[2080,2048][int]: tau boo
No bad pixels, min=0., max=0. (old)
Line storage mode, physdim [2080,2048], length of user area 2511 s.u.
Created Fri 21:57:24 15-May-2009, Last modified Fri 21:57:24 15-May-
2009
Pixel file "n70061.fits" [ok]
EXTEND  =                    T / FITS dataset may contain extensions
COMMENT    FITS (Flexible Image Transport System) format defined in
Astronomy and
COMMENT   Astrophysics Supplement Series v44/p363, v44/p371, v73/p359,
v73/p365.
COMMENT   Contact the NASA Science Office of Standards and Technology
for the
COMMENT   FITS Definition document #100 and other FITS information.
OBJECT  = 'tau boo '           / Object name
OBSERVAT= 'MCDONALD'           / Observatory
EXPTIME =            1200.000 / Actual integration time
DARKTIME=            1200.152 / Total elapsed time
IMAGETYP= 'object  '           / Object, dark, bias, etc.
DATE-OBS= '2006-04-12'         / Date (yyyy-mm-dd) of obs.
UT      = '05:08:55.29'        / Universal time
ST      = '11:33:54.60'        / Sidereal time
RA      = '13:47:15.57'        / Right ascension
DEC     = '+17:27:31.8'        / Declination
EQUINOX =              2000.00 / Equinox of coordinate system
TELTKRA =                 15.0 / Track rate in arcsec/sec
TELTKDEC=                  0.0 / Track rate in arcsec/sec
POINT   = 'mean    '           / Point type
HA      = '-02:13:24.29'       / Hour angle
ZD      = '33.10   '           / Zenith distance
AIRMASS =                 1.19 / Airmass
TELESCOP= 'mcd107x '           / Telescope name
HOSTCOMP= 'oberon  '           / Host computer name
HOSTOPS = 'SunOS 5.8'          / Host computer operating system
PROGRAM = 'ICE V2-10Feb2003'   / Data acquistion program
DETECTOR= 'TK3     '           / Detector name
DETSIZE = '2048X2048'          / Detector size for DETSEC
MICROCOD= 'TK3_2002'           / Detector microcode name
CONTTYPE= 'McDonald Obs. V2'   / Detector controller type
BP      = 'V2.0 #4 Rev B'      / Backplane ID
PS      = 'V2.0 #4 Rev B'      / Power supply ID
CD      = 'V2.0 #4 Rev B'      / Clock driver ID
TC      = 'V2.0 #4 Rev A'      / Temperature controller ID
DSP     = 'V2.0 #4 Rev A'      / Digital signal processor ID
ASP1    = 'V2.0 #6 Rev C'      / Analog Signal Processor #1 ID
PH      = 'V2.0 #4 Rev C'      / Penthouse ID
AMPLIFIE= '3       '           / Amplifier(s) in use
ASPGAIN =                    1 / ASP gain setting
INTEGRAT=                    1 / Integrator setting
DETTEMP =              -105.00 / Detector temperature (Celsius)
CRYOTEMP=              -192.97 / Cold sink temperature (Celsius)
CONTTEMP=                23.04 / Controller temperature (Celsius)
SERVOPWR=                 0.69 / Servo heater power (watts)
```

```
NCCDS   =                    1 / Number of CCDs in detector
NAMPS   =                    1 / Number of amplifiers used
INSTRUME= 'cs23-e2 '           / Instrument
CCDSUM  = '1 1     '           / On-chip summation
TILTPOS = ' 4847.60'           / Tilt position
ORDER   = '71      '           / Spectral order
PRISM   = '-649    '           / Prism encoder
ECHELLE = '3981    '           / Echelle encoder
RDNOISE3=                      2.55 / Readout noise for amplifier 3
(electrons)
GAIN3   =                0.5840 / Gain for amplifier 3 (electrons per
ADU)
CCDSIZE = '2048X2048'          / CCD size
CCDSEC  = '[1:2048,1:2048]'    / Orientation to full frame
AMPSEC  = '[1:2048,1:2048]'    / Amplifier section
DETSEC  = '[1:2048,1:2048]'    / Detector section
ORIGSEC = '[1:2048,1:2048]'    / Original size full frame
DATASEC = '[1:2048,1:2048]'    / Image portion of frame
TRIMSEC = '[1:2048,2:2047]'    / Region to be extracted
BIASSEC = '[2053:2080,2:2047]' / Overscan portion of frame
```

All FITS files of the observation run are inspected for corruption, saturation or other defects by using DS9.

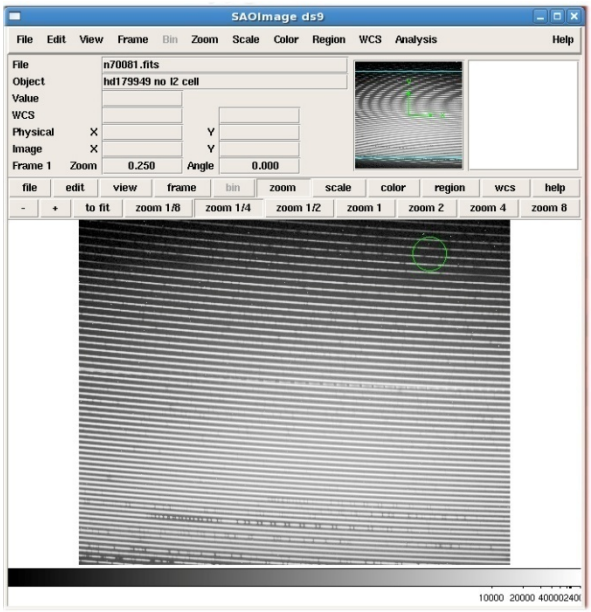

Figure 3.2 SAOImage DS9 (Screenshot)

3.2.1.2. *Inventory*

For each observation night, the observer has a set of FITS files that consist of BIAS, FLAT, DARK, THAR and OBJECT frames. OBJECT is also referred as STELLAR. A short description of these files is given below.

BIAS: Zero seconds exposure image – image of the noise that is generated by electrons on the surface of the CCD chip. Usually several BIAS frames are taken at the beginning of an observation night.

FLAT: A taken image when the slit of the spectrograph is uniformly illuminated by an incandescent light bulb on the light path. At some observatories, where it is not feasible to use incandescent bulb, FLAT's are taken by pointing telescope to a white screen or twilight sky.

FLAT is commonly referred as Flat-Field. FLAT images are essential pieces of data reduction as they represent the characteristic of the CCD chip under uniformly illuminated slit. Sensitivity differences among pixels can only be normalized by dividing OBJECT (or stellar) imaged by FLAT. This normalization is called FLAT correction or Flat-Fielding. Usually several FLAT frames are taken at the beginning of an observation night. Nightly FLAT's are averaged out to compute best (optimistic) FLAT image of the night.

DARK: Dark is the recorded noise of the CCD camera under certain exposure time when CCD's shutter is closed. The exposure time of Dark images are set to be the same as stellar images to figure the generated "Dark Current" when taking stellar images. Dark is not always necessary when using nitrogen cooled CCD cameras (i.e., McDonald Observatory's TK3 Coudé Spectrograph at the 2.7 m telescope) where the effect of dark is negligible.

THAR: An emission line spectrum taken from Thorium-Argon source (arc lamp) located in the light path. Arc lamp generates bright emission lines that are sufficiently spaced along the optic window to identify at least 3-4 emission lines per order. Identified lines and their corresponding wavelengths are used as reference points to correlate pixel numbers with wavelengths. The correlation function, which is called dispersion correlation function, allows to perform this task is computed by IRAF.

A previous study was done by Carlos Allende Prieto (2001) at the McDonald Observatory to identify and compute wavelengths of bright emission lines generated by Th-Ar (arc) lamp on the light path of the 2.7 m telescope. Identified features were recorded and published at *"The Spectrum of the Th-Ar Hollow-Cathode Lamp Used with the 2d Coudè spectrograph"*. At later stage of data reduction, called wavelength calibration, allows to identify Th-Ar emission lines on the CCD chip and to enter the corresponding wavelengths. It will let IRAF to find the best mathematical expression (dispersion correlation) to match pixels with corresponding wavelengths. THAR frames are usually taken within a few hours, depending on how critical the accuracy in wavelength is, during observation night to avoid effects by

temperature, humidity, and pressure changes. Change in atmospheric conditions may alternate the refraction index of the air, which may cause slight shifts of spectrum on CCD chip.

OBJECT: Star's spectrum (or taken CCD picture using starlight) which contains number of absorption and emission lines on continuous spectrum.

Sample BIAS, FLAT, THAR and OBJECT frames are represented in the Figure 3.3.

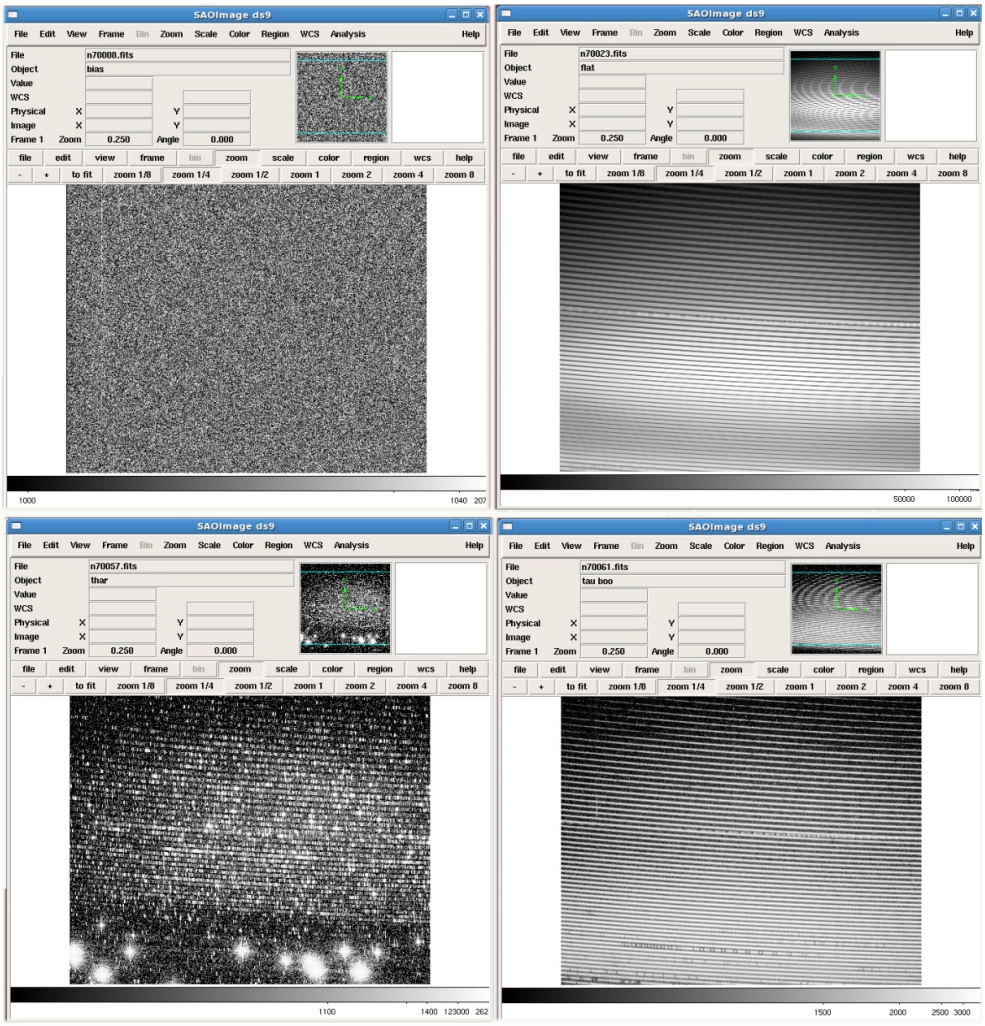

Figure 3.3 Top left: Sample BIAS image. Bias is noise produced by surface electrons of the CCD chip which are captured by zero-seconds exposure. Top right: Sample FLAT image which is obtained when the slit of the spectrometer is uniformly illuminated. Bottom left: Sample Th-Ar (arc) image. Arc image is a broad bright-emission spectrum which is generated by a Th-Ar lamp on the light path. Bottom right: Sample OBJECT (or Stellar) image which is produced by star light.

3.2.1.3 Bad Pixel Information of CCD chip – bad.pix file

Most CCD chips have defective pixels. If defective areas exist on the CCD chip, coordinates of the bad pixels should be known to obtain an accurate data reduction. Bad pixel information (bad pixel file – bad.pix) is usually obtained from technical support staff at the observatory. If that file is not available, a good BIAS and FLAT frames can be inspected to identify bad pixels. Note that bad.pix file is used by IRAF to ignore data stored by defective pixels on the CCD chip.

Bad pixels typically appear as either dark or bright, thin vertical lines starting from either top or bottom of the CCD frame. CCDs scan pixels vertically when reading data from CCD chip. If a bad is pixel found, hardware of CCD fails to read, and ignores the rest of the line.

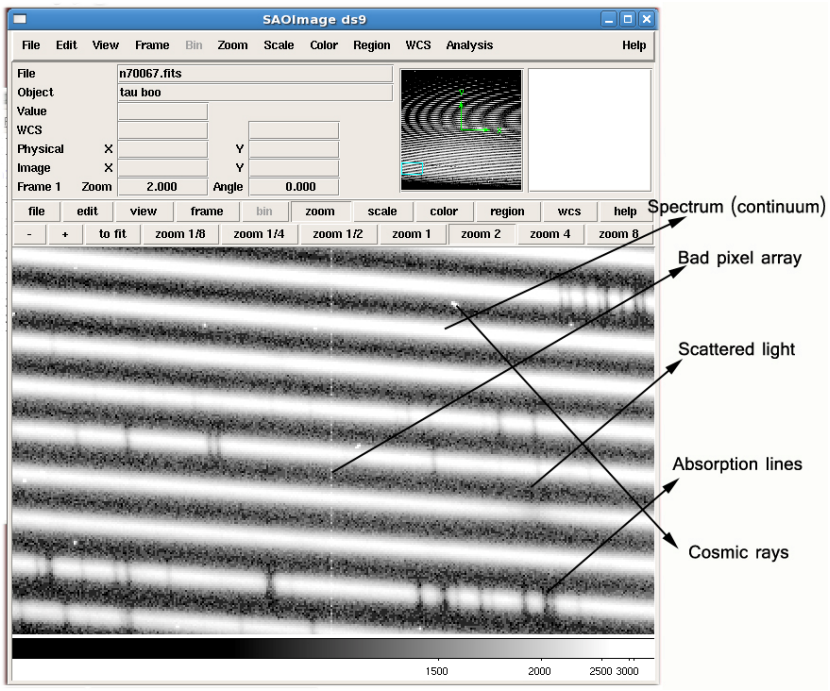

Figure 3.4 A typical spectrum as it read from FITS file. The typical features, such as bad pixels, scattered light and cosmic rays are shown.

The Figure 3.5 is the content of the bad.pix file. In this file, columns 200, 201, 216 are entirely marked as “bad” (0 – 2048). Columns 1635 and 1636 are marked as “bad” from rows 1112 to 2048.

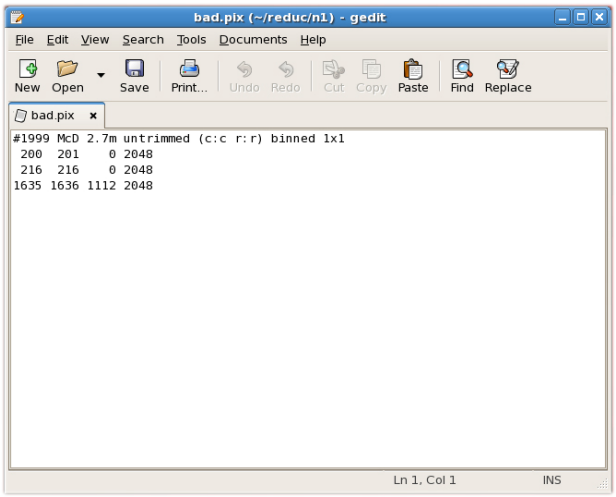

Figure 3.5 Content of the bad.pix file

3.2.2 Reduction Procedures

3.2.2.1. Running the IRAF for the first time

In order to create the login file, login.cl, **mkiraf** command is used in the terminal window. Terminal type is specified as “xgterm”.

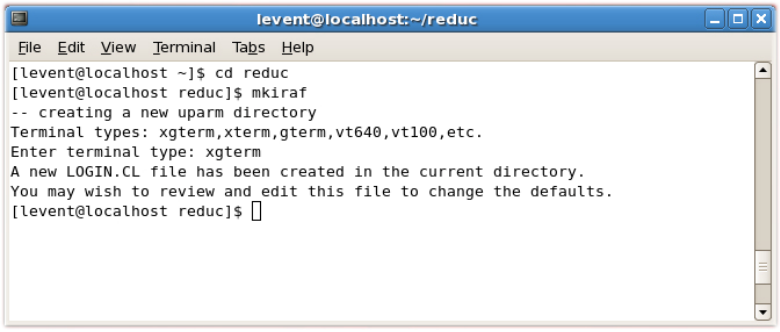

Figure 3.6 mkiraf command

IRAF must be started in the xgterm window. Note that xgterm is started by the command **xgterm &**.

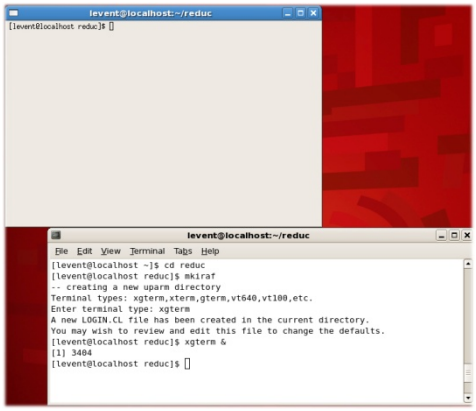

Figure 3.7 xgterm window

cl command starts the IRAF In the xgterm window. There are several different file formats supported by IRAF. Following commands are used to check and set the image type.

show imtype **:** displays the current image type

set imtype = "fits, noinherit" : sets the image type to "fits"

In the scope of this project, *imred*, *ccdred* and *echelle* packages of IRAF are used when reducing echelle spectra. Each package contains large number of utilities that assist during data reduction.

3.2.2.2. Combining BIAS frames

As can be seen from the observation log, several BIAS exposures are taken for each night before the actual observation run starts. These BIAS exposures are combined to obtain "the best" BIAS which represents the characteristics of the CCD's internal noise. Combined BIAS image is the mathematical mean of all of the BIAS images. In order to perform mathematical operation on images, such as multiplication, division or addition, FITS images are considered as matrices consisting of pixels which each pixel containing a number that is a

fraction of intensity. If 2K CCD chip is utilized, each FITS image will represent a 2048x2048 matrix. Combining several matrixes in such size is not an easy task by hand; but simply done in seconds by IRAF's **zerocombine** command.

Each task in IRAF has large set of parameters specific to the task being performed. An IRAF task may have over 30 parameters to set before it performs desired operation. The task **epar** is used to set parameters of other tasks. Once parameters are set, IRAF stores the parameters for convenience for next time use.

For example, **epar zerocomb** command is used to set parameters of **zerocomb** task.

Table 3.1 lists all the parameters of **zerocomb** that we used to reduce data from McDonald Observatory's 2.7 m Telescope's TK3 detector. Those parameters may vary for different reduction procedures and detectors. Some of the parameters are directly obtained from the FITS header of the corresponding files.

Table 3.1 Parameters of ZEROCOMBINE task

input	=	@bias
output	=	zero.fits
combine	=	average
reject	=	ccdclip
ccdtype	=	
process	=	no
delete	=	no
clobber	=	no
scale	=	none
statsec	=	
nlow	=	0
nhigh	=	1
nkeep	=	1
mclip	=	yes
lsigma	=	3.
hsigma	=	3.
rdnoise	=	RDNOISE3
gain	=	GAIN3
snoise	=	0.
pclip	=	-0.5
blank	=	0.
mode	=	ql

Note: **CTRL-D** keystrokes update and exit the **epar**.

Note: When **zerocomb** task is started, IRAF prompts for “List of zero level images to combine (@bias):

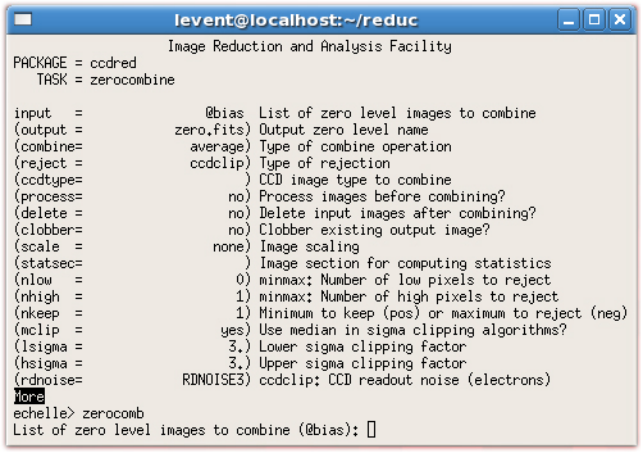

Figure 3.8 IRAF prompts to list zero level of images

Output of this task will be *zero.fits* file. The output file is inspected via DS9, it will look like any other BIAS image.

3.2.2.3. Combining Flat Frames

Similar to BIAS, Flat frames will be combined into single *flat.fits* image file by using **flatcomb** command. Parameters used are given at the Table 3.2.

Table 3.2 Parameters of FLATCOMBINE task

input	=	@flat
output	=	flat.fits
combine	=	average
reject	=	ccdclip
ccdtype	=	
process	=	no
delete	=	no
clobber	=	no
scale	=	none
statsec	=	
nlow	=	1
nhigh	=	1
nkeep	=	1
mclip	=	yes
lsigma	=	3.
hsigma	=	3.
rdnoise	=	RDNOISE3
gain	=	GAIN3
snoise	=	0.
pclip	=	-0.5
blank	=	1.
mode	=	ql

flatcomb task produces the *flat.fits* file. Combined flat image will look like any other flat image.

3.2.2.4. Bias (zero) subtraction

Bias is the (zero level) noise produced in the CCD electronics; therefore, it is named “zero”. Bias is subtracted from all FITS images using task **ccdpro**. Bias subtraction is performed for Bias (itself), Flat, Comp and Object files. In fact, Bias subtraction from Bias itself (with other words - Bias minus Bias) is not an actual subtraction, but it is performed to trim images to certain size (see *biassection* and *trimsection* parameters). It should be noted from the table below that *zerocorrection* is set to “no” when processing Bias images.

Table 3.3 Parameters of CCDPRO task to perform BIAS subtraction

images	=	zero.fits
output	=	zero_c.fits
ccdtype	=	
max_cache	=	0
noproc	=	no
fixpix	=	yes
oversca	=	yes
trim	=	yes
zerocor	=	no
darkcor	=	no
flatcor	=	no
illumcor	=	no
fringecor	=	no
readcor	=	no
scancor	=	no
readaxis	=	line
fixfile	=	bad.pix
biassec	=	[2053:2080,3:2046]
trimsec	=	[3:2046,3:2046]
zero	=	
dark	=	
flat	=	
illum	=	
fringe	=	
min replace	=	1.
scantype	=	shortscan
nscan	=	1
interactive	=	yes
function	=	spline3
order	=	20
sample	=	*
naverage	=	1
niterate	=	3
low_reject	=	3.
high_reject	=	3.
grow	=	0.
mode	=	ql

Bad pixel file is pointed at *fixfile*. Bad pixels will be fixed if *fixpix* parameters is set to “yes”. Bad pixels will be either interpolated or discarded. *biassec* and *trimsec* parameters are obtained from the CCD header.

ccdpro command asks the following questions before proceed:

List of CCD images to correct (zero.fits):

Fit overscan vector for zero.fits interactively (yes):

When *interactive* parameter is set to “yes”, IRAF shows overscan region that needs a fit with certain function and order. The fit is shown with dashed lines in white color (by default). Fit function and order can be changed by using keyboard shortcuts. Overscan region of the Bias image and keyboard shortcuts are display below.

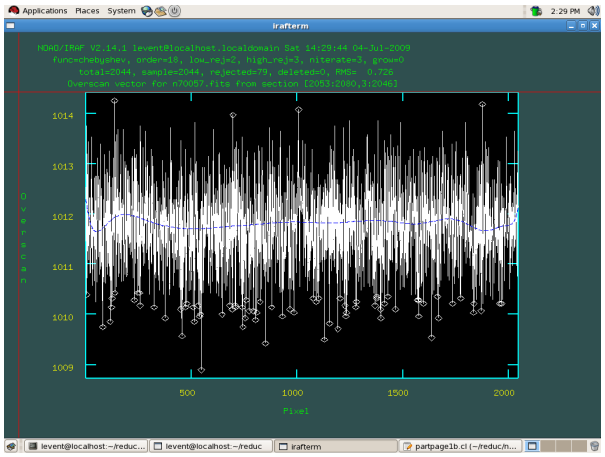

Figure 3.9 Ovescan region of BIAS

Below are some of the useful commands to perform BIAS subtraction task in IRAF.

:c 4 = change the fit color to number 4 (blue)

:o 22 = change the order of the fit to 22

:low 2 = change the low_reject (sigma) to 2

F key = redraw the graph.

? = help

Bias subtraction will also be performed for Flat, Comp and Objects. Most **ccdpro** parameters will remain the same except following ones.

Table 3.4 Parameters of CCDPRO task to perform FLAT division

images	=	flat.fits
output	=	flat_c.fits
zerocor	=	yes
zero	=	zero_c.fits

After updating the parameters with **CTRL-D** and running **ccdpro** to process flat, IRAF's graphic interface shows the overscan vector for flat.

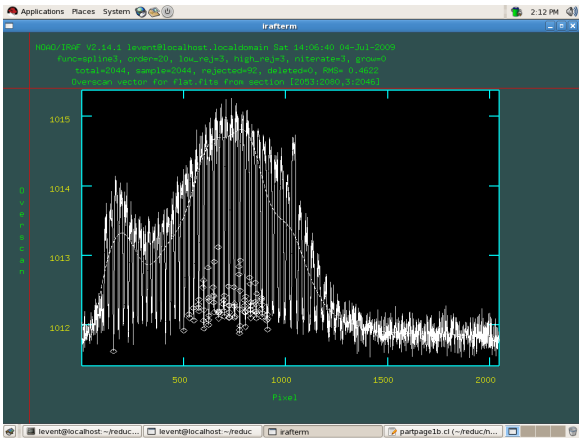

Figure 3.10 Overscan region of FLAT

When making fit, SPLINE3 or CHEBYCHEV functions usually return the best results.

A similar operation is performed for comp and object images by editing *images* and *output* parameters of the **ccdpro** task accordingly. Figure 3.11 and Figure 3.12 below shows the overscan fits for sample comp and object images.

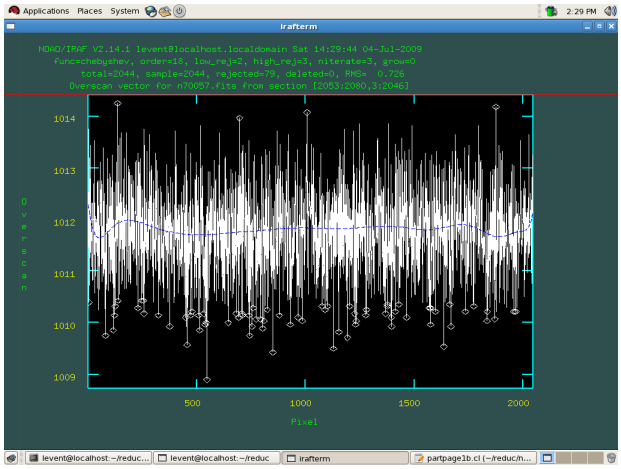

Figure 3.11 Overscan Vector for comp image. Blue line indicates the best fit.

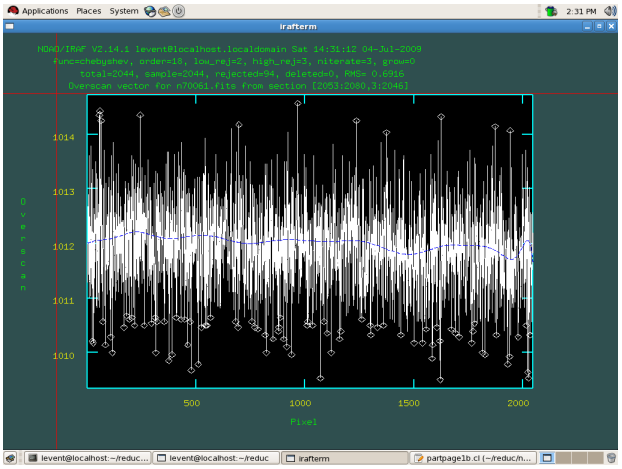

Figure 3.12 Overscan Vector for object image. Blue line indicates the best fit.

3.2.2.5. Finding Apertures – using APALL

Apertures and their width are determined in IRAF by **apall** task. This is one of the most important tasks of data reduction to minimize the noise and other artificial effects. One of the brightest of the program stars is selected to determine the apertures. The brightest star has the highest signal-to-noise ratio; therefore, it has the sharpest aperture pattern on the CCD chip. **apall** task has large number of parameters. The table below shows the list of parameters used to reduce our program stars.

Table 3.5 Parameters of APALL task to determine the apertures

input	=	n70061_c.fits
output	=	
apertures	=	
format	=	echelle
references	=	
profiles	=	
interactive	=	yes
find	=	yes
recenter	=	no
resize	=	no
edit	=	yes
trace	=	yes
fittrace	=	yes
extract	=	no
review	=	no
line	=	INDEF
nsum	=	10

Table 3.5 – *Continued*

lower	=	-9.
upper	=	9.
apidtable	=	
b_function	=	chebyshev
b_order	=	1
b_sample	=	-10:-5,5:10
b_naverage	=	-3
b_niterate	=	2
b_low_reject	=	3
b_high_reject	=	3
b_grow	=	0
width	=	15
radius	=	8
threshold	=	0
nfind	=	68
minsep	=	5.
maxsep	=	1000.
order	=	increasing
aprecenter	=	
npeaks	=	INDEF
shift	=	No
llimit	=	INDEF
ulimit	=	INDEF
ylevel	=	0.03
peak	=	yes
bkg	=	yes
r_grow	=	0
avglimits	=	no
t_nsum	=	10
t_step	=	10
t_nlost	=	10
t_function	=	legendre
t_order	=	4
t_sample	=	*
t_naverage	=	1
t_niterate	=	1
t_low_reject	=	3.
t_high_reject	=	3.
t_grow	=	0.
background	=	none
skybox	=	1
weights	=	none
pfit	=	fit1d
clean	=	no
saturation	=	INDEF
readnoise	=	RDNOISE3
gain	=	GAIN3
lsigma	=	3.
usigma	=	3.
nsubaps	=	1

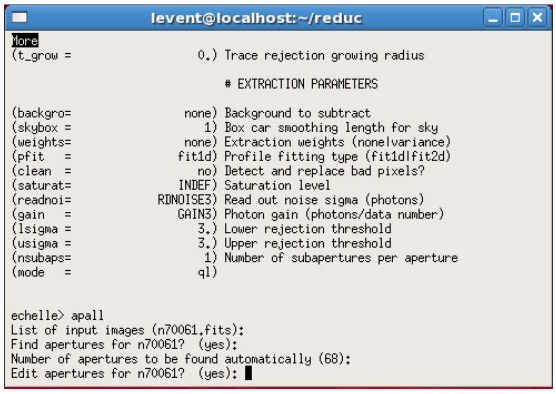

Figure 3.13 Starting APALL task

Figure 3.13 shows the startup screen of **apall** task asking the number of apertures expected in the echelle spectrum. This number is (approximately) known by the observer as it depends on the setup of echelle spectrograph. IRAF usually accurately finds most apertures. IRAF takes a 10 Å wide slice from the middle of the CCD chip (see Figure 3.14), and plots the sum of each row (in the 10 Å window) as a function of the row numbers (see top-left figure of Figure 3.15).

The purpose of this step is to adjust the apertures width to take all available light in and to set the sharp boundary between spectra features and scattered light region. As it can be seen from the Figure 3.15, some of the weak apertures may not be identified automatically (top and bottom-right figures), or IRAF may (accidentally) identify cosmic rays as apertures (bottom-left figure). In some cases, cosmic rays can be in apertures (top-right figure). It is not possible to avoid such cosmic rays as they are superposed on to actual spectra, and will be eliminated through the data reduction.

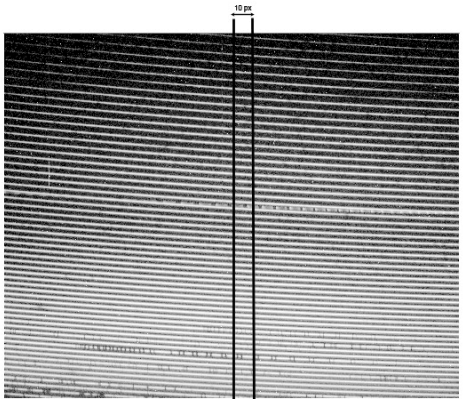

Figure 3.14 10Å wide window that is used by IRAF to find apertures

apall's GUI (Graphical User Interface) utilizes large number of keyboard keystrokes to manipulate apertures. Most USEFUL commands are summarized below.

? : See Help

w-e-e : Zoom (hit W key, point the mouse to the left-bottom corner of the area to be zoomed, hit E key, then point the mouse to the right top corner of the area to be zoomed, hit E key)

w-a :View All (or Zoom Out)

:nsum :Specify the number of columns to be added (by default 10). Command must be followed by a number.

a :toggle All flag (select All)

c :center an aperture(s)

d :delete an aperture(s)

n :define a new aperture centered at the cursor

s :shift the center(s) of the current aperture to the cursor position

t :trace aperture position

f :find apertures

o :order aperture numbers

q :quit (or proceed to the next step)

I :Interrupt (nothing saved)

For example, necessary tasks to perform for the apertures in the Figure 3.15 are listed below.

- Add aperture between apertures 1 & 2 (command n)
- Remove aperture 50 (command d)
- Add apertures on the left end (command n)
- Reorder the apertures (command o while the cursor is on ap.1)
- Check centers of the apertures

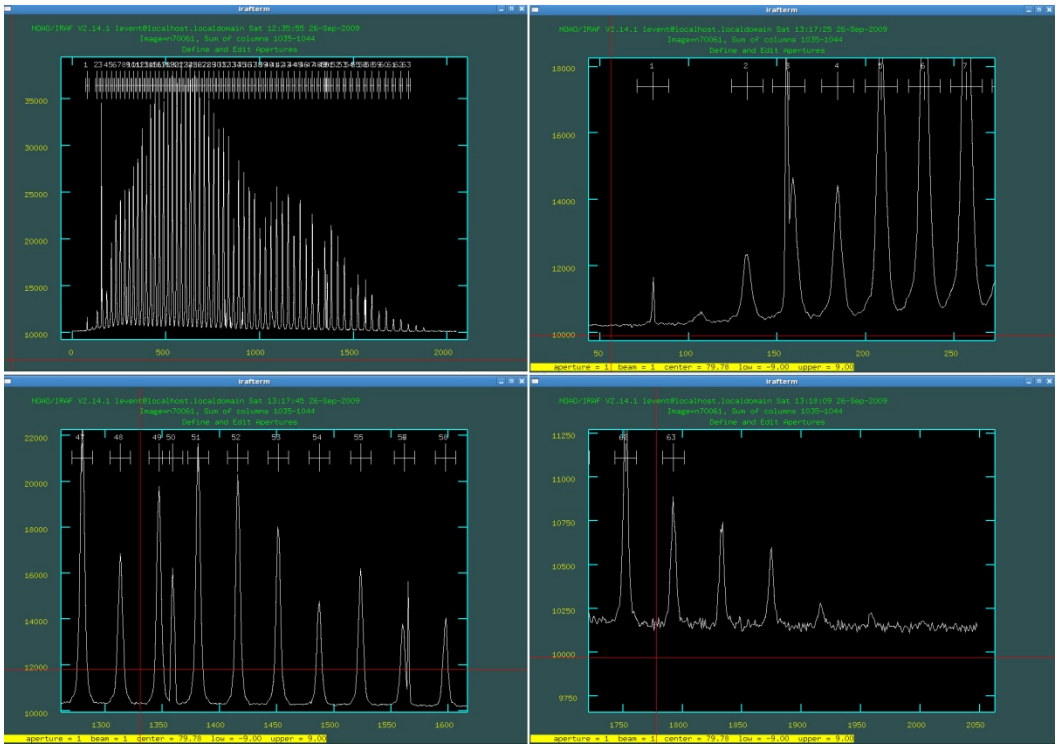

Figure 3.15 APALL task. Top left figure: identified apertures. Top right figure: a cosmic ray in the aperture 3. Bottom left figure: a cosmic ray identified as an aperture. Bottom right figure: (Automatically) unidentified orders.

At the first attempt, 67 orders are identified in this frame. After necessary corrections are performed, ‘q’ (quit) command will be used to proceed to the next step.

In some cases, 10 Å is not sufficient to obtain a clear plot to determine the boundary of apertures. In this case, the width of the window can be increased by **:nsum** command (for example: **:nsum 20**).

In the next step, IRAF asks a few questions about tracing the apertures interactively. "*yes*" answer is given to all of these questions. IRAF traces and makes a fit to individual apertures. If the fit doesn't seem to be correct, it can be corrected by deleting data points with big discrepancy (if any) and/or by changing the order of the fit. The 'q' command is used to proceed to the next step.

3.2.2.6. Finding Apertures on the Edge of the CCD Chip

At this step, **apall** command is used one more time to find the apertures that falls the edge of the CCD chip. As orders are fainter at edges, their peak in *apall* window may not be identifiable. To avoid any unidentifiable orders, the 10 pixels window is increased to 20 pixels by **nsum** command. It can be recalled from the previous section that the 10Å window used by IRAF to plot the orders is located at the center of the CCD chip. It can be seen from Figure 3.14 that some orders located close the right-top corner and left-bottom corner never falls in that window. In order to include them, the window must be moved all the way right and all the way left of CCD chip. This task is done by **line** command of IRAF GUI.

Usage: **line** *starting pixel number*

line 0 will move the window all the way to the left

line 2044 will move the window all the way to the right

The newly discovered apertures are added by '**n**' keyboard keystroke, then followed by '**t**' keystroke to trace the aperture to check the "fit". If the apertures are not noticeable, increasing *nsum* value may help finding more apertures. To get sum of 20 pixels, nsum command should be run as follows:

:nsum 20

3.2.2.7. Resizing Apertures

apresize task allows IRAF to change size of apertures if they are not adjusted by *apall* command appropriately. The aperture sizes are checked to make sure that the light is fulfilling the apertures so there is no scattered light leak into apertures (see Figure 3.16).

The table below shows the parameter set used with the task **apresize**. The bright star with the highest S/N ratio, which is also used in the previous step to determine apertures, will be used in the “references”.

Table 3.6 Parameters of APRESIZE task

apertures	=	
references	=	n70061_c.fits
interactive	=	yes
find	=	no
recenter	=	no
resize	=	yes
edit	=	yes
line	=	INDEF
nsum	=	1
llimit	=	-9.
ulimit	=	9.
ylevel	=	0.6
peak	=	yes
bkg	=	no
r_grow	=	0
avglimits	=	no

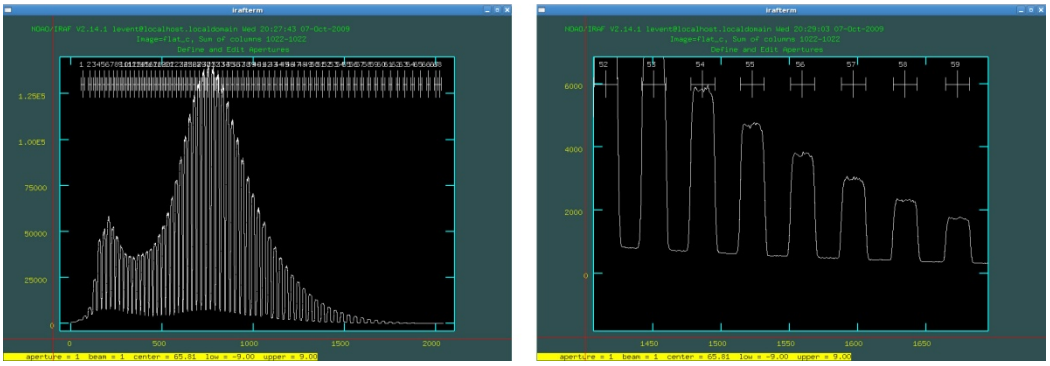

Figure 3.16 Apresize task of IRAF. Left figure shows the scattered light on the bottom. Right Figure shows the apertures appropriately filled.

After making necessary adjustments, *q* keyboard keystroke is used to proceed to the next step: removing the scattered light.

*3.2.2.8. Removing Scattered Light with task:**apscatter***

Although the width of apertures is set accurately, the effect of scattered light is not negligible. The effect of scattered light can be seen Figure 3.16 (left figure) as elevated base. Ideally, the figure should have a flat base terminating at zero level. **apscatter** task of IRAF allows user to create a best model for the scattered light, and subtract it from the entire data set. **apscatter** task is used with the parameters shown at Table 3.7.

Table 3.7 Parameters of APSCATTER task

apertures	=	
scatter	=	
references	=	flat1_c.fits
interactive	=	yes
find	=	yes
recenter	=	no
resize	=	no
edit	=	yes
trace	=	no
fittrace	=	yes
subtract	=	yes
smooth	=	yes
fitscatter	=	yes
fitsmooth	=	yes
line	=	INDEF
nsum	=	10
buffer	=	1
apscat1	=	
apscat2	=	

When **apscatter** task starts, IRAF asks set of questions and will first display the apertures. '*q*' command proceeds to the next step where the scattered light be modeled. IRAF GUI displays vertically scanned chip from the middle (columns 1022- middle of the 2044 pixels chip). IRAF's default fit is shown in the Figure 3.17. The aim of this task is to make the best fit that will sweep the bottom of the data set (as in Figure 3.18).

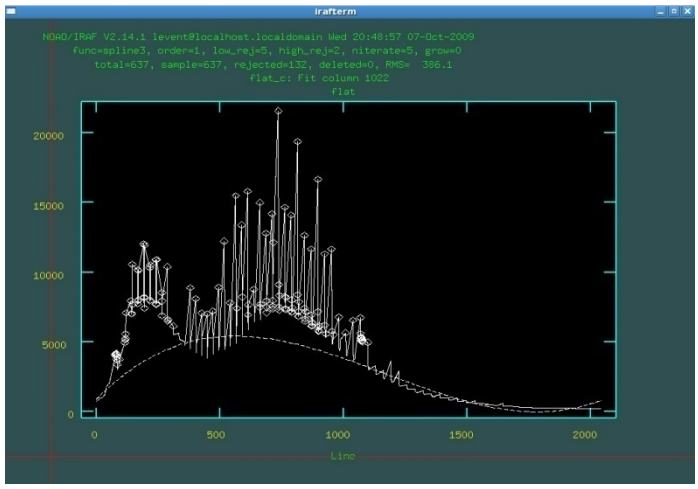

Figure 3.17 APSCATTER task. Bottom gap represents the scattered light. IRAF's default fit to the boundary of the scattered light is shown with white dashes.

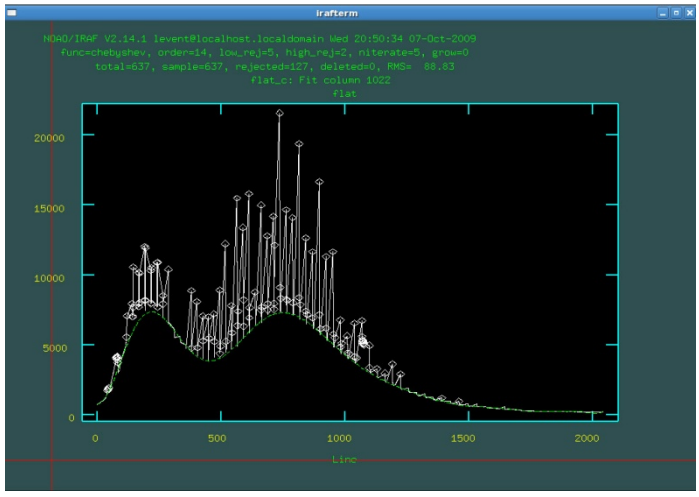

Figure 3.18 APSCATTER task. The fit is adjusted by changing fit function to chebyshev, increasing the order and iteration parameters to match the boundary of the scattered light.

Some useful commands of this task are as follows:

:f *change function (ex: :f chebyshev)*

:o *change order (ex: :o 12)*

:n *change iteration time*

:low *set lower rejection limit (ex:to change the limit to 3 sigma, :low 3)*

:high *set higher rejection limit*

After finding the best fit for column 1022, different columns should also be scanned and checked to make sure that the currently modeled fit represents the scattered light for the entire chip. *q* keystroke is used to scan different columns. With *q* keystroke, IRAF asks whether the user would like to quit (q) or scan different column (c). It is not necessary to work on every individual column. Working on 4-5 (almost) equally spaced columns is sufficient to perform this task (for example columns 400 – 800 – 1400 – 1800).

The Figure 3.19 shows that previously made fit works well on 3 different column of the data set.

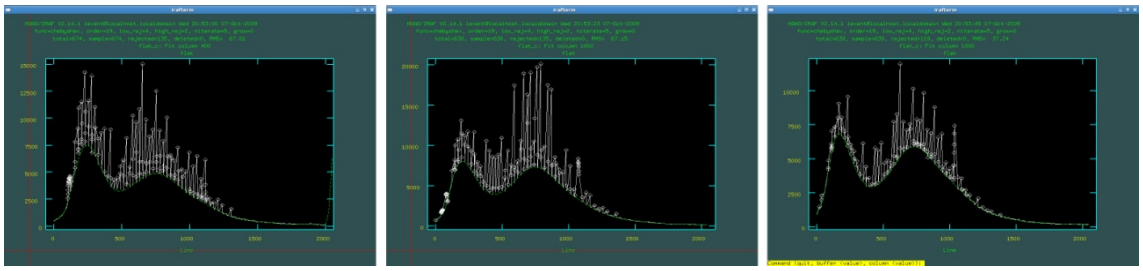

Figure 3.19 Checking the scattered light fit for 3 different columns of the CCD chip

When the best fit is figured, '*q*' keystroke is used to proceed to the next step. This time, IRAF will scan the chip horizontally (lines instead of columns). Same task is performed to find the best fit for 4-5 equally space lines.

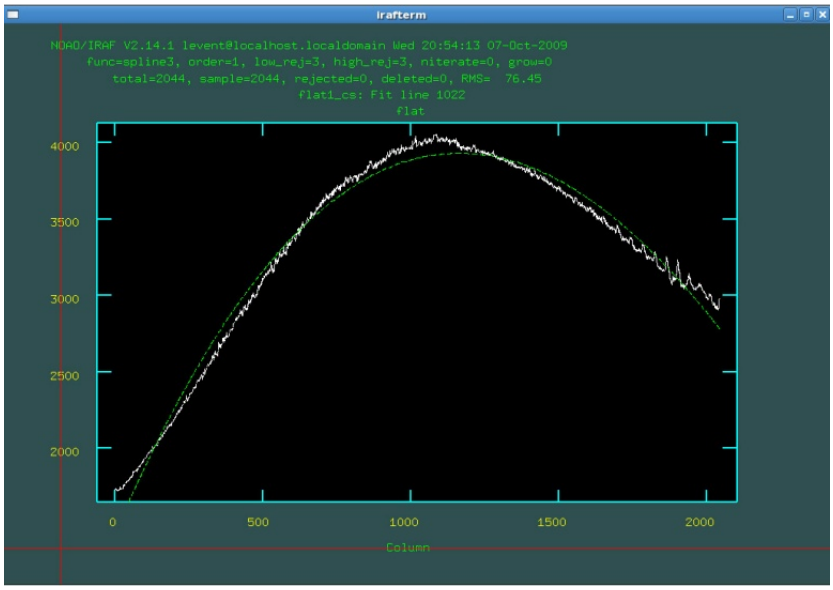

Figure 3.20 The default fit made by IRAF to the horizontally scanned column 1022

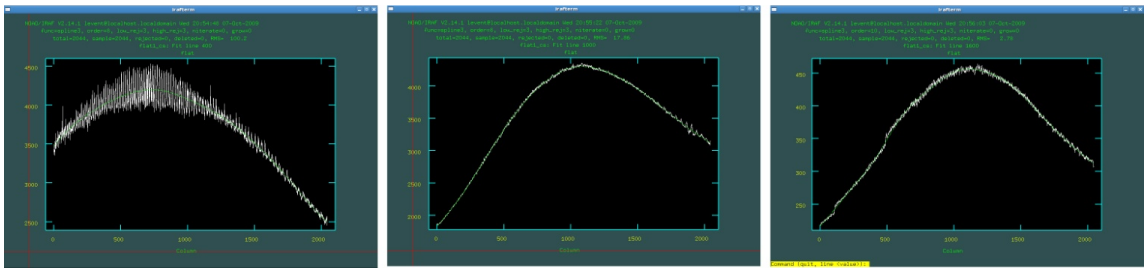

Figure 3.21 Adjusted fit is tested for columns 400, 1000, and 1600.

During this task, IRAF computes the best model for the scattered light through the CCD chip, and subtracts it from the entire flat image.

3.2.2.9. Smoothing Flat: ***apflatten***

This is the last step of the flat preparation. **apflatten** task works on a similar GUI, plots the individual apertures and smoothens data points with the best fit function. The parameters that are used to smoothen the flat via **apflatten** tasks are given in Table 3.8.

Table 3.8 Parameters of APFLATTEN task

apertures	=	
references	=	flat1_cs.fits
interactive	=	yes
find	=	no
recenter	=	no
resize	=	no
edit	=	yes
trace	=	no
fittrace	=	no
flatten	=	yes
fitspec	=	yes
line	=	INDEF
nsum	=	10
threshold	=	10
pfit	=	fit1d
clean	=	no
saturation	=	INDEF
readnoise	=	0
gain	=	1
lsigma	=	4
usigma	=	4
function	=	spline3
order	=	4
sample	=	*
naverage	=	1
niterate	=	3
low_reject	=	3
high_reject	=	3
grow	=	0

When IRAF GUI shows the apertures, success in removing the scattered light can be seen from the base line of the data set. '*q*' keystroke proceeds to the next step to smooth the entire flat data set. Very similarly, the user determines the best fit for individual apertures for the entire data set.

3.2.2.10. Division of spectra by flat:

All previous efforts were performed to prepare FLAT to be used as the "normalization function". Difference in illumination on the edges of the CCD chip and sensitivity differences have been discussed at the beginning of this chapter. Flat represents the response of the CCD chip under uniformly illuminated slit. Therefore, it can be used as a normalization function.

Division of star spectrum by flat (or normalization function) will clean the spectrum from the aforementioned effects.

This task is performed by IRAF's **ccdpro** task with the *flatcor* parameter is set to yes. The *flat* parameter is pointed to the previously smoothened flat file.

The parameters used for flat division are listed in the Table 3.9.

Table 3.9 Parameters of CCDPRO task to perform FLAT division

output	=	@object1_c
ccdtype	=	
max_cache	=	0
noproc	=	no
fixpix	=	no
overscan	=	no
trim	=	no
zerocor	=	no
darkcor	=	no
flatcor	=	yes
illumcor	=	no
fringecor	=	no
readcor	=	no
scancor	=	no
readaxis	=	line
fixfile	=	
biassec	=	
trimsec	=	
zero	=	
dark	=	
flat	=	flat1_csf.fits
illum	=	
fringe	=	
minreplace	=	1
scantype	=	shortscan
nscan	=	1
interactive	=	yes
function	=	spline3
order	=	20
sample	=	*
naverage	=	1
niterate	=	3
low_reject	=	3
high_reject	=	3
grow	=	0

3.2.2.11. Removal of scattered light from flat corrected spectra

Previously, scattered light was removed from the flat image by using IRAF's task **apscatter**. After stellar images are normalized by flat division, the scattered light should also be removed from each flat corrected star (stellar) spectrum. There is no need for changing any parameter of **apscatter** task.

3.2.2.12. Final touches: resizing stellar and Th-Ar spectra

Just a step away to extract spectrum from images, all stellar and arc (Th-Ar) images are resized using the task **apresize**. In fact, the aim of this task is not to resize the images as *trimsection* and *biassection* parameters are not changed. However, this task is performed to make sure that (a) the light is filling the apertures entirely, (b) there is no scattered light, and (c) the size of all the images are identical (*trimsection* and *biassection*).

3.2.2.13. Extraction of the stellar spectra

The 2-dimensional image is converted to a 2-dimensional spectrum by the **apall** task. During this task, IRAF shows the cross-section of the image, and then extracts all of the apertures, which are identified and adjusted in the previous steps. The parameters used to perform this task by **apall** are listed in the Table 3.10.

Table 3.10 Parameters of APALL task
to extract 2-dimensional spectrum from 2-dimensional image

output	=	@object1_csfe
apertures	=	
format	=	echelle
references	=	
profiles	=	
interactive	=	yes
find	=	yes
recenter	=	yes
resize	=	yes
edit	=	yes
trace	=	no
fittrace	=	no
extract	=	yes
extras	=	no
review	=	yes
line	=	INDEF
nsum	=	10
lower	=	-10
upper	=	10
apidtable	=	
b_function	=	chebyshev
b_order	=	1
b_sample	=	-10:-5,5:10
b_naverage	=	-3
b_niterate	=	2
b_low_reject	=	3
b_high_reject	=	3
b_grow	=	0
width	=	15
radius	=	8
threshold	=	0
minsep	=	5
maxsep	=	1000
order	=	increasing
aprecenter	=	
npeaks	=	INDEF
shift	=	no
llimit	=	INDEF
ulimit	=	INDEF

Table 3.10 – *Continued*

ylevel	=	0.029999999329448
peak	=	yes
bkg	=	yes
r_grow	=	0
avglimits	=	no
t_nsum	=	10
t_step	=	10
t_nlost	=	10
t_function	=	legendre
t_order	=	4
t_sample	=	*
t_naverage	=	1
t_niterate	=	1
t_low_reject	=	3
t_high_reject	=	3
t_grow	=	0
background	=	none
skybox	=	1
weights	=	variance
pfit	=	fit1d
clean	=	yes
saturation	=	INDEF
readnoise	=	RDNOISE3
gain	=	GAIN3
lsigma	=	3
usigma	=	3
nsubaps	=	1

3.2.2.14. Extraction of the comparison spectra

The extraction of the comparison spectra is performed in a very similar manner to stellar spectra with slightly different parameters of **apall**. *Interactive*, *find*, *recenter*, *edit*, *trace*, *extras* and *review* parameters are set to "*no"* when extracting arc spectra. *Background* and *weights* parameters are set to *none*.

3.2.2.15. Wavelength calibration

Wavelength calibration of Echelle spectra is performed in 3 steps. The first step is the identification of Th-Ar lines via **ecidentify** task of IRAF. The second step is assigning the Th-Ar

references to the stellar spectra using **refspec** task. The third step is applying dispersion function to the extracted spectra using the task **ecdispcor**.

ecidetify: The Th-Ar Atlas that is used to identify Th-Ar lines was obtained from the McDonald Observatory. The atlas is called “The Spectrum of the Th-Ar Hollow-Cathode Lamp Used With the *2dcoudé* Spectrograph”, Carlos Allende Prieto (2001). IRAF represents the first order of the extracted spectra when **ecidentify** task is started. Usually it is extremely complicated to identify lines in the first and last orders, and it is highly recommended to start identifying lines from the middle orders. Usually, the identification of 3-4 lines per order result in an accurate wavelength calibration. In this scope of work, almost every line in every aperture was identified to allow very accurate wavelength calibrations.

The identification of lines is performed by pointing cursor onto a line and hitting the **m** (mark) key. After the identification of a sufficient number of lines, the fit is made by **f** keystroke. The fit should be a trend. Some points with high residuals can be deleted (as necessary) by **d** keystroke. If the trend is not clearly visible, **:xorder** and **:yorder** values can be increased to see the trend. IRAF also shows the RMS value of the fit. The goal is obtaining a RMS value smaller than 0.04. If the RMS value is higher, then the removal of points with high residuals, and identification of more lines may be necessary to obtain a lower the RMS value.

The parameters used to perform **ecidentify** task are listed in the Table 3.11.

Table 3.11 Parameters of ECIDENTIFY task

database	=	database
coordlist	=	linelists$thar.dat
units	=	
match	=	1
maxfeatures	=	1000
zwidth	=	10
ftype	=	emission
fwidth	=	4
cradius	=	5
threshold	=	0
minsep	=	2
function	=	chebyshev
xorder	=	2
yorder	=	2
niterate	=	0

Table 3.11 – *Continued*

lowreject	=	3
highreject	=	3
autowrite	=	no
graphics	=	stdgraph
cursor	=	

refspec: A simple text file is created by name *ref.table* as the reference table. File names of the stellar spectra are listed in the first column of the table. In the second column the file names of the Th-Ar spectra are indicated next to each stellar spectrum to be matched. A sample content of the ref.table file is shown below.

n10064_cfse.fits n10063_ce.fits

n10065_cfse.fits n10063_ce.fits

n10066_cfse.fits n10068_ce.fits

n10067_cfse.fits n10068_ce.fits

…

It is up-to user how to match the reference spectrum. Usually the closest Th-Ar file is used if more than one Th-Ar is taken during the observation night. The frequency of taking Th-Ar exposures depends of the scope of the study. For example, extra-solar planet studies require highly accurate wavelength calibration in order to detect small wavelength shifts.

Table 3.12 Parameters of REFSPEC task

references	=	ref.table
apertures	=	
refaps	=	
ignoreaps	=	yes
select	=	average
sort	=	ut
group	=	
time	=	yes
timewrap	=	22
override	=	yes
confirm	=	yes
assign	=	yes
logfiles	=	STDOUT,logfile
verbose	=	no

dispcor: This task calculates the dispersion function and compute the correlation between pixel numbers of the CCD chip and the corresponding wavelengths. The Table 3.13 lists the parameters used to run this task.

Table 3.13 Parameters of DISPCOR task

linearize	=	no
database	=	database
table	=	
w1	=	INDEF
w2	=	INDEF
dw	=	INDEF
nw	=	INDEF
flux	=	yes
samedisp	=	no
global	=	no
ignoreaps	=	no
confirm	=	no
listonly	=	no
verbose	=	yes
logfile	=	

3.2.2.16. Applying radial velocity and heliocentric corrections to the spectra with ***Astutil***

Finally, radial velocity corrections due to orbital speed of Earth and heliocentric corrections are applied. These corrections are performed by **rvcor** and **dopcor** tasks included in the **astutil** package. Due to their small number of parameters, **rvcor** and **dopcor** can be directly typed in with its parameters:

```
rvcor (files="", images="@allobjects_w2", header+,
input+,imupda+, epoch=INDEF, observa=")_.observatory", vsun=20,
ra_vsun=18, dec_vsu=30, epoch_v=1900.)

dopcor ("@allobjects_w2", "@allobjects_wh", "-vhelio", isveloc+,
add-, dispers+, flux-, factor=3, aperture="", verbose+)
```

*3.2.2.17. Adding overlapping orders of the spectra with **onedspec***

scopy task of *onedspec* package extracts subset of apertures and performs necessary format conversions.

```
Scopy (“@allobjects_wh2”, ”@allobjects_wh1”, w1=INDEF, w2=INDEF,
apertures=””, bands=””, beams=””, apmodulus=0,
format=”onedspec”, renumber=no, offset=0, clobber=no, merge=no,
rebin=yes, verbose=no)
```

scopy task extracts orders into separate files. For example, if there are 69 orders in a FITS file, there will be 69 output files named *filename.fits.0001.fits, filename.fits.0002.fits,…*

3.2.2.18. Converting FITS to TXT

Although FITS files are readable by many astronomy applications such as IDL, the spectra still should be converted an ASCII based text in most cases. **wspectext** task performs necessary conversion. **wspectext** is very simple task to run.

```
wspectext (“filename.fits”, “filename.txt”, header=no,
wformat=””)
```

However, due to the large number of files to perform TXT conversion, it is very convenient to create a table for input and output files. For example, *allspecsin.txt* consists of fits filenames, *allspecsout.txt* consists of same filenames with .txt extension.

```
wspectext (“@allspecsin.txt”, “@allspecsout.txt”, header=no,
wformat=””)
```

The data reduction is completed at this point. The above procedures have been performed for the entire observation run on April 2006. For verification, the entire data reduction was also performed in parallel by our collaborator, Dr. Seth Redfield, Assistant Professor at Wesleyan University, who mentored me to facilitate observations and data reduction within the scope of this project. The comparison of Dr. Redfield’s results with my own results indicated no difference.

CHAPTER 4

DATA ANALYSIS

4.1 Selected Target: HD 179949

A large number of program stars has been observed during the observation run at the McDonald Observatory in 2006. Their data have been reduced at UT Arlington. However, one of the program stars, HD 179949, is selected as the main focus of this study due to its confirmed PIE effect by Shkolnik et al (2003).

HD 179949 is a 6^{th} magnitude star in the constellation Sagittarius, and it is located 27 light years away from Earth. HD 179949 is a main sequence star with F8.5 spectral classification. Its close-in giant planet, named as HD 179949b, is at an orbital distance of about 0.04 Astronomical Unit (AU) from its host star. For comparison, HD179949b is about 10 times closer to its host star than Mercury to the Sun. Stellar properties of HD 179949 (Table 4.1), planetary properties of HD 179949b (Table 4.2), and HD 179949's location in the night sky (Figure 4.1) are given below.

Table 4.1 Stellar Properties of HD 179949

Parameter	HD 179949	Reference
Spectral Type	F8.5 V	*a*
RA	19 15 33.23	*b*
DEC	-24 10 45.67	*b*
V	6.25	*b*
T_{eff}	6202±52	Ribas et al. (2003)
$M_*(M_\Theta)$	1.24±0.10	Tinney et al. (2001)
Distance (pc)	27.0±0.5	b
Age (Gyr)	2.05	Donahue (1993)
$R_*(Ro)$	1.193±0.030	Ribas et al. (2003)
[Fe/H]	0.226±0.050	Gonzales & Laws (2007)

References:
a: data from SIMBAD (*http://simbad.u-strasbg.fr*)
b: adopted from the Hipparcos catalogue. See ESA (1997)

Table 4.2 Planetary Properties of HD 179949b

Orbital Period (days)	Epoch(JD 2,400,000+)	Mass ($M_{jupiter}$)	Semi-major axis (AU)	Eccentricity
3.092514 (±0.000032)	T_t=11001.510 (±0.020)	0.916 (±0.076)	0.0443 (±0.0026)	0.022 (±0.015)

References: Butler et al. (2006)

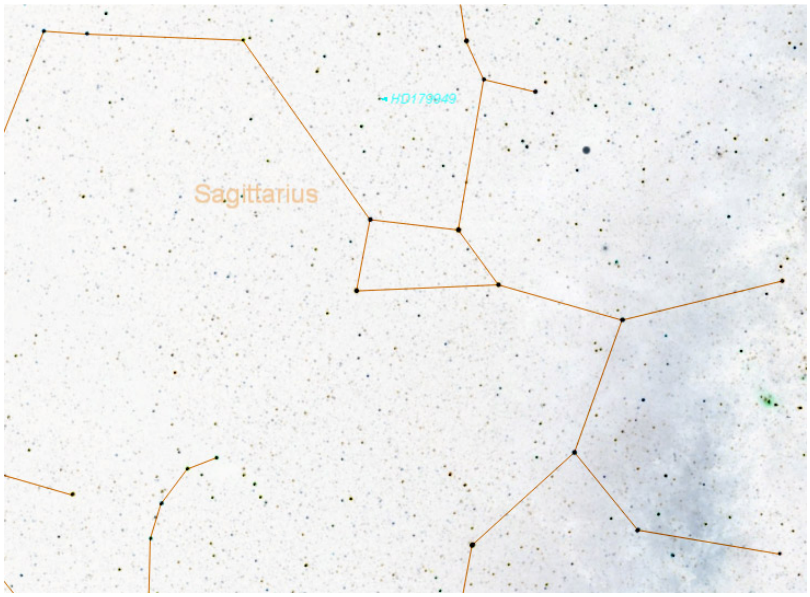

Figure 4.1 Location of HD179949 in the night sky
(*Ref: StarryNight Pro* http://www.starrynight.com)

4.2 Previous Study on HD 179949

Shkolnik et al. pursued a total of 6 observations during August 2001, July 2002, August 2002, September 2003, September 2005, and June 2006. They describe data reduction and analysis procedures as well as preliminary results in 2003 as follows:

Their high-resolution (R=110,000) spectra with high signal-to-noise ratio (500 in the continuum, 150 in the H and K cores) are obtained from Canada-France-Hawaii Telescope (CFHT), which is a world-class 3.6 m telescope located at Mauna Kea. If compared with the spectra acquired at the McDonald Observatory in the scope of this project, the resolutions are about 2 times, signal-to-noise ratios are about 3 times greater; however, Shkolnik's spectra is only covering 60 Å centering 3947 Å in single image. We acquired full optical bandwidth (3400 Å – 10,900 Å) for each exposure, which may allow further analysis beyond Ca II lines as necessary.

Ca II H and K lines are strong chromospheric lines that allows ground based choromosphere studies as their wavelength falls in optical window unlike other chromospheric lines (such as Mg II). If chromosphere of a star is heated by an external mechanism (such as

magnetic interaction), emission lines should be produced in chromospheric lines, such as Ca II. Ca II emission should appear as weak emission on strong absorption line. This situation is called “line reversal”. The effect is so weak that it is not noticeable by visually comparing spectra. Therefore, statistical analysis required to reveal line reversals.

Shkolnik et al. reported preformed tasks during data reduction as follows:

- Appropriate dark exposures are subtracted from stellar, arc and flat field exposures
- flats are combined and normalized to a mean value 1 along each row of the dispersion axis
- Nightly stellar exposures are averaged to define a single aperture for spectral extraction
- Residual background between orders are subtracted
- Spectra from stellar, comparison and flat field exposures are extracted
- Stellar and comparison spectra are divided by flat
- Wavelength calibration is done using Th-Ar arcs
- Heliocentric and radial velocity corrections are applied

Although data reduction performed by Shkolnik et al. was very similar to the data reduction procedures described in the previous chapter, there are several differences such as using DARK images instead of BIAS, combining stellar spectra for each night, and normalizing combined flat value to 1.

Shkolnik’s extracted and flat-fielded spectrum, which is represented by Shkolnik (2003), is shown in the Figure 4.2.

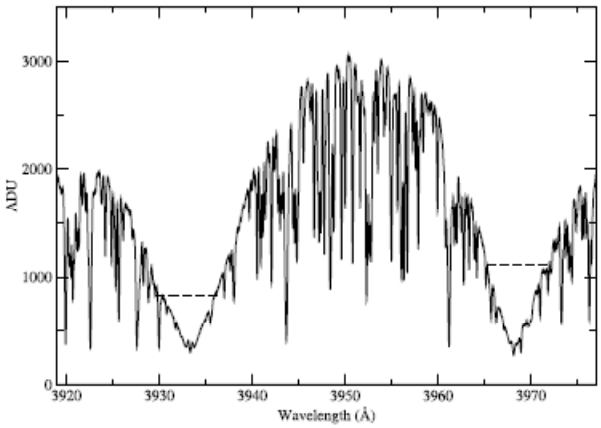

Figure 4.2 Sample spectrum from Shkolnik's observation run.
Spectra is 60Å wide, centering 3947Å. Dashed lines are showing normalization levels. *Figure credit: Shkolnik et al. (2003)*

From 2001 and 2002 observation runs, Shkolnik et al. also measured differential radial velocities (ΔRV) to compute the phase of the planet accurately. The RV analysis is discussed in Walker et al. (2003), and Shkolnik et al. reported the error on the phase as ±0.03. The ephemerides reported by Shkolnik et al. in 2003 are shown in Table 4.3.

Table 4.3 2002 ephemerides reported by Shkolnik et al.
Figure credit: Shkolnik et al. (2003)

EPHEMERIDES, 2002 JULY

Star	HJD at $\phi = 0$ (days)	δ(HJD)[a] (days)	Revised P_{orb} (days)	$\delta(P_{orb})$[a] (days)
τ Boo	2452478.770	0.099	3.31245	0.00033
HD 179949.....	2452479.823	0.093	3.09285	0.00056
HD 209458.....	2452481.129	0.106	3.52443	0.00045
51 Peg	2452481.108	0.127	4.23067	0.00024
υ And.....	2452481.889	0.139	4.61794	0.00064

[a] Uncertainties in the respective measurements.

Shkolnik et al. reported the procedure of statistical analysis in order to reveal the PIE effect from the spectra as follows:

- 7 Å spectrum centering Ca II H and K cores at 3933 Å and 3968 Å are extracted
- End points of each extracted spectrum are set to 1 for normalization

- All spectra are grouped by date and nightly means are computed for both H and K cores
- Overall average over all nights is calculated
- Nightly residuals from the overall average are computed
- Low order curvatures from each residual spectrum are removed
- The residuals were smoothed over 21 pixels
- Mean Absolute Deviation (MAD) were calculated

$$MAD = N^{-1} \sum |data_i - mean|$$

As there is no clear continuum for the H and K cores of the 60 Å spanning spectra, Shkolnik et al. preferred working in 7Å extracted spectrum pieces centered at H and K cores for normalization. Relative flux was used since there was no flux calibration done for the spectra; it was necessary for the scope of this study. Therefore, the relative flux levels were different due to different S/N ratios of each exposure. The end points of each spectrum were set to 1 to normalize each spectrum (see Figure 4.3). Then, spectra were grouped by date. Each group was co-added together to construct a single representative spectrum for each night. Co-addition is a standard task for consecutive exposures that allows improving S/N ratio and eliminating momentary effects, such as cosmic rays, etc. Computing overall average and nightly residuals are very straight forward processes. Figure 4.4 represents the over-plotted nightly residuals (smoothed over 21 pixels) reported by Shkolnik et al. (2003). 21 pixels is an experimental number to make the data cleaner looking. Mean Absolute Deviation (MAD) was also calculated (see top figure of Figure 4.4). MAD plot demonstrates the magnitude of fluctuation in the Ca II K core. Shkolnik et al. reported that the same analysis was also performed for Ca II H core where the effect seemed to have a lower magnitude. Strong photospheric line Al I was also analyzed by extracting in 7Å and 2Å spectra, and no fluctuation was reported.

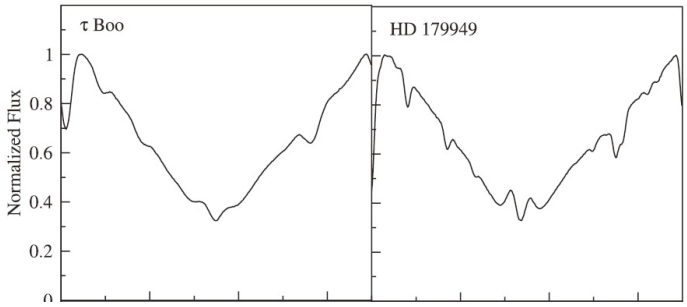

Figure 4.3 7Å extracted spectra from K cores.
End points of the extracted spectra are set to 1 for normalization.
Figure credit: Shkolnik et al. (2005)

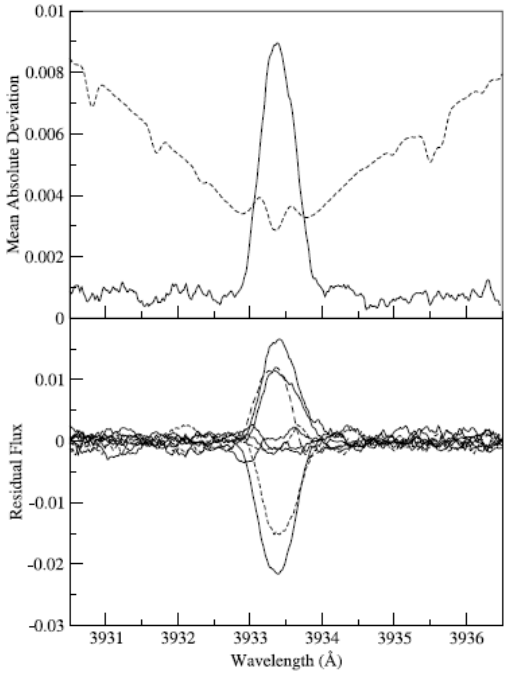

Figure 4.4 Top Figure: Mean Absolute Deviation (MAD) of K core. Dashed line is the overall average spectrum (scaled vertically) shown to indicate the activity is confined in the K core. Bottom Figure: Nightly residuals (smoothed over 21 pixels) of the K core. Residuals are calculated from the overall average. *Figure credit: Shkolnik et al. (2003)*

Integrated K residuals are also plotted as a function of phase to illustrate the phase dependency of the emission (see Figure 4.5). Though the number of data points is not sufficient to arrive to a conclusion, the figure indicates that the period of the activity is modulated by the orbital period of the planet. Two different bright-spot models are computed and represented by

solid and dashed lines, respectively. The normalized flux at the lowest data point is set as zero, and all others are scaled accordingly. Please also note that the graph is repeated twice to show the complete cycle.

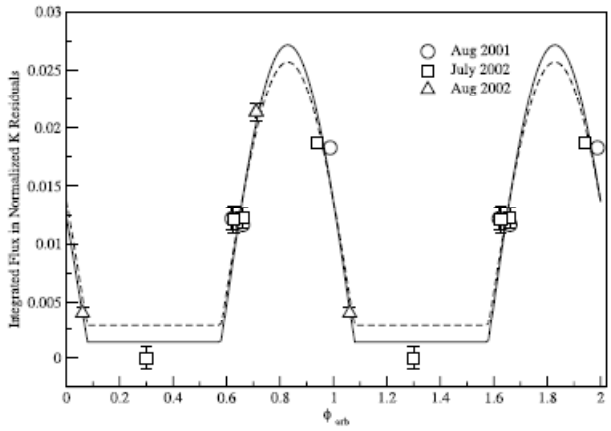

Figure 4.5 Integrated K residuals. Solid and dashed lines are best-fit bright-spot models. The lowest residual set to zero, all others scaled accordingly. *Figure credit: Shkolnik et al. (2003)*

In 2005, Shkolnik et al. reports a further study to attempt to monitor more PIE effect phenomena on a larger number of sun-like stars hosting CEGP's, based on their observation run on September 2003. At this time, they utilized the Very Large Telescope (VLT) and CFHT to acquire data. New ephemerides are computed for the CFHT stars that can be seen at the Table 4.4.

Table 4.4 2003 ephemerides reported by Shkolnik et al. *Figure credit: Shkolnik et al. (2005)*

2003 September Ephemerides

Star	$\sigma_{\Delta RV}$ (m s^{-1})	HJD at $\phi = 0$ (days)	δ(HJD)[a] (days)	Revised P_{orb} (days)	$\delta(P_{orb})$[a] (days)
τ Boo	33	2452892.864	0.066	3.31250	0.00026
HD 179949	19	2452894.114	0.062	3.09246	0.00031
HD 209458	17	2452893.653	0.070	3.52490	0.00020
51 Peg	15	2452895.868	0.085	4.23092	0.00014
υ And	9	2452892.615	0.092	4.61750	0.00052

[a] Uncertainties in the respective measurements.

New data points from 2003 observation run is shown in the Figure 4.6 .New data points are indicated with diamond symbols. Although Shkolnik et al. didn't comment on the inconsistency of the newly observed data points, they conclude that the behavior of enhanced activity is synched with the orbital period of the planet, not with the rotation period of the star; therefore, the effect must be due to star-planet interaction, not star spots. Moreover, the effect was observed once per planetary 360° phase, implyin g that the effect is magnetic, not tidal.

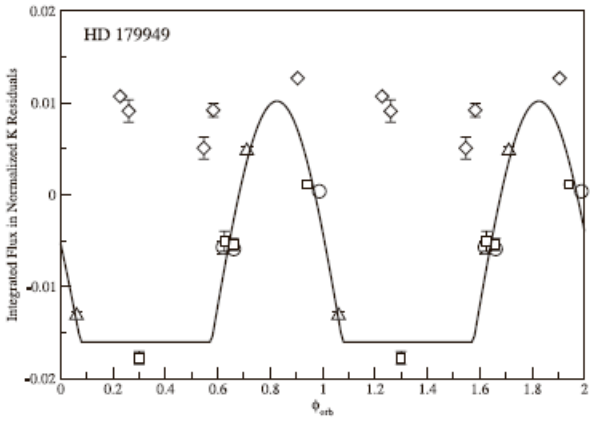

Figure 4.6 Updated phase diagram with 2003 data. Symbols show data from different observing runs: circles (2001 August), squares (2002 July), triangles (2002 August), diamonds (2003 September). *Figure credit: Shkolnik et al. (2008)*

Shkolnik et al. noticed that the peak point of the activity did not coincide with the sub-planetary point $\emptyset = 0$. There is about 60° lead in the activity relative to planetary position. This can be seen from the Figure 4.6 noting that the peak of the activity is around $\emptyset = 0.8$.

The Sun and Tau Cet were also among the program stars selected to verify that enhanced stellar activity is not due to a statistical error, but does originate from star-planet interaction. However, one of the program stars, Tau Boo, which is also hosting a Hot Jupiter, demonstrated insignificant variation in 2001, and demonstrated very little enhanced activity in 2002 and 2003 at $\phi = 0.4 - 0.5$, which is modulated with P_{orb} and P_{rot}. Based on this data, it is impossible to arrive on a conclusion about planet induced heating. Although there is some uncertainty about the rotation period of Tau Boo, its planet is believed to be synched orbit ($P_{orb} = P_{rot}$).

In 2008, Shkolnik et al. draw attention to a different characteristic of star-planet interactions, the on/off nature. After observations of the same program stars in 2005 and 2006, Shkonik et al. arrive at the conclusion that the PIE effect is not appearing during every observation, and "turns off" unexpectedly. Shkolnik et al. (2008) report total of six observations of HD 179949 as of 2008, noting that four showed emission due to star-planet interaction. An unexplained phase shift of emission peak is also reported when data from 2005 is over-plotted onto previous data (see Figure 4.7).

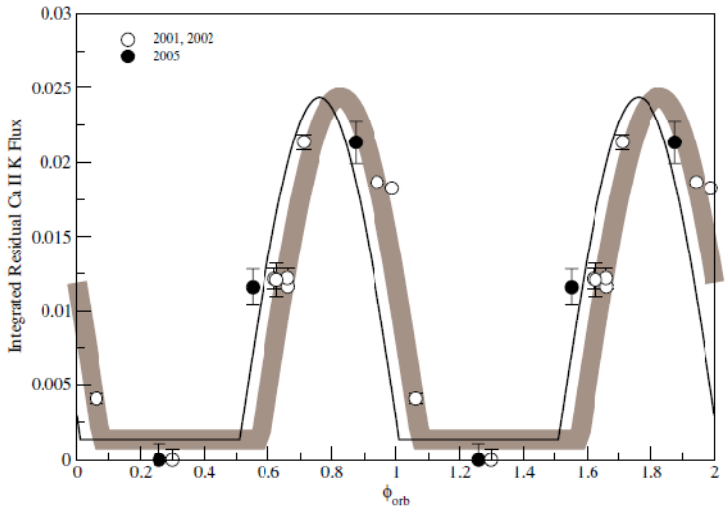

Figure 4.7 2005 update on the phase diagram. New fit suggests slight phase shift in the activity on HD 179949 system. *Figure credit: Shkolnik et al. (2008)*

The amount of shift is reported as -0.07 between 2002 and 2005. 2003 and 2006 data is studied separately as they did not show correlation with data from 2001, 2002, and 2005. Shkolnik et al. suggested that the activity is synchronized with the rotation of the star (P_{rot}) rather than orbital period of the planet (P_{orb}). The 2003 and 2006 data plotted as a function of 7 day rotation period of the star is shown in the Figure 4.8. All the points in the figure are shifted vertically such that minimum of the curves are zero. The reported phase shift between 2003 and 2006 data points was -0.17.

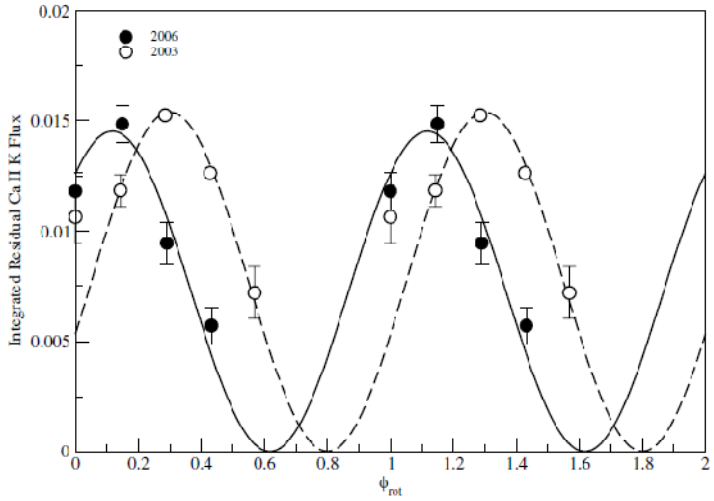

Figure 4.8 Integrated K residuals from 2003 and 2006 observation runs plotted as a function of 7 days orbital period of the star. *Figure credit: Shkolnik et al. (2008)*

While the Ca II emission varied with the orbital period of 3.092 days during the four out of six observation runs (August 2001, July 2002, August 2002, and September 2005), the emission varied with the orbital period of 7 days during the observation runs of September 2003 and June 2006. A similar effect had been observed for υ And at one out of four observations indicating the effect is modulated with the stellar rotation rather than the planet's orbital period. This on/off behavior was also modeled by Cranmer & Saar (2007).

In efforts to reveal the PIE effect from the McDonald data, Shkolnik et al.'s procedure is followed step-by-step to verify and confirm the results of their previous work. Although there was a about 1-meter disadvantage in telescope size, and one third of resolution compared to Shkolnik et al.'s work, the Ca II emission due to planet-related interaction was clearly seen after careful data reduction and analysis. Our data set had a resolution of R = 50,000, and a signal-to-noise ratio of 200 around Ca II H and K continuum, and 50 in the H and K cores. The signal-to-noise ratio as function of wavelength of one of the selected exposures is shown in the Figure 4.9. Although the entire data set consist of the full optical bandwidth, all of our analysis has been done between 3915 Å and 3985 Å, which covers the Ca II H and K lines with plenty of

spacing left and right to the line cores. The indicated wavelength range is extracted from the Aperture 56 of the reduced CCD images.

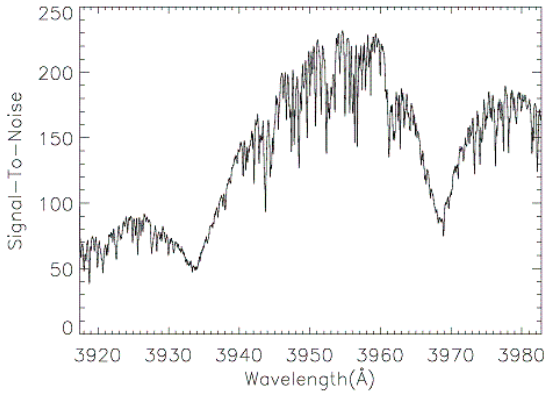

Figure 4.9 Signal-to-noise ratio as function of wavelength.
The data extracted from Aperture 56 of reduced CCD images.

All the work to follow the procedures by Shkolnik et al. (2003) on the McDonald data is done based on IDL (Interactive Data Language) distributed by ITT Visual Information Solutions. Several routines had to be developed in addition to built-in IDL routines. Some IDL routines were downloaded from Goddard High Resolution Spectrograph (GHRS) Library, and modified to consider the McDonald data. GHRS website can be accessed at http://www.stsci.edu/hst/ghrs and the public domain library can be accessed at http://www.astro.washington.edu/docs/idl/htmlhelp/slibrary43.html. The complete list of routines and explicit codes are provided in the Appendix. The routines are developed such way that not only works for HD 179949, but also any other McDonald data.

The data analysis procedure is step-by-step listed and explained below. For each step, the IDL routine used is also indicated. All routines are combined under a pipeline macro called *main.pro*.

4.3 Data Analysis of HD 179949 spectra

4.3.1 Blaze correction (blaze.pro):

The reduced data have a low order curvature on all orders that needs to be corrected before performing any analysis. As indicated in the previous chapter, the Flat-Field is the exposure when the diffraction slit is illuminated uniformly by a hollow-cathode lamp. Differences in the temperature of hollow-cathode lamp and target stars result in slightly different intensity distribution for the orders. Therefore, the flat-fielded (or flat corrected) spectra still carry a low order curvature. To correct this effect, the combined flat image is processed like a stellar image (except flat-fielding) during data reduction. The reduced image provides a low-order function called Blaze function (see Figure 4.11). Dividing data set by the blaze function results in the necessary correction.

In the Figure 4.10, the reduced data set for Aperture 56 is shown as “raw” data. Blaze function (Figure 4.11) and blaze corrected data set (Figure 4.12) are also shown below.

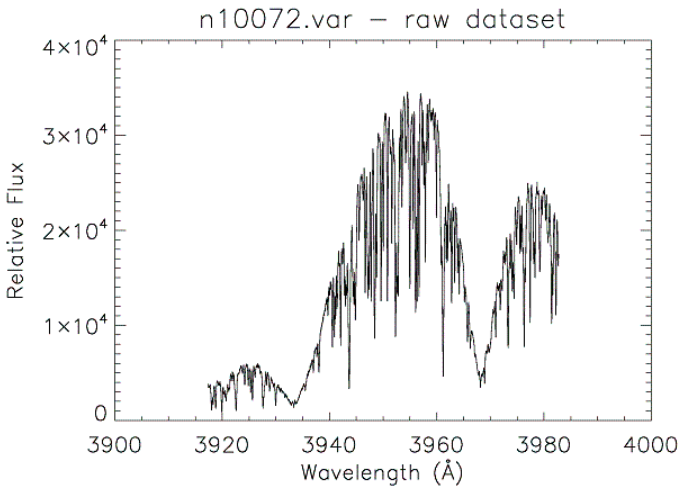

Figure 4.10 Raw data before blaze correction. The data carries low-order curvature.

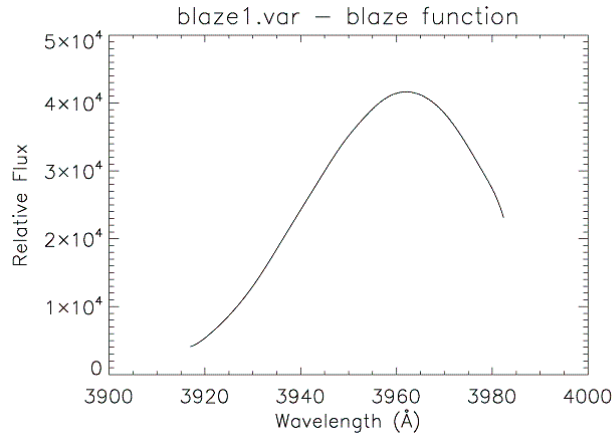

Figure 4.11 Blaze function. Blaze function is created by processing a flat field exposure like a stellar data.

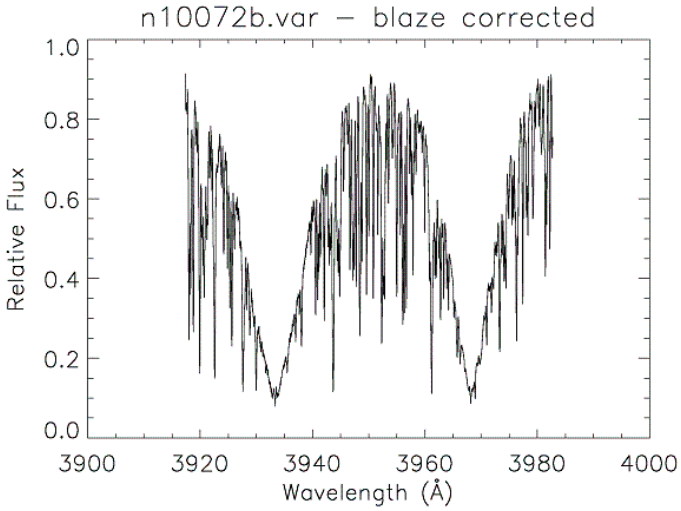

Figure 4.12 Blaze corrected (divided) spectrum

The IDL routine *blaze.pro* performs following tasks:

- Finds stellar images by using the name convention of the McDonald Observatory
- For each stellar exposure
    - Extracts the order 56 (3915 Å – 3985 Å) from the full bandwidth of spectra
    - Extracts the blaze function from the appropriate image
    - Perform division of stellar data set by blaze function

- Saves the corrected spectrum with "*b*" postfix

4.3.2 Extracting 7Å chunks centering at a specified wavelength of a spectrum (extract.pro)

A 7Å chunk centering at a specified wavelength is extracted from the rest of the spectrum. This task is repeated for Ca II H and K lines as well as Al I line. The extracted K line is shown in the figure below.

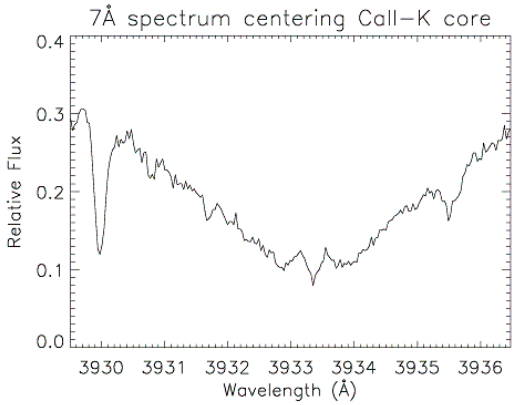

Figure 4.13 A 7 Å extracted spectrum centering K core

4.3.3 Normalizing the spectra (normX.pro)

This step is instructed in Shkolnik et al. (2003) as setting the end points of each 7 Å wide spectrum to 1. Each extracted spectrum is shifted vertically to set left shoulder to 1 similar to Figure 4.3. In order to shift the spectra, flux values are multiplied by an appropriate value. Although this is a manual task that requires some judgment, the used IDL codes are saved in a file (*normX.pro*) to allow the reproduction of the results. In the naming convention, *X* stands for the number of the night. Figure 4.14 and Figure 4.15 show the spectra set before and after normalization.

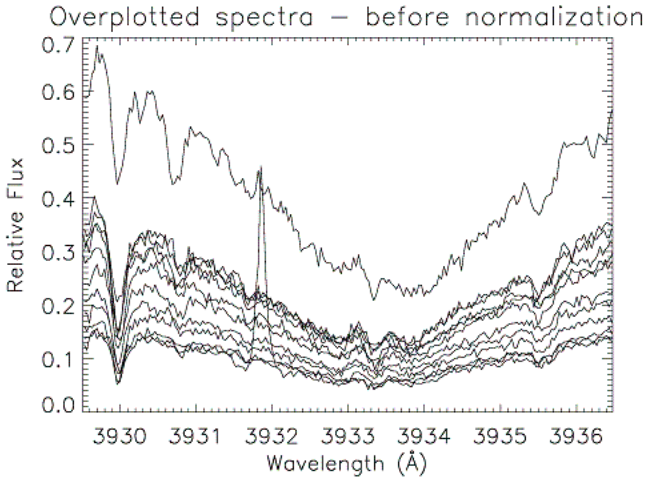

Figure 4.14 Over-plotted spectra. All available spectra set is over-plotted in the same figure. Level flux differences indicate different S/N ratios.

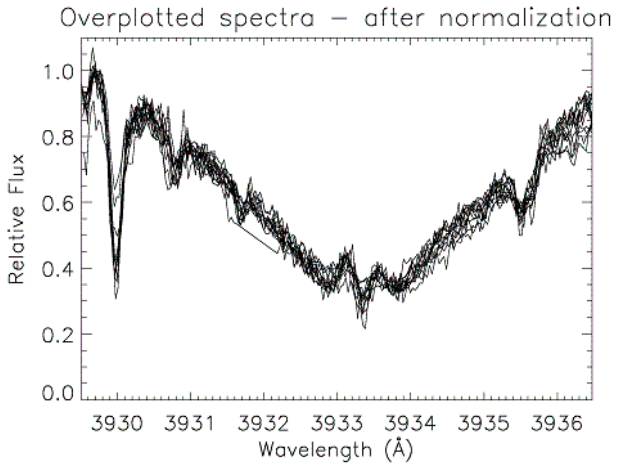

Figure 4.15 All spectra shifted vertically to set left end-points to 1.

4.3.4 *Co-addition of spectra to compute nightly means (coadd.pro):*

Spectra are grouped for each night and co-added to produce one mean (co-added) spectrum for each night. The signal-to-noise ratio is considered as the statistical weight when computing nightly mean. Two external routines, *HRS_Combine* and *HRS_Offset*, are used from the GHRS library when developing the routine *coadd*. Both *HRS_Combine* and *HRS_Offset* are

modified in the scope of this project to consider the McDonald data. Various obsolete codes are also updated for current versions of IDL. *HRS_Combine* routine cross correlates each succeeding spectrum to determine the wavelength shifts between each spectrum, and then shifts the spectrum via *HRS_Offset* routine by an appropriate amount. Mean spectrum for each night is then calculated from the shifted spectra.

4.3.5 Fine tuning to the co-added spectra:

Nightly mean spectra are over-plotted and any necessary fine vertical shifts are performed to match the general trend in the relative continuum. This task is performed by multiplying flux values by an appropriate number which is not larger than 2%.

4.3.6 Calculating overall mean spectrum and finding residuals (residual.pro):

To calculate the mean spectrum from all six spectra, flux values are interpolated to a reference wavelength array. The first night's first observation is taken as a reference wavelength array. The interpolation is performed by an IDL task *quadterp*, which is a 3-point Lagrangian interpolater using the average of the two quadratics derived from the four nearest point. Interpolated new dataset is saved with "*i*" postfix in its filename.

After lining up the flux points, the arithmetic mean flux is calculated for each consecutive wavelength. The mean spectrum is also saved into a file, "*fluxave.var*". The mean spectrum over-plotted onto the overall spectra is shown in Figure 4.16.

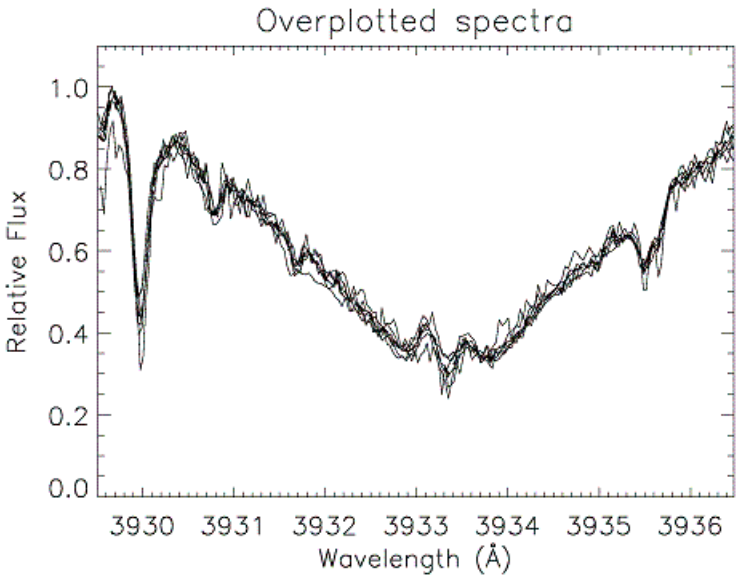

Figure 4.16 Mean spectrum (shown by thick black line) over-plotted onto all spectra

The residuals from the mean spectrum ($data_i - mean$) are computed. Value 1 is added to the fluxes of each spectrum to avoid zero and negative values in flux. This will avoid the "division by zero" problem in the next step when a low-order curvature is removed from the residuals. Addition of 1 to each flux shifts the baseline of fluctuation from zero to one. Each residual is saved into a different file with "*r*" postfix. One of the residuals (after addition of 1) is shown in the Figure 4.17 below.

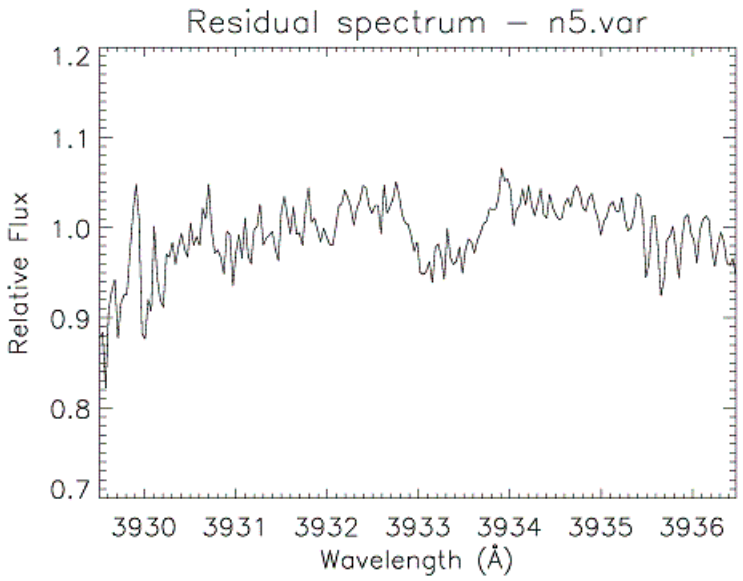

Figure 4.17 Residuals of April 11 (night5). Flux values are added 1 to avoid zero values in the data set.

4.3.7 Removal of low-order curvature from residuals (curve.pro):

Each residual demonstrates a low-order curve trend line. However, finding the appropriate function and order of the best fit is not a straight-forward task because of the different behavior of the line core due to PIE effect (see Figure 4.17). Therefore, the line core must be ignored when making the fit.

Curve routine allows the user to set boundaries for the portion of the spectra to be ignored, and set the magnitude of order of the polynomial fit. Our practice showed that order of two led to the most plausible results. A fit to a selected residual is shown in the figure below. *Curve* routine divides flux values of each residual with the corresponding fit.

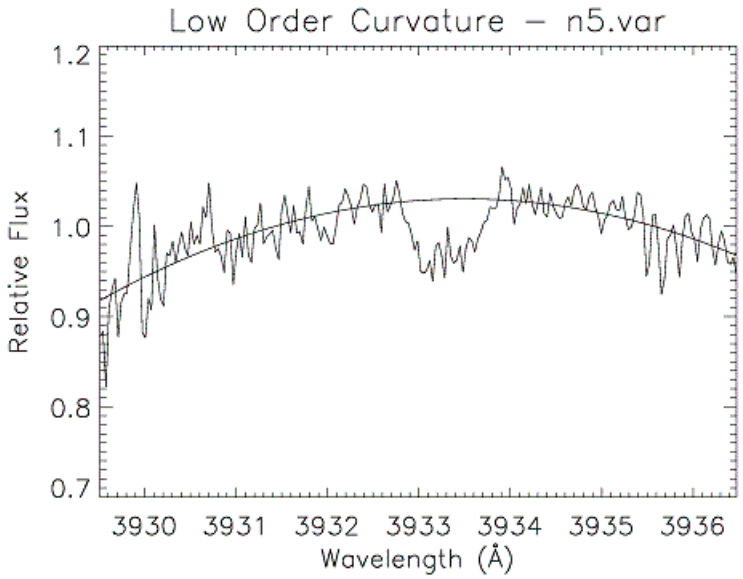

Figure 4.18 Low order fit to remove the low-order curvature from residuals. Polynomial fit with order of two used. The core of the line is ignored when making the fit.

If this step was performed before the base line is shifted to one, the fit would likely cross x-axis, where the flux value is zero. Therefore, the division by zero error would occur. After removal of the low-order curvature, the baseline of fluctuation is retracted to zero by subtraction of 1. Output files were saved with a "*c*" postfix. See Figure 4.19 for the sample residual with the low-order curvature is removed.

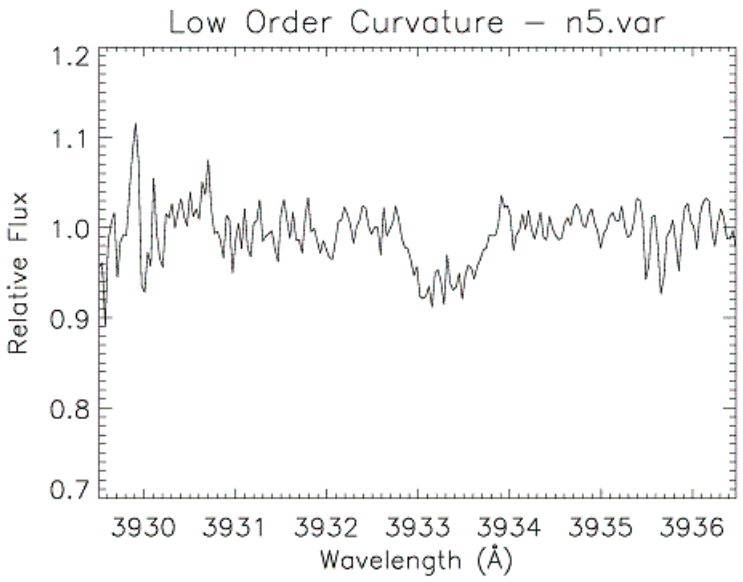

Figure 4.19 Sample residual which low-order curvature is removed

4.3.8 Smoothing data over 21 pixels (smoothen.pro)

Smooth function of IDL is utilized to smoothing the flux over 21 pixels. The correct amount of smoothing makes the PIE effect clearer, as it cleans momentary fluctuations unrelated to the PIE effect. Smoothing over 21 pixels was suggested by Shkolnik et al. (2003), and it worked best for our data set as well (see Figure 4.20). Smoothed residuals over 21 pixels are over-plotted in the Figure 5.1, which is similar to the figure by Shkolnik et al. (2003). This is an exciting result as the figure show fluctuation confirming that the effect was indeed observed during the McDonald run in 2006.

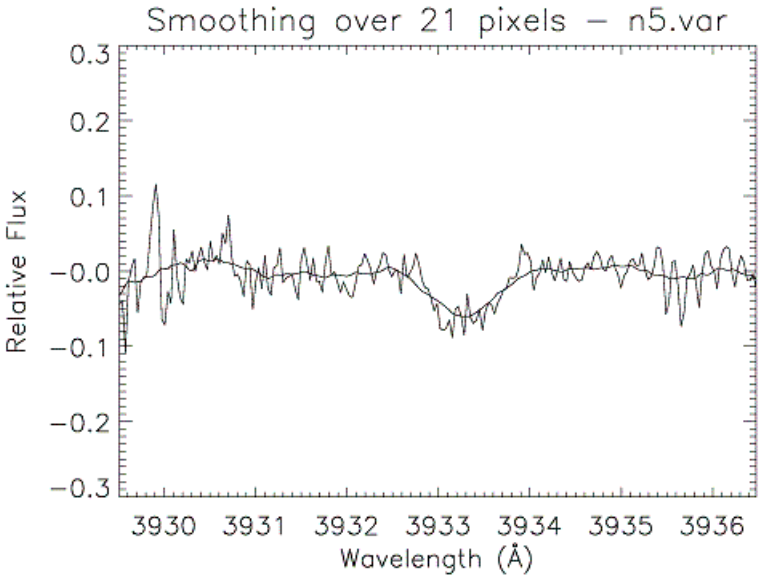

Figure 4.20 Sample residual smoothed (over 21 pixels) is plotted over unsmoothed residual

4.3.9 Mean Absolute Deviation (MAD) figure (mad.pro):

Mean Absolute Deviation is computed from each residual. The equation for the computation of the MAD was given by Shkolnik et al. (2003) as

$$MAD = N^{-1} \sum |data_i - mean|$$

Computed MAD values are shown in the Figure 5.2.

4.3.10 Computing error bars from nightly variations (errorX.pro):

Error bars are computed from nightly variations of each spectrum. Shkolnik et al. (2005) reported the error bars as 1-σ of intranight variations.

To compute nightly variations, extracted 7 Å portions of the raw data set is used to avoid any normalization, co-addition and smoothing of errors. Therefore, the computed error bars demonstrates the best realistic case. IDL's *STDDEV* task is used to compute the standard deviation. Generated error arrays are saved with "*e*" postfix to be used in the next step.

4.3.11 Phase dependency of the PIE effect (phase.pro):

Each residual flux is integrated to reveal the phase dependence of the PIE effect. Trapezoidal integration is used. The lowest data point is considered zero, and all others are scaled accordingly. Data points from different epochs are shown with different symbols. The solid line represents the best-fit bright-spot model as discussed by Shkolnik et al. (2003) with the spot is on 30° latitude and a stellar inclination of $i = 87°$. The dashed line is the same spot-model with $i = 83°$.

The error bars as computed at the previous step are used. There is no error bar associated with the data point, where $\phi = 0.575$, as the data point was derived from one spectrum. Therefore, there is no nightly variation. To provide a realistic estimate of the error range to this data point, the largest error bar is used.

CHAPTER 5

RESULTS AND DISCUSSION

The residuals smoothed over 21 pixels are over-plotted in the Figure 5.1 (top figure), where each nightly residuals are shown with different line styles. The lines drawn with different line styles are solid (April 5), dotted (April 6), dashed (April 7), dash-dot (April 8), dash-dot-dot (April 9) and long-dashed (April 11). The figure indicates the fluctuation in the K core due to star-planet interaction consistent with Shkolnik et al.'s (2003) results (at the bottom of Figure 5.1). When compared, top and bottom figures show very similar characteristics such as similar fluctuation between wavelengths 3932.5 Å and 3934 Å. For most residuals (except the residual from April 9, which is shown with dash-dot-dot line style), the fluctuation intensity is between 0.1 and 0.2, which is also consistent with the results by Shkolnik et al. However, the residual from April 9 is an interesting data point, and will be discussed in the rest of this chapter.

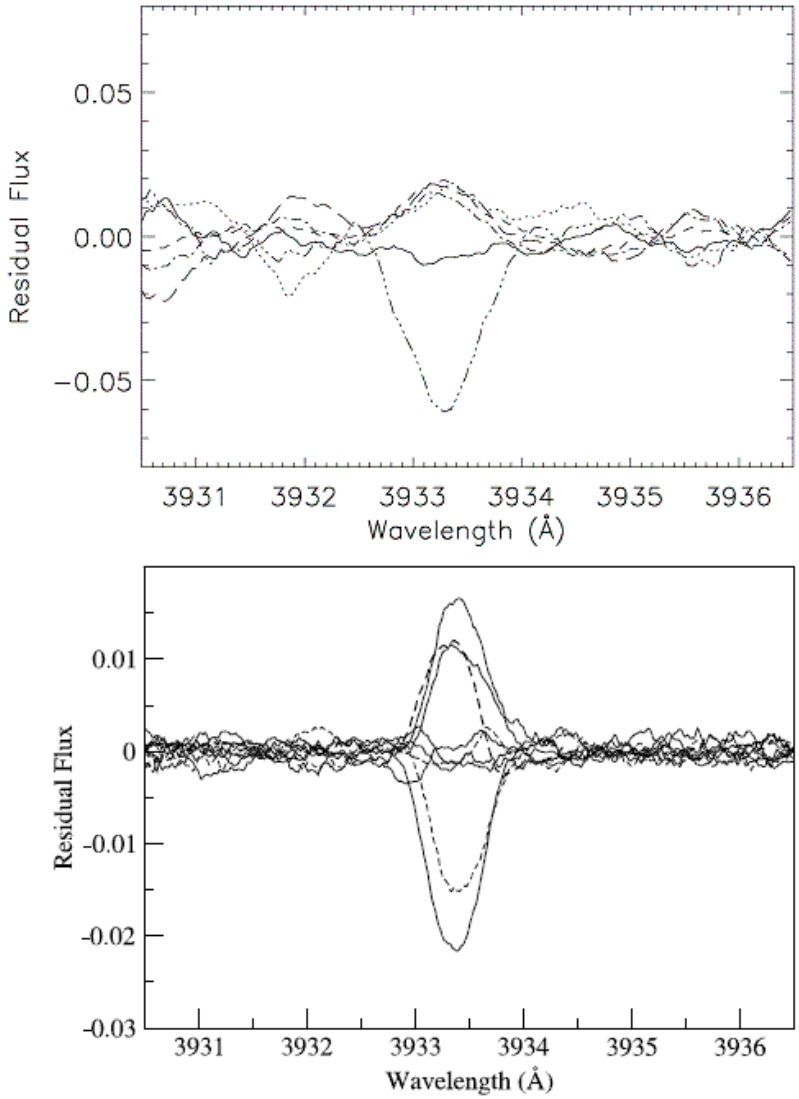

Figure 5.1 Top Figure: Residual flux of the CaII K core of HD 179949 between April 5, 2006 and April 11, 2006. Residual flux is computed from average mean and smoothed by 21 pixels. The graph consist of solid (April 5), dotted (April 6), dashed (April 7), dash-dot (April 8), dash-dot-dot (April 9) and long dashed (April 11) lines. Bottom Figure: Integrated K residuals by Shkolnik et al (2003). Bottom figure is shown for comparison. *Figure credit: Shkolnik et al. (2003)*

The mean absolute deviation in the Ca II K core is computed as discussed in the previous chapter. The calculated MAD as well as the MAD represented by Shkolnik et al. (2003) are shown in the Figure 5.2 (top and bottom figures). The overall average over all spectra, which is used to deduce the nightly residuals, is shown with dashed-lines indicating the mean

absolute deviation is confined in the K core. This result is also consistent with Shkolnik et al. (2003) except that the peak of deviation is slightly higher in our results, probably due to exceptional data point from April 9.

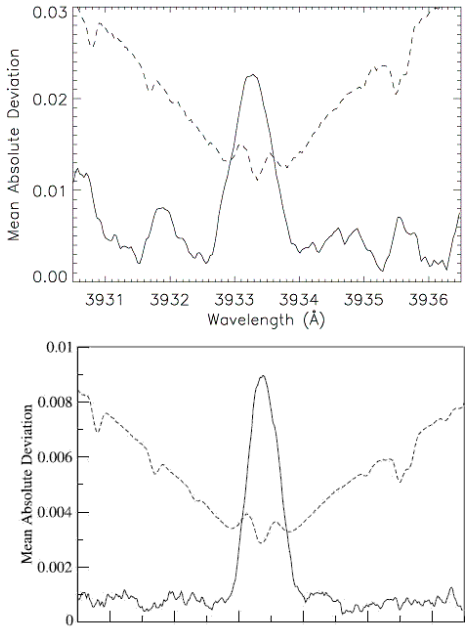

Figure 5.2 Top Figure: Solid line is the Mean Absolute Deviation (MAD) of the Ca II K core of HD 179949. MAD is calculated as indicated in the Shkolnik et al. (2003) $MAD = N^{-1}\sum|data_i - mean|$ for N spectra. The units are the intensity as a fraction of normalized flux. Bottom Figure: the MAD figure given by Shkolnik et al. (2003). *Figure credit: Shkolnik et al. (2003)*

A similar analysis has been done for Ca II H line at 3968 Å and Al I line at 3944 Å. The H line showed very similar variation with about 2/3 intensity of that for the K core. Al I line showed no significant fluctuation in 2 Å window analysis; however, there is a noticeable fluctuation when the width of the window is set to 7 Å, which may imply low level magnetic interaction at the photosphere layer. The Al I line is a strong photospheric line located between Ca II H and K lines in the spectrum, and analyzed to distinguish between chromospheric and (possible) photospheric activities. The analysis for the H core of Ca II, residual flux, MAD, and Al I (residual flux only) are shown in the Figure 5.3 and Figure 5.4, respectively.

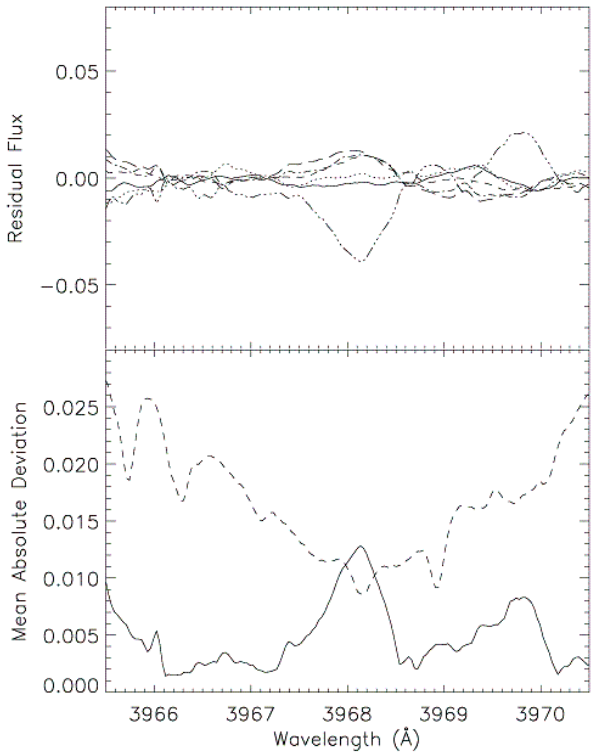

Figure 5.3 Top Figure: Residuals of the H core. Bottom Figure: Computed MAD for the H core. Dashed lines represent the mean spectrum (scaled vertically).

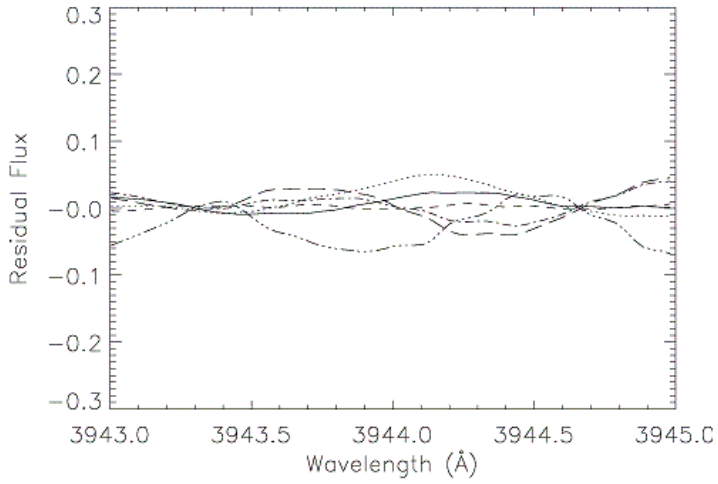

Figure 5.4 Residuals of Al I line (in 2 Å window). The Al I line is a strong photosperic line and shows no apparent fluctuation.

To illustrate the modulation of the PIE effect, the Ca II K residuals are integrated and plotted as function of phase of the planet (see Figure 5.5). Integrated residuals are grouped by orbital period of the planet. Each orbital coverage is distinguished by different symbols. The scale of the figure is adjusted as indicated by Shkolnik et al. (2003), which is described as setting the lowest residual's flux to zero, and scaling other points accordingly. The best-fit bright-spot models from Shkolnik et al. (2003) are shown with solid and dashed lines in the same figure. The solid line is the model for a spot at 30° latitude with stellar inclination $i = 87°$. The dashed line is the same model with $i = 83°$.

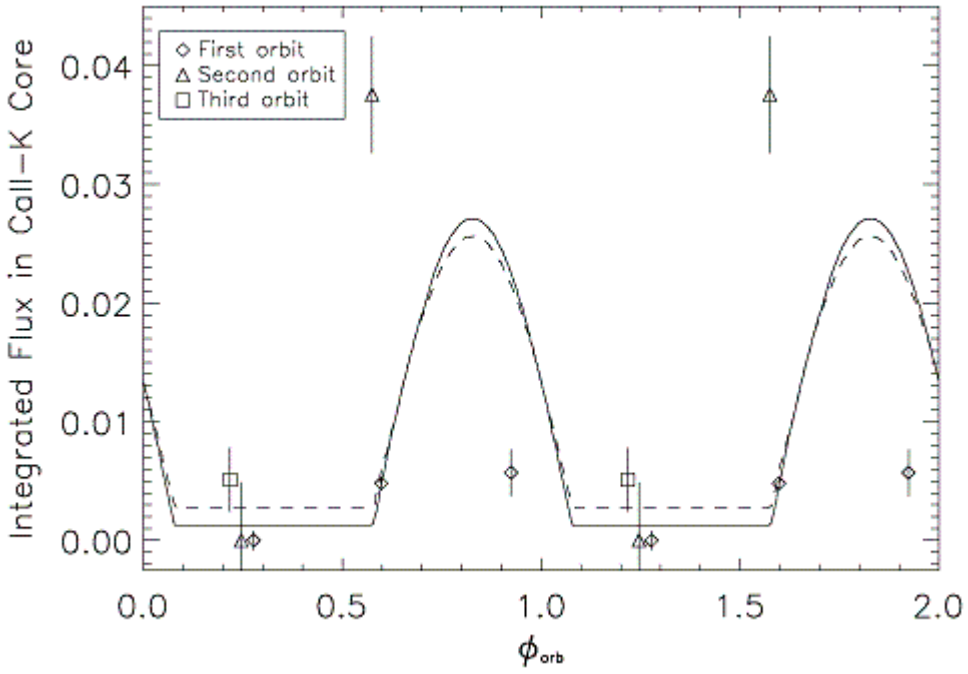

Figure 5.5 Integrated K residuals as function of phase of the planet. Lowest residual's flux is set to zero, and all others scaled accordingly. Error bars are calculated from nightly variations. 1-σ is used to calculate the error bars. The best-fit bright-spot models from Shkolnik et al. (2003) are shown with solid and dashed lines in the same figure. The solid line is the model for a spot at 30° latitude with stellar inclination $i = 87°$. The dashed line is the same model with $i = 83°$.

The figure does not indicate any planet induced activity during the first orbital period of the planet. However, strong emission was detected during the second orbital period when planet is at phase $\emptyset = 0.575$. This is an interesting result as the activity is thought to be at its

"off" state (according to the data from the first orbital period); therefore a weaker activity was expected to modulate around 7 days period. But this result suggests that the activity may even switch between on/off states within one orbital period (3.09 days).

Another interesting result is the observed strong emission occurring at the phase $\emptyset = 0.575$, when the planet is (almost) in the blind spot of the star. Shkolnik et al. previously suggested that peak occurs at phase about $\emptyset = 0.8$. Although observing the activity when the planet is still behind the star seems unreasonable, the following two aspects may be critical in understanding these phenomena: 1. The accuracy of the calculated phases is uncertain due to previously detected phase shifts at the HD 179949 star-planet system. 2. Magnetic interaction is not likely carried by straight field lines. Therefore, the magnetic field geometries may be complex (Parker Spirals, Parker E. N., 1958). These two factors are discussed below.

The phase shifts in the HD 179949 system are first detected by Shkolnik et al. when the observational data spanning 6 years were analyzed. New fit functions suggested phase shifts of -0.07 between 2002 and 2005 data points, and -0.17 between 2003 and 2006 data points. The cause of these phase shifts are currently unknown, and it is thought to be related with the star-planet interaction.

We did not derive the ephemerides from the observational data, but used available 2003 ephemerides provided by Shkolnik et al (2005). As mentioned in the previous paragraph, Shkolnik et al. reported phase shifts with an amount of -0.17 between 2003 and 2006 observations; therefore, (almost) the same amount of the shift may be applicable to our 2006 observations at the McDonald Observatory. In order to see the effect of proposed shift on observational data, the suggested bright-spot models are shifted by -0.17 in phase (see Figure 5.6). This figure suggests that the shift may be real as data points now show a better correlation with the bright-spot models. However, I would like to note that the bright-spot fits are shifted to test the correlation while the observational data maintained as calculated because the proposed shift is currently empirical.

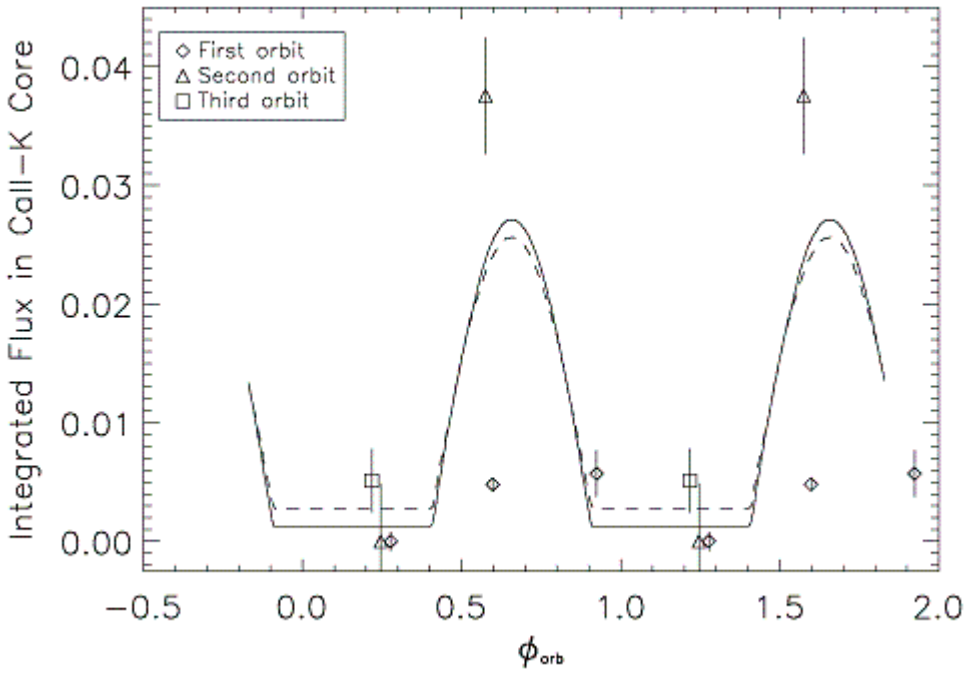

Figure 5.6 Integrated K residuals (as in Figure 5.5) with bright-spot models shifted to test correlation with the observational data. The amount of shift, which is -0.17 is discussed in the text. The observational data is maintained as calculated because the proposed shift is currently empirical.

The peak point of the planet induced activity is estimated by Shkolnik et al. to occur when the planet is about at the third quadrature ($\emptyset \approx 0.8$). This initial estimation was based on best-fit bright-spot models created with aid of first available data points (see Figure 5.5 and Figure 5.6). However, a lack of sufficient number of observational data and detected phase shifts created a large uncertainty about the phase of the peak point of activity.

As previously indicated by Shkolnik et al. and others, the planet-induced activity is leading the phase of the planet, and this phase lead may allow us to understand magnetic field geometries such as Parker spirals of stellar winds. Parker spiral is the shape of the Sun's magnetic field, which is twisted into a spiral due to magnetohydrodynamic influence of the solar wind associated with solar rotation. The spiral model and the solar wind were predicted by E.

Parker in the mid 1950s. The figure below indicates Parker's prediction about the shape of the solar magnetic field.

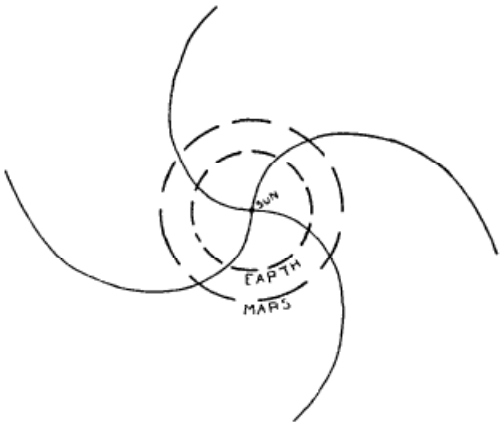

Figure 5.7 Parker Spirals of the Sun.
Figure ref: Parker (1958)

The shape of spirals at the HD 179949 may be more complicated and "twisted" noting that the planet may be behind the star while the terminator of the field line that carries the interaction may be facing to Earth. This is speculated in Figure 5.8. The activity shows a peak on April 9, 2006 when the terminator of the Parker spiral is facing to Earth (black line). I would like to note that the Parker spirals in this figure are only speculation, and not based on detailed computations.

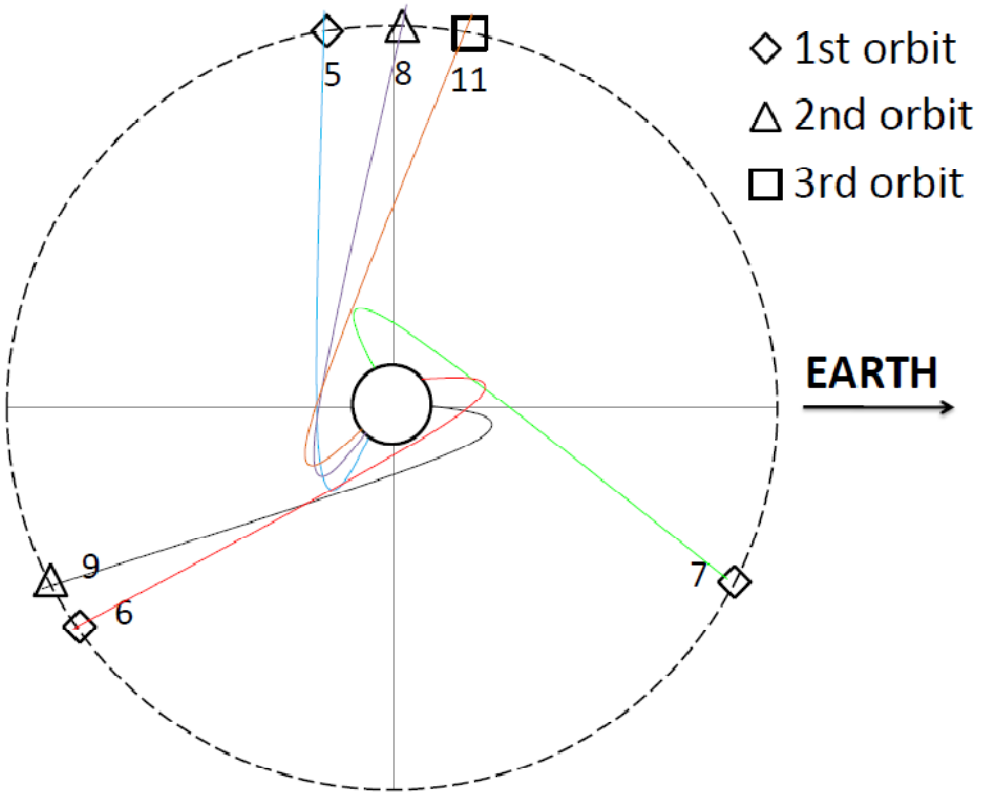

Figure 5.8 Positions of the planet during McDonald observation run on April 2006. Each orbital period is distinguished by different symbols. Numbers represent the day of April (i.e. 5 is April 5, 2006). Size of the star and size of the orbit is scaled. Colored lines are speculated Parker spirals.

The latest four ephemerides of HD 179949 system are listed in Table 5.1. Calculated phases from the four different epochs are listed in the Table 5.2. The inconsistency of calculated phases from different epochs may imply changes in the mechanical properties in the system as function of time due to star-planet interaction. Figure 5.9 shows the change in phase as function of time, where it shows a low-order polynomial trend. Data points are computed from $\Delta\text{phase} = \phi - \phi_{\text{Butler}}$ where ϕ are phases obtained from Table 5.2. The trend shown in Figure 5.9 may be critical for our understanding of the nature of the HD 179949 star-planet system; However, it is not discussed in the scope of this project as further study and observations are

required to understand its nature. Nevertheless, I would like to note that the studied phase shift is not unique to HD 179949 system, and was detected in other studied CEGP's by Shkolnik et al (2005) as well.

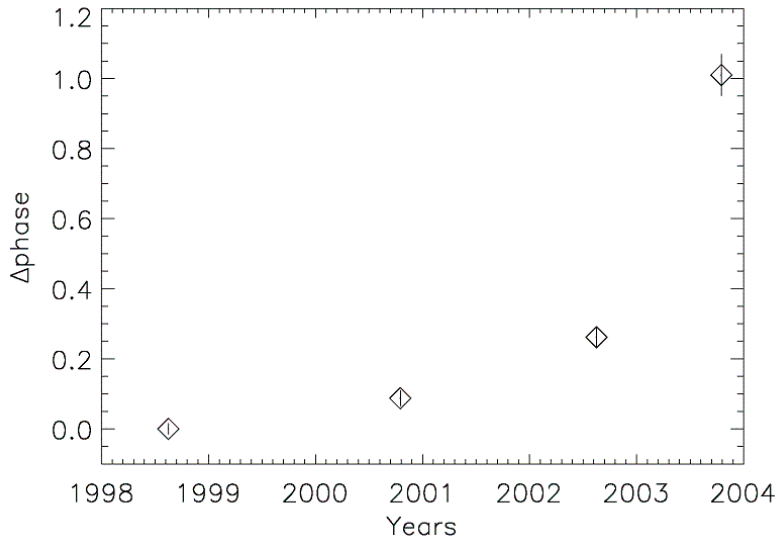

Figure 5.9 Phase shift of HD 179949 star-planet system. Δphase = ϕ - ϕ_{Butler} Four different ϕ is used from Table 5.2

Table 5.1 Four Different Ephemerides of HD179949b

	Butler et al.	Exoplanet.eu	Shkolnik	
	(1998 July)	(2000 Sept)	(2002 July)	(2003 Sept)
Epoch (JD)	2451001.51000	2451793.98000	2452479.823	2452894.11
Period (days)	3.092514	3.0925	3.09285	3.09246

Table 5.2 Calculated Phases of HD179949b With Four Different Ephemerides From Table 1.1

			Shkolnik	
Night of	ϕ_{Butler}	$\phi_{exoplanet}$	ϕ_{2002}	ϕ_{2003}
April 5	0.2676	0.0163	0.1906	0.2776
April 6	0.5878	0.3365	0.5108	0.5978
April 7	0.9141	0.6628	0.8370	0.9241
April 8	0.2362	0.9850	0.1591	0.2463
April 9	0.5647	0.3135	0.4877	0.5749
April 11	0.2078	0.9566	0.1307	0.2180

CHAPTER 6

CONCLUSION

We have covered (almost) three planetary orbits of the close-in giant planet of HD 179949 system during 10-days of observation run at the McDonald Observatory. We were able to acquire data from HD 179949 which 6 out of 10 nights. Our data analysis confirmed previous results by Shkolnik et al. (2003), who showed the first observational evidence of Planet Induced Emission (PIE) in Ca II H and K lines. The PIE phenomenon, which was first suggested by Cuntz et al (2000), is now known to occur concerning the H and K lines on 5 other systems hosting CEGP's. Besides H and K, the effect has also been identified on the Ca II IR triplet by Saar & Cuntz (2001), and in coronal X-rays by Kashyap et al. (2008) and Saar et al. (2008).

The results of our highly limited observations can be summarized as follows:

- The results appear to confirm the on/off nature of the PIE phenomenon as previously indicated by Shkolnik et al. (2008) based on six observational runs obtained in 2001, 2002, 2003, 2005, and 2006 with each observational run covering one planetary orbit.
- Shkolnik et al. reported that the modulated PIE effect disappeared in 2003 and in June 2006; however, we have a single data point obtained on April 9, 2006 suggesting the PIE effect to be present. This particular data point also seems to indicate that the activity in the HD 179949 system may be somewhat stronger than previously thought.
- No PIE effect was observed during other orbital periods, which seems to be consistent with the interpretation that the PIE effect is due to magnetic star-planet interaction carried along the Parker spiral of the stellar wind (Saar et al. 2004).

- Our results seems to confirm the evolution of the phase difference of star-planet interaction which may be related with the time dependency of magnetic cycle of HD 179949 (McIvor et al. 2006, Lanza 2008, Cohen et al. 2009)..
- The PIE effect was appeared nearly at the sub-planetary point ($\emptyset = 0.511$). However, no activity was detected nearly at the same phase ($\emptyset = 0.488$) 3 days earlier.
- Our results also suggested slight evidence for planet related photospheric fluctuations as a result of analysis of the strong photospheric line Al I λ3944 Å best visible in 7Å window. A photospheric PIE effect was previously suggested for τ Boo A based on COROT data (Walker et al. 2008). The on/off nature of the chromospheric PIE effect appears to be consistent with its magnetic nature as well as a flare (rather than a wave) interpretation as previously argued by Rubenstein & Shafer (2000), Zarka et al. (2001), Saar et al. (2004), and others.

APPENDIX A

OBSERVATION LOG TABLES

TABLE A.1 APRIL 5/6 OBSERVATION LOG

Date (2006)	UT	Target	Filename	Exposure Time (seconds)	Seeing (arcsecs)
5/6 Apr	8:39	tau cet	n10064.fits	1200	2.6
	9:04	tau cet	n10065.fits	1200	
	9:37	hd142373	n10066.fits	900	
	9:56	hd142373	n10067.fits	900	
	10:20	hd187123	n10069.fits	1200	
	10:44	hd187123	n10070.fits	1200	
	11:08	hd187123	n10071.fits	1200	
	11:31	hd179949	n10072.fits	1200	
	11:54	hd179949	n10073.fits	1200	

TABLE A.2 APRIL 6/7 OBSERVATION LOG

Date (2006)	UT	Target	Filename	Exposure Time (seconds)	Seeing (arcsecs)
6/7 Apr	1:45	hd73256	n20053.fits	1200	4.1
	2:08	hd73256	n20054.fits	1200	
	2:31	hd73256	n20055.fits	1200	
	2:58	hd49674	n20056.fits	1200	
	3:21	hd49674	n20057.fits	1200	
	3:44	hd49674	n20058.fits	1200	
	4:15	tau boo	n20060.fits	600	
	4:28	tau boo	n20061.fits	600	
	4:42	tau boo	n20062.fits	600	
	4:55	tau boo	n20063.fits	600	
	5:08	tau boo no I2	n20064.fits	600	
	5:27	hd102195	n20066.fits	1200	
	5:50	hd102195	n20067.fits	1200	
	6:13	hd102195	n20068.fits	1200	
	6:37	rho crb	n20069.fits	600	
	6:50	rho crb	n20070.fits	600	
	7:09	hd149026	n20072.fits	1200	
	7:32	hd149026	n20073.fits	1200	
	7:55	hd149026	n20074.fits	1200	
	8:18	hd149026	n20075.fits	1200	
	8:41	hd149026	n20076.fits	1200	
	9:04	hd149026	n20077.fits	1200	
	9:36	hd189733	n20079.fits	1200	
	9:59	hd189733	n20080.fits	1200	
	10:47	tau boo	n20081.fits	600	
	11:00	tau boo	n20082.fits	600	
	11:17	hd179949	n20084.fits	1200	
	11:40	hd179949	n20085.fits	1200	
	12:03	hd179949	n20086.fits	1200	

TABLE A.3 APRIL 7/8 OBSERVATION LOG

Date (2006)	UT	Target	Filename	Exposure Time (seconds)	Seeing (arcsecs)
7/8 Apr	1:42	hd45067	n30053.fits	900	5.0
	2:00	hd45067	n30054.fits	900	
	2:20	hd73256	n30055.fits	1200	
	2:43	hd73256	n30056.fits	1200	
	3:06	hd73256	n30057.fits	1200	
	3:37	hd49674	n30059.fits	1200	
	4:00	hd49674	n30060.fits	1200	
	4:23	hd49674	n30061.fits	1200	
	4:50	tau boo	n30062.fits	600	
	5:03	tau boo	n30063.fits	600	
	5:17	tau boo	n30064.fits	300	
	10:47	tau boo	n30067.fits	600	
	11:00	tau boo	n30068.fits	600	
	11:14	tau boo	n30069.fits	600	
	11:30	hd179949	n30070.fits	1200	
	11:53	hd179949	n30071.fits	1200	

TABLE A.4 APRIL 8/9 OBSERVATION LOG

Date (2006)	UT	Target	Filename	Exposure Time (seconds)	Seeing (arcsecs)
8/9 Apr	1:44	hd73256	n40052.fits	1200	2.3
	2:07	hd73256	n40053.fits	1200	
	2:30	hd73256	n40054.fits	1200	
	2:57	hd43587	n40055.fits	900	
	3:15	hd43587	n40056.fits	900	
	3:39	hd49674	n40058.fits	1200	
	4:02	hd49674	n40059.fits	1200	
	4:25	hd49674	n40060.fits	1200	
	4:51	tau boo	n40061.fits	300	
	4:59	tau boo	n40062.fits	300	
	5:07	tau boo	n40063.fits	300	
	5:15	tau boo	n40064.fits	300	
	5:23	tau boo	n40065.fits	300	
	5:31	tau boo	n40066.fits	300	
	5:44	hd102195	n40068.fits	1200	
	6:07	hd102195	n40069.fits	1200	
	6:30	hd102195	n40070.fits	1200	
	7:00	hd149143	n40071.fits	1200	
	7:23	hd149143	n40072.fits	1200	
	7:47	hd149143	n40073.fits	1200	
	8:19	hd149026	n40075.fits	1200	
	8:42	hd149026	n40076.fits	1200	
	9:05	hd149026	n40077.fits	1200	
	9:32	tau boo	n40078.fits	300	
	9:40	tau boo	n40079.fits	300	
	9:48	tau boo	n40080.fits	300	
	9:56	tau boo	n40081.fits	300	
	10:04	tau boo	n40082.fits	300	
	10:12	tau boo	n40083.fits	300	
	10:26	hd187123	n40085.fits	1200	
	10:49	hd187123	n40086.fits	1200	
	11:13	hd179949	n40087.fits	1200	
	11:36	hd179949	n40088.fits	1200	
	11:59	hd179949	n40089.fits	1200	

TABLE A.5 APRIL 9/10 OBSERVATION LOG

Date (2006)	UT	Target	Filename	Exposure Time (seconds)	Seeing (arcsecs)
9/10 Apr	1:50	hd73256	n50049.fits	1200	2.1
	2:13	hd73256	n50050.fits	1200	
	2:36	hd73256	n50051.fits	1200	
	3:05	epsilon ori	n50053.fits	10	
	3:10	epsilon ori	n50054.fits	40	
	3:14	epsilon ori	n50055.fits	40	
	3:17	epsilon ori	n50056.fits	40	
	3:24	tau boo	n50057.fits	300	
	3:32	tau boo	n50058.fits	300	
	3:40	tau boo	n50059.fits	300	
	3:48	tau boo	n50060.fits	300	
	3:56	tau boo	n50061.fits	300	
	4:04	tau boo	n50062.fits	300	
	4:21	hd49674	n50064.fits	1200	
	4:44	hd49674	n50065.fits	1200	
	5:07	hd49674	n50066.fits	1200	
	5:32	hd102195	n50067.fits	1200	
	5:55	hd102195	n50068.fits	1200	
	6:18	hd102195	n50069.fits	1200	
	6:46	hd149143	n50071.fits	1200	
	7:09	hd149143	n50072.fits	1200	
	7:32	hd149143	n50073.fits	1200	
	8:01	hd149026	n50074.fits	1200	
	8:24	hd149026	n50075.fits	1200	
	8:47	hd149026	n50076.fits	1200	
	9:17	tau boo	n50078.fits	300	
	9:25	tau boo	n50079.fits	300	
	9:33	tau boo	n50080.fits	300	
	9:41	tau boo	n50081.fits	300	
	9:49	tau boo	n50082.fits	300	
	9:57	tau boo	n50083.fits	300	
	10:07	hd182572	n50084.fits	600	
	10:20	hd182572	n50085.fits	600	
	10:39	hd187123	n50087.fits	1200	
	11:02	hd187123	n50088.fits	720.2	
	11:36	hd179949	n50089.fits	1200	
	11:59	hd179949	n50090.fits	1200	

TABLE A.6 APRIL 10/11 OBSERVATION LOG

Date (2006)	UT	Target	Filename	Exposure Time (seconds)	Seeing (arcsecs)
10/11 Apr	1:43	hd49674 no I2 ce	n60052.fits	1200	
	2:07	hd49674	n60053.fits	1200	
	2:30	hd49674	n60054.fits	1200	
	2:53	hd49674	n60055.fits	1200	
	3:16	hd49674	n60056.fits	1200	
	4:12	tau boo	n60057.fits	600	
	4:25	tau boo	n60058.fits	600	
	4:39	tau boo	n60059.fits	600	
	4:52	tau boo	n60060.fits	600	
	5:10	tau boo	n60061.fits	600	
	5:23	tau boo	n60062.fits	600	
	5:36	tau boo	n60063.fits	600	
	5:53	hd102195 no I2 c	n60065.fits	1200	
	6:19	hd102195	n60066.fits	1200	
	6:42	hd102195	n60067.fits	1200	
	7:05	hd102195	n60068.fits	664.2	
	7:20	hd142373	n60069.fits	300	
	7:28	hd142373	n60070.fits	300	
	7:39	hd142373 no I2 c	n60071.fits	300	
	7:47	hd142373 no I2 c	n60072.fits	300	
	7:59	hd149026 no I2 c	n60074.fits	1200	
	8:22	hd149026	n60075.fits	1200	
	8:45	hd149026	n60076.fits	479.4	
	9:31	hd149026	n60077.fits	1200	
	9:54	hd149026	n60078.fits	1200	
	10:24	hd179949	n60079.fits	1200	
	10:47	hd179949	n60080.fits	1200	
	11:10	hd179949	n60081.fits	1200	

TABLE A.7 APRIL 11/12 OBSERVATION LOG

Date (2006)	UT	Target	Filename	Exposure Time (seconds)	Seeing (arcsecs)
11/12 Apr	2:04	beta aur	n70054.fits	300	1.7
	3:04	alpha leo	n70055.fits	600	
	3:17	alpha leo	n70056.fits	480	
	3:32	hd49674	n70058.fits	1200	
	3:55	hd49674	n70059.fits	1200	
	4:32	hd49674	n70060.fits	1200	
	5:08	tau boo	n70061.fits	1200	
	5:31	tau boo	n70062.fits	1200	
	5:55	tau boo	n70063.fits	1200	
	6:20	tau boo	n70064.fits	600	
	6:34	tau boo	n70065.fits	600	
	6:47	tau boo	n70066.fits	600	
	7:00	tau boo	n70067.fits	600	
	7:13	tau boo	n70068.fits	600	
	7:26	tau boo	n70069.fits	600	
	7:39	tau boo	n70070.fits	600	
	7:52	tau boo	n70071.fits	600	
	8:16	hd149026	n70073.fits	1200	
	8:39	hd149026	n70074.fits	1200	
	9:03	hd149026	n70075.fits	1200	
	9:27	hd189733 no I2 c	n70076.fits	1200	
	9:50	hd189733 no I2 c	n70077.fits	1200	
	10:13	hd189733 no I2 c	n70078.fits	1200	
	10:38	hd189733 no I2 c	n70079.fits	1200	
	11:08	hd179949 no I2 c	n70081.fits	1200	
	11:31	hd179949	n70082.fits	1200	
	11:54	hd179949	n70083.fits	1200	

TABLE A.8 APRIL 12/13 OBSERVATION LOG

Date (2006)	UT	Target	Filename	Exposure Time (seconds)	Seeing (arcsecs)
12/13 Apr	3:31	tau boo	n80052.fits	300	
	3:39	tau boo	n80053.fits	300	
	3:47	tau boo	n80054.fits	300	
	3:55	tau boo	n80055.fits	300	
	4:03	tau boo	n80056.fits	300	
	4:11	tau boo	n80057.fits	300	
	4:23	hd49674	n80058.fits	1200	
	6:58	hd149026	n80061.fits	1200	
	7:21	hd149026	n80062.fits	1200	
	7:44	hd149026	n80063.fits	1200	
	8:07	hd149026	n80064.fits	1200	
	11:36	hd179949	n80067.fits	900	
	11:54	hd179949	n80068.fits	900	

TABLE A.9 APRIL 13/14 OBSERVATION LOG

Date (2006)	UT	Target	Filename	Exposure Time (seconds)	Seeing (arcsecs)
13/14 Apr	1:44	hd43587	n90052.fits	600	
	1:58	hd43587	n90053.fits	600	
	2:15	hd49674	n90054.fits	1200	

APPENDIX B

IDL ROUTINES DEVELOPED FOR DATA ANALYSIS

MAIN.PRO

```
;** Main Script to perform analysis in the K core **
;**
;** Routines Called:
;** 1.extract
;** 2.coadd
:** 3.hrs_combine
;** 4.hrs_offset
;** 5.residual
;** 6.curve
;**
;** Corrections:
;** 1. Remove n20086.var : different target
;** 2. Shift Wavelength of n50090.var by -0.73
;**
;** Prepare Directory
;** Files: n?00??.var
:** Blaze: blaze?.var
;**
;** Run
;**
;** Step1: Blaze correction to the spectra
    .r blaze.pro
;**
;** Step2: Take 7A chunks
    spawn,'ls n*b.var',list ; Create an array to include the blazed
spectra
    for i = 0,n_elements(list)-1 do begin
    extract,list(i),3933 ; CaII-K
    wait,3
    endfor
;**
;** Step3: Set end points to 1
    .r norm1
    .r norm2
    .r norm3
    .r norm4
    .r norm5
    .r norm7
;**
;** Step4: Co-add each night
    coadd,'n10072b_7Anorm.var','n10073b_7Anorm.var',OUT='n1.var'
    coadd,'n20084b_7Anorm.var','n20085b_7Anorm.var',OUT='n2.var'
    coadd,'n30070b_7Anorm.var','n30071b_7Anorm.var',OUT='n3.var'

coadd,'n40087b_7Anorm.var','n40088b_7Anorm.var','n40089b_7Anorm.var',O
UT='n4.var'
    $cp n50090b_7Anorm.var n5.var
    coadd,'n70082b_7Anorm.var','n70083b_7Anorm.var',OUT='n7.var'

;** Some Adjustments - fine adjustments on co-added data - major
features are matched !
```

```
    restore,'n4.var
    flux=flux*0.98
    error=error*0.98
    save,wave,flux,error,filename='n4.var'
    restore,'n5.var
    flux=flux*1.01
    error=error*.1.01
    save,wave,flux,error,filename='n5.var'
    restore,'n7.var
    flux=flux*0.98
    error=error*0.98
    save,wave,flux,error,filename='n7.var'

;**Step5: Calculate overall mean (create: fluxave.var) and compute
residuals

   residual,'n1.var','n2.var','n3.var','n4.var','n5.var','n7.var'

;**Step6: Low order curvature removal


curve,'n1ir.var','n2ir.var','n3ir.var','n4ir.var','n5ir.var','n7ir.var
',LOW=3932.5,HIGH=3934.5,ORDER=2

;**Step7: Smoothing and Plotting

   .r see

;**Step8: Save smoothed data

   .r smoothen

;**Step9: MAD plot

   .r mad

end
```

B.2.BLAZE.PRO

```
;*************************************************************
;* Step 1: ***Blaze Calibration for .var files in a directory***
;* a. Interpolate blaze onto wave of each spectrum
;* b. Divide each spectrum by BLAZE
;* c. Calculate new ERROR array
;* d. Calculate S/N ratio
;* e. Calculate the "weight" of each flux value
;*
;* Output1: filenameb.var
;* Output2: filenameb.ps
;*************************************************************

spawn,'ls n?00??.var',list ;create array (list) with nYXXXX.var files
in the directory
; Y represent the number of the night

print,'Performing operations...'
print,' '

for j=0,n_elements(list)-1 do begin

;**Set variables ***
wavebl=dblarr(2044)
fluxbl=dblarr(2044)
wavei=dblarr(2044)
fluxi=dblarr(2044)
errori=dblarr(2044)
;*******************

blaze = 'blaze' + strmid(list(j),1,1)+'.var' ;blaze is blaze of
corresponding night
restore, blaze
wavebl[*]=wave[56,*] ;Extract Aperture 56 from 2D wave of blaze
fluxbl[*]=flux[56,*] ;Extract Aperture 56 from 2D flux of blaze
flux=0 ;flush the variables
wave=0 ;flush the variables
flux=dblarr(2044) ; re-define the variables
wave=dblarr(2044) ; re-define the variables

restore, list[j]
print,list[j] + '/' + blaze
wavei[*]=wave[56,*]   ;Extract wave of Aperture 56 into 1D wavei
fluxi[*]=flux[56,*]   ;Extract flux of Aperture 56 into 1D fluxi
errori[*]=error[56,*] ;Extract error of Aperture 56 into 1D errori

quadterp, wavebl, fluxbl, wavei, fluxbli ; INTERPOLATE BLAZE'S FLUX
ONTO WAVE

fluxb=fluxi/fluxbli   ; DIVIDING FLUX BY BLAZE
errorb=errori/fluxbli ; DIVIDING ERROR BY BLAZE
```

```
signal=fluxb/errorb ; CALCULATING S/N RATIO
weight=signal ; CHECK THIS !! WEIGHT IS SQRT OF S/N

; FLUSH SOME VARIABLES
wave = 0
flux = 0
error = 0
; ASSIGN NEW VARIABLES
wave = wavei
flux = fluxb
error = errorb
;
outname=strsplit(list[j],'.',/extract)+'b.var'
;save,wavei,fluxb,errorb,signal,weight,filename=outname[0]        ;save
output file with 'b' postfix
save,wave,flux,error,filename=outname[0]  ;save  output  file  with  'b'
postfix

;**OUTPUT TO X
!p.multi=[0,2,2,0,1]
plot,wavei,fluxi,title='raw'
plot,wavebl,fluxbl,title='blaze function'
plot,wavei,fluxb,title='blazed'
;**OUTPUT TO PS
set_plot,'ps
outname=strsplit(list[j],'.',/extract)+'b.ps'
device,file=outname[0]
!p.multi=[0,2,2,0,1]
plot,wavei,fluxi,title='raw'
plot,wavebl,fluxbl,title='blaze function'
plot,wavei,fluxb,title='blazed'
device,/close
set_plot,'x
wait,3

; FLUSH VARIABLES HERE ...
wave = 0
wavei = 0
wavebl = 0
fluxbl = 0
fluxb = 0
flux = 0
error = 0
errorb = 0
signal = 0
weight = 0
; VARIABLES ARE FLUSHED ...

endfor

print,'Blaze division is done!...'

end
```

B.3. EXTRACT.PRO

```
;#Extract 7 Angstrom chunk centering specified wavelenghth from data
;#usage: extract, filename.var, centering wavelength
;# wave, flux and error arrays are assumed in the input .var file
;#

pro extract,filename,wavelength

;SET BOUNDARIES
lowlimit = wavelength - 3.5
highlimit = wavelength + 3.5

j=0

print,'Processing :' + filename
print,'wavelength :' + string(wavelength)
restore,filename ; Open file
;***CALCULATE THE SIZE OF 7A CHUNK***
for i = 0,n_elements(wave) -1 do begin
  if wave(i) gt lowlimit and wave(i) lt highlimit then j = j+1
endfor

print, 'Size of the array (points) :' + string(j)

wavearr=dblarr(j); Set new array dimensions
fluxarr=dblarr(j); Set new array dimensions
errorarr=dblarr(j); Set new array dimensions
j = 0

;***CONSTRUCT THE ARRAY***
for i = 0,n_elements(wave) -1 do begin
  if wave(i) gt lowlimit and wave(i) lt highlimit then begin
      wavearr(j) = wave(i)
      fluxarr(j) = flux(i)
      errorarr(j) = error(i)
      j = j+1
  endif
endfor

wave = 0 ; Flush
flux = 0 ; Flush
error = 0 ; Flush
wave = wavearr ; Set new name
flux = fluxarr ; Set new name
error= errorarr ; Set new name

;**OUTPUT TO X
!p.multi = 0
set_plot,'x
plot,wave,flux,xrange=[lowlimit,highlimit],xstyle=1,title=filename
;**OUTPUT TO PS
```

```
!p.multi=0
set_plot,'ps
outname=strsplit(filename,'.',/extract)+'_7A.ps'
device,file=outname[0]
plot,wave,flux,xrange=[lowlimit,highlimit],xstyle=1,title=filename
device,/close
set_plot,'x
outname=strsplit(filename,'.',/extract)+'_7A.var'
save,wave,flux,error,filename=outname[0]

print, 'Output file :' + outname[0]
print, ' '

return ; EXTRACT
end ; EXTRACT
```

B.4.NORM1.PRO

```
;**Step 3:normalize 1.night
;**Set end points to 1 and fit with a straight line
;**
;**

!p.multi=0
;set_plot,'ps
;device,file='norm1.ps'

restore,'n10072b_7A.var'
line=dblarr(n_elements(wave))
line=line+1
plot,wave,line,linestyle   =   2,yrange=[0.0,1.2],title='n10072b(rd)   -
n10073b(gr)'

restore,'n10072b_7A.var'
flux=flux*3.27
error=error*3.27
signal=flux/error
oplot,wave,flux,color='0000FF'x
save,wave,flux,error,filename='n10072b_7Anorm.var'

restore,'n10073b_7A.var'
flux=flux*2.85
error=error*2.85
signal=flux/error
oplot,wave,flux,color='00FFFF'x
save,wave,flux,error,filename='n10073b_7Anorm.var'

;device,/close
end
```

B.5.COADD.PRO

```
;*********************************************************
;** Co-Add up to 5 spectra                               *
;** Usage: coadd,'file1.var','file2.var',...,OUT=outname.var*
;**                                                      *
;** This procedure assumes all co-added spectra be in same*
;** size                                                 *
;**                                                      *
;** data structure of HRS_combine input:                 *
;** wavearr(*,0) : first spectrum's wave                 *
;** fluxarr(*,0) : first spectrum's flux                 *
;** errarr(*,0)  : first spectrum's error                *
;** wavearr(*,1) : second spectrum's wave                *
;** ................................                     *
;**                                                      *
;** Performed operations:                                *
;** 1. open each file                                    *
;** 2. For each file, convert single wave,flux,err arrays *
;**    into wave(*,i), flux(*,i), err(*,i)               *
;**    where i is the # of spectrum                      *
;** 3. call HRS_Combine routine to co-add spectra        *
;** 4. Save combined spectra                             *
;**                                                      *
;** Levent Gurdemir (2009)                               *
;*********************************************************
;** Expected Inputs:                                     *
;** files that contain arrays: WAVE, FLUX, ERROR         *
;**                                                      *
;**                                                      *
;*********************************************************

pro coadd,p1,p2,p3,p4,p5,OUT=outname

;night = 'n1' ;number of the night
;spawn,'ls '+string(night)+'*norm.var',list ;create array (list)
on_error,2

list=strarr(n_params(0))
list(0) = p1 ; p1 must be exist
list(1) = p2 ; p2 must be exist
if keyword_set(p3) then list(2) = p3
if keyword_set(p4) then list(3) = p4
if keyword_set(p5) then list(4) = p5

restore,list(0) ;restore the first file in the list to read the size
of the wave
wavearr=dblarr(n_elements(wave),n_params(0)) ;set new array's size
fluxarr=dblarr(n_elements(wave),n_params(0))
errarr=dblarr(n_elements(wave),n_params(0))

for j=0,n_elements(list)-1 do begin
```

```
restore,list(j)
print, 'processing...' + list(j)
wavearr(*,j)=wave
fluxarr(*,j)=flux
errarr(*,j)=error
endfor

print, 'ploting ...'
plot,wavearr(*,0),fluxarr(*,0)
for j=0,n_elements(list)-1 do begin
oplot,wavearr(*,j),fluxarr(*,j),linestyle=j+1
endfor

print,'combining ...'

hrs_combine,wavearr,fluxarr,errarr,wl,fl_total

wave=0
flux=0
error=0

wave=wl
flux=fl_total
error=errarr

;save,wl,fl_total,err,filename=night[0]+'.var'
save,wave,flux,error,filename=outname

end
```

B.6. HRS_COMBINE.PRO

```
;Modified from original HRS_COMBINE for McDonald data
;Levent Gurdemir - 2009
;
;*PURPOSE:  Combine  (co-add)  the  different  readouts  into  single
spectrum.
;
;*CALLING SEQUENCE:
;     HRS_COMBINE, wave, flux, ERR, wl, fl_tot, /swidth
;
;*PARAMETERS:
;  INPUT:
;     wave  - (REQ) - (0) - (S)        - wave(*,i) = wave1, wave2,...,
wavei
;     flux  - (REQ) - (0) - (S)        - flux(*,i) = flux1, flux2,...,
fluxi
;     ERR   - (REQ) - (0) - (S)          - err(*,i) = err1, err2,...,
erri
;
;*KEYWORDS:
;     swidth      - (OPT) - (0) - (I,R,L,D) - Search width (pixels)
for
;                                     cross correlation.
;  OUTPUT:
;     WL    - (REQ) - (2) - (I,R,L,D) - Wavelength array.
;     FL_TOT  - (REQ) - (2) - (I,R,L,D) - Flux array.
;     VAR   -  (OPT)  -  (1)  -  (I,R,L,D)  -  Shift  vector  (in  pixels)
between
;                                          each    spectra    and    the
reference
;                                          spectrum.
;     ERR   - (OPT) - (2) - (I,R,L,D) - Statistical error array for
the
;                                        overall spectrum.
;*SYSTEM VARIABLES USED:
;     !DUMP ** removed ** !DUMP is not used anymore by IDL
;     !PSYM
;     !C
;     !ERR
;     !NOPLOT
;*SUBROUTINES CALLED:
;     HRS_OFFSET
;*EXAMPLES:
;
;*PROCEDURE:
;     From the flux array, number of readouts is determined.
;     Using  the  first  spectrum  as  a  reference,  the  program  cross
correlates
;     each  succeeding  spectrum,  determines  the  wavelength  shift,
shifts the
;     spectrum by the appropriate amount and then coadds to generate a
final
```

```
;     flux vector.

pro hrs_combine,wavearr,fluxarr,errarr,wl,fl_tot,SWIDTH=swidth

on_error,2

if (not(keyword_set( swidth))) then swidth=15.0

;
;  Extract the reference spectrum
;
wl=wavearr(*,0)
;
;eps=eps(*,0)  ;  Data  quality  array  has  been  removed  in  this
modification
;
; determine the number of readouts
;
sz=size(fluxarr)
ndim=sz(0)
;Test  the  array  for  2-dimensions  **  removed  as  !dump  variable  is
obselete!
;if ndim ne 2 then begin
;  if !dump gt 1 then $
;     print,' Unable to find multiple readouts...returning'
;  flt_tot= flux
;  return
;endif
;
;if !dump gt 1 then begin ; **removed as !dump variable is obselete
      print,' '
      print,'Number of data points = ',sz(1),'   readouts = ',sz(2)
      print,' '
;end

nmax=sz(2)-1            ; nmax = number of columns in the flux array
(number of spectra)
var=fltarr(sz(2)) ; define var array as large as number of spectra in
the flux
var(0)=0.         ; set the first number in the array to zero.
;
;  calculate error vector
;
errs=fltarr(n_elements(errarr(*,0)))           ;
for i=0,nmax do errs=errs + errarr(*,i)*errarr(*,i)   ;
delta(err)={[(err1)^2+(err2)^2+...+(errn)^2]^1/2}/n
errarr=sqrt(errs)/float(sz(2))                 ;
;
; determine the data point separation in angstroms
;
dwl=(max(wl)-min(wl))/(n_elements(wl)-1.) ; calculate delta(wavearr)
;if !dump gt 1 then $
      print,'wavelength separation of data points = ',dwl,' A'
```

```
;
; use the first flux spectra as the reference
;
fl_ref=fluxarr(*,0)
fl_tot=fluxarr(*,0)
;
; Now process each of the other spectra and add to the final
;
;if !dump gt 1 then $
;     print,' shifts found (pixels)'
for i=1,nmax do begin
  fl=fluxarr(*,i)
;
;   determine the shift (in pixels) between this spectrum and the
reference
;
  hrs_offset,fl_ref,fl,offset,0,swidth,corr           ;   JKF   3/16/91
(incr. width)
  if offset eq 0.0 then begin
      print,' '
      print,' Error: Unable to cross-correlate readout:',i-1
      print,'    Hint:    Increase    SEARCH    WIDTH...current    search
width:',swidth
      print,' Action: returning'
      return
  end

; if !dump gt 1 then $
      print,'OFFSET: ',offset
;
;   convert the shift to angstroms
;
  shft=dwl*offset
  var(i)=offset
;
;   PERFORM THE SHIFT to get a new wavelength array
;
  wl1=wl+shft
; if !dump gt 1 then begin
      plot,wavearr(*,0),fluxarr(*,0)
      oplot,wavearr(*,i),fluxarr(*,i)
      wait,3
      plot,wavearr(*,0),fluxarr(*,0)
      oplot,wl1,fl
      wait,3
;end
;
;   put the flux back onto the wavelength samples of the reference
;
  linterp,wl1,fl,wl,fl1
;
;   coadd this spectrum to the total
;
```

```
  fl_tot=fl_tot+fl1
;
endfor
;
   fl_tot=fl_tot/(nmax+1)
;
return ; HRS_COMBINE
end ; HRS_COMBINE
```

B.7 HRS_OFFSET.PRO

```
;+++++++++++++++++++++++++++++++++++++++++++++++++++++++++++++++++++++++++
++++++++++
;+
;
;*NAME: HRS_OFFSET  ** Modified by Levent Gurdemir ** 2009
;
;*CLASS:
;     Data Reduction
;*CATEGORY:
;
;*PURPOSE:  Determine  the  shift  (in  pixels)  of  one  spectrum  with
respect to
;        another.
;*CALLING SEQUENCE:
;     HRS_OFFSET, s1, s2, OFFSET, approx, width, CORR
;*PARAMETERS:
;     INPUTS:
;     s1    - (REQ) - (1) - (I,R,L,D) - First spectrum.
;     s2    - (REQ) - (1) - (I,R,L,D) - Second spectrum.
;     approx      - (OPT) - (0) - (I,L)     - Approximate offset.
;     width - (OPT) - (0) - (I,L)     - Search width.
;     OUTPUTS:
;     OFFSET      - (REQ) - (0) - (I,R,L,D) - Offset of s2 from s1 in
data points.
;     CORR  - (REQ) - (1) - (I,R,L,D) - Output correlation vector.
;
;*SYSTEM VARIABLES USED:
;     !DUMP  ** removed ** !DUMP is not used anymore by IDL
;     !PSYM
;     !C
;     !ERR
;*EXAMPLES:
;
;*RESTRICTIONS:
;     Both s1 and s2 must be on the same wavelength scale.
;*NOTES:
;
;*PROCEDURE:
;     The cross correlation between S1 and S2 is determined and a non-
linear
;     fit  to  the  peak  of  the  correlation  is  used  to  determine  the
exact
;     offset.
;*MODIFICATION HISTORY:
;     Ver 1.0     - xx/xx/xx - D. Lindler   - GSFC
;     Ver 2.0 - 02/08/91 - K. Feggans   - GSFC - Moved to DAF.
;     Ver 3.0 - 02/11/91 - R. Robinson  - GSFC - Prolog added.
;     Ver  4.0  -  02/11/91  -  J.  Blackwell  -  GSFC  -  Modified  to  conform
with
;                                                GHRS DAF standards.
;     27-apr-1992 JKF/ACC           - update !DUMP options.
```

```
;     21-aug-2009 Levent Gurdemir - remove !DUMP
;-
;---------------------------------------------------------------------
----------
pro hrs_offset,s1,s2,offset,approx,width,corr
;
      if n_params(0) lt 4 then approx = 0
      if n_params(0) lt 5 then width = 15
;
; extract template from spectrum 2
;
      ns = n_elements(s1)
      ns2 = ns/2
      width2 = width/2
      nt2 = ns2 - width2 - abs(approx) - 1
      center = ns2
      template2 = s2(center-nt2:center+nt2)
      nt = nt2*2+1
;
; correlate
;
      corr = fltarr(width)                ;correlation matrix
      mean2 = total(template2)/nt
      sig2 = sqrt(total((template2-mean2)^2))
      diff2 = template2 - mean2

      for i=0,width-1 do begin
            center = ns2 - width2 + i + approx
            template1 = s1(center-nt2:center+nt2)
            mean1 = total(template1)/nt
            sig1 = sqrt(total((template1-mean1)^2))
            diff1 = template1 - mean1
            corr(i) = total(diff1*diff2)/sig1/sig2
      end
;     if !dump gt 2 then begin ; ** removed ** as !dump variable is
obselete
            diff = corr-min(corr)
            !c = 0
            plot,diff,title='HRS_OFFSET      Cross-correlation      '+
!stime,psym=-1
            wait,5
            !c = 0
;     end
;
; Find maximum
;
      maxc = max(corr) & k=!c
      if (!c eq 0) or (!c eq (width-1)) then begin
            print,'HRS_OFFSET-  maximum  on  edge  of  search  area,
ABORTING'
            !err = -1
            offset = 0.0
            return
```

```
      end
;
; USE QUADRATIC REFINEMENT
;
      Kmin=(corr(K-1)-corr(K))/(corr(K-1)+corr(K+1)-2.*corr(K))-0.5
      offset = K + Kmin - width2 + approx
;     if !dump gt 2 then print,offset   ; ** removed ** as !dump
varible is obselete
      print,offset

return ; HRS_OFFSET
end ; HRS_OFFSET
```

B.8.RESIDUAL.PRO

```
;** Calculate Overall Mean and Residuals
;**
;** Levent Gurdemir 2009
;**
;** usage: residual,'file1.var',file2.var',...  (7 files max)
;** output: *i.var  :wave interpolated outputs
;** output: *r.var  :residuals
;** output: fluxave.var : overall mean
;**
;** Procedure:
;** 1. Open input files
;** 2. Interpolate all waves onto first spectra's wave
;** 3. Calculate average flux : fluxave=sum(flux)/numberof(flux)
;** 4. Calculate residuals for each spectra : fluxres=flux-fluxave
;**
;**
;*****************************************************************
pro residual,p1,p2,p3,p4,p5,p6,p7
;**Step 1: Calculate the Overall Average
list=strarr(n_params(0))
list(0) = p1 ; p1 must be exist
list(1) = p2 ; p2 must be exist
if keyword_set(p3) then list(2) = p3
if keyword_set(p4) then list(3) = p4
if keyword_set(p5) then list(4) = p5
if keyword_set(p6) then list(5) = p6
if keyword_set(p7) then list(6) = p7

restore,list[0]       ;open first .var file as reference
iwave=wave
fluxave=flux ;fluxave will be used to calculate average flux!
errorave=error

print, 'saving the reference file : '+list[0]
outname=strsplit(list[0],'.',/extract)+'i.var'
save,wave,flux,error,filename=outname[0]
plot,wave,flux
wait,2

for j=1,n_elements(list)-1 do begin ;
restore,list[j]
print,'interpolating flux for ... '+list[j]
quadterp, wave, flux, iwave, iflux; interpolate fluxi array onto wave:
newarray=wave,iflux
quadterp, wave, error, iwave, ierror; interpolate error array
wave=0
flux=0
error=0
wave=iwave
flux=iflux
error=ierror
```

```
outname=strsplit(list[j],'.',/extract)+'i.var'
save,wave,flux,error,filename=outname[0]   ;save  output  file  with  'i'
postfix
oplot,wave,flux
wait,2

;Also calculate an average flux
fluxave=fluxave+flux
errorave=errorave+error

endfor

fluxave=fluxave/j
errorave=errorave/j
flux=fluxave
error=errorave
save,wave,flux,error,filename='fluxave.var'
oplot,wave,flux,color='0000FF'x
wait,2

;**Step2: Compute Residuals

fluxres=dblarr(n_elements(wave)) ;Residual

for j=0,n_elements(list) -1 do begin ;
inname=strsplit(list[j],'.',/extract)+'i.var'
restore,inname[0]
print,'Calculating Residuals for :'+inname[0]
fluxres=flux-fluxave + 1  ; 1 added to avoid zero values in residuals
errorres=error+errorave   ; absolute errors add (not subtract!)
plot,wave,fluxres
outname=strsplit(inname[0],'.',/extract)+'r.var'
save,wave,fluxres,errorres,filename=outname[0]
wait,2
endfor
end
```

B.9.SMOOTHEN.PRO

```
;** Save smoothed data
;** sf = smoothing factor
;** Levent Gurdemir (2009)

sf = 21
restore,'n1irc.var
flux=smooth(newfluxres-1,sf,/EDGE_TRUNCATE)
error=smooth(newerrorres,sf,/EDGE_TRUNCATE)
save,wave,flux,error,filename='n1ircs.var'
restore,'n2irc.var
flux=smooth(newfluxres-1,sf,/EDGE_TRUNCATE)
error=smooth(newerrorres,sf,/EDGE_TRUNCATE)
```

```
save,wave,flux,error,filename='n2ircs.var'
restore,'n3irc.var
flux=smooth(newfluxres-1,sf,/EDGE_TRUNCATE)
error=smooth(newerrorres,sf,/EDGE_TRUNCATE)
save,wave,flux,error,filename='n3ircs.var'
restore,'n4irc.var
flux=smooth(newfluxres-1,sf,/EDGE_TRUNCATE)
error=smooth(newerrorres,sf,/EDGE_TRUNCATE)
save,wave,flux,error,filename='n4ircs.var'
restore,'n5irc.var
flux=smooth(newfluxres-1,sf,/EDGE_TRUNCATE)
error=smooth(newerrorres,sf,/EDGE_TRUNCATE)
save,wave,flux,error,filename='n5ircs.var'
restore,'n7irc.var
flux=smooth(newfluxres-1,sf,/EDGE_TRUNCATE)
error=smooth(newerrorres,sf,/EDGE_TRUNCATE)
save,wave,flux,error,filename='n7ircs.var'

end
```

B.10. CURVE.PRO

```
;** Low Order Curvature Removal with given parameters: **
;**
;** This procedure makes a low order fit to given data set
;** Given wavelength window is ignored while making the fit
;** Centered feature is protected while making fit
;**
;** This procedure can be used while making fits to continuum on line
profiles
;**
;** Levent Gurdemir and Seth Redfield 2009
;**
;**                                                                  usage:
curve,'file1.var',file2.var',...,LOW=lowerlimit,HIGH=higherlimit,ORDER
=order
;** LOW= lower limit of wavelength window to be ignored
;** HIGH= higher limit of wavelength window to be ignored

pro curve,p1,p2,p3,p4,p5,p6,p7,LOW=low,HIGH=high,ORDER=order

;**Construct list array outof input parameters
list=strarr(n_params(0))
list(0) = p1 ; p1 must be exist
if keyword_set(p2) then list(1) = p2
if keyword_set(p3) then list(2) = p3
if keyword_set(p4) then list(3) = p4
if keyword_set(p5) then list(4) = p5
if keyword_set(p6) then list(5) = p6
if keyword_set(p7) then list(6) = p7

;**Make Fit

for j=0,n_elements(list)-1 do begin
restore,list(j)
temp=min(abs(wave-low),count1)  ;find index value of low limit
temp=min(abs(wave-high),count2) ;find index value of high limit
result=poly_fit([wave(0:count1),wave(count2:*)],[fluxres(0:count1),flu
xres(count2:*)],order)
fit=poly(wave,result) ;make fit onto wave
;fluxres=fluxres+1
;fit=fit+1
newfluxres=fluxres/fit ; divide flux values to fit to remove curvature
newerrorres=errorres/fit ; divide error values to fit
;newfluxres=newfluxres-1
plot,wave,fluxres,ystyle=3
oplot,wave,fit,color='0000FF'x
outname=strsplit(list[j],'.',/extract)+'_fit.var'
save,wave,fit,filename=outname[0] ; save fit file
outname=strsplit(list[j],'.',/extract)+'c.var'
save,wave,newfluxres,newerrorres,filename=outname[0]
wait,2
endfor; end
```

B.11.MAD.PRO

```
;** Plots Mean Absolute Deviation
;** MAD equation is given in Shkolnik (2003)
;** MAD = (1/N)*SUM(abs(data[i]-mean)) for N spectra
;** in the *ircs files, flux values are already 'data[i]-mean' as they
are 'residuals'.
;**
;** Levent Gurdemir (2009)
;**

data=0

restore,'n1ircs.var'
data=abs(flux)
restore,'n2ircs.var'
data=data + abs(flux)
restore,'n3ircs.var'
data=data+abs(flux)
restore,'n4ircs.var'
data=data+abs(flux)
restore,'n5ircs.var'
data=data+abs(flux)
restore,'n7ircs.var'
data=data+abs(flux)

data=data/6

plot,wave,data,xrange=[3930.5,3936.5],xstyle=1,yrange=[0,0.030],ytitle
='Mean       Absolute       Deviation',charsize=1.5,xtitle='Wavelength
('+string("305B)+')',background=255,color=0,charthick=2

;** Over plot AVERAGE FLUX onto MAD plot
restore,'fluxave.var'
flux=flux/27 ; to scale average flux
oplot,wave,flux,linestyle=2,color=0

end
```

B.12.PHASE.PRO

```
;** Phase plot
;** Levent Gurdemir 2009
;**
;** This procedure generates Shkolnik (2003) Figure 6: phase plot
;** K line residuals are integrated
;** plotted against phase
;** Phase values are manually calculated and entered based on Shkolnik
2003 epherimedes.
;**
;** procedures used: integral
;**         integral(X,Y,xmin,xmax)
;** integrated between 3932.45A and 3934.15A
;**  Corresponding  errors  are  computed  from  n?e.var  files  which  are
standard deviations of each night
;**         cerror(wave,error,xmin,xmax) used to sum-up all errors


xmin = 3932.45
xmax = 3934.15

;*** Integrate K lines between xmin and xmax, and compute errors:

restore,'n1ircs.var'
restore,'n1e.var'  ; open error file (nightly variations)
intfluxn1 = integral(wave,flux,xmin,xmax)
interrorn1=  cerror(wave_b,error_c,xmin,xmax)  ;  compute  error  from
nightly variations
print, 'integrated flux for n1  : ' + string(intfluxn1)
print, 'integrated error for n1 : ' + string(interrorn1)

restore,'n2ircs.var'
restore,'n2e.var'
intfluxn2 = integral(wave,flux,xmin,xmax)
interrorn2= cerror(wave_b,error_c,xmin,xmax)
print, 'integrated flux for n2  : ' + string(intfluxn2)
print, 'integrated error for n2 : ' + string(interrorn2)

restore,'n3ircs.var'
restore,'n3e.var'
intfluxn3 = integral(wave,flux,xmin,xmax)
interrorn3= cerror(wave_b,error_c,xmin,xmax)
print, 'integrated flux for n3  : ' + string(intfluxn3)
print, 'integrated error for n3 : ' + string(interrorn3)

restore,'n4ircs.var'
restore,'n4e.var'
intfluxn4 = integral(wave,flux,xmin,xmax)
interrorn4= cerror(wave_b,error_c,xmin,xmax)
print, 'integrated flux for n4  : ' + string(intfluxn4)
print, 'integrated error for n4 : ' + string(interrorn4)

restore,'n5ircs.var'
```

```
;;;;    'restore,'n5e.var' ; !!! There is no such file (single data
point)
intfluxn5 = integral(wave,flux,xmin,xmax)
;;;; interrorn5= cerror(wave,error,xmin,xmax)
interrorn5=0.0048921014 ; Error can not be calculated due to single
data point, the largest error value (n4) is used
print, 'integrated flux for n5  : ' + string(intfluxn5)
print, 'integrated error for n5 : ' + string(interrorn5)

restore,'n7ircs.var'
restore,'n7e.var'
intfluxn7 = integral(wave,flux,xmin,xmax)
interrorn7= cerror(wave_b,error_c,xmin,xmax)
print, 'integrated flux for n7  : ' + string(intfluxn7)
print, 'integrated error for n7 : ' + string(interrorn7)

;*********************************************************
;*** Prepare Phase Plot **********************************
;*********************************************************

intflux1=dblarr(6,2)
intflux2=dblarr(4,2)
intflux3=dblarr(2,2)

phase1=dblarr(6)
phase2=dblarr(4)
phase3=dblarr(2)

intflux1(0,0) = abs(intfluxn1) ; First orbit
intflux1(1,0) = abs(intfluxn2) ; First orbit
intflux1(2,0) = abs(intfluxn3) ; First orbit
intflux2(0,0) = abs(intfluxn4) ; Second orbit
intflux2(1,0) = abs(intfluxn5) ; Second orbit
intflux3(0,0) = abs(intfluxn7) ; Third orbit

intflux1(0,1) = interrorn1
intflux1(1,1) = interrorn2
intflux1(2,1) = interrorn3
intflux2(0,1) = interrorn4
intflux2(1,1) = interrorn5
intflux3(0,1) = interrorn7

intflux1(3,0)  =  abs(intfluxn1)  ;Repeat  same  plot  one  more  time
(Shkolnik Fig.6)
intflux1(4,0)  =  abs(intfluxn2)  ;Repeat  same  plot  one  more  time
(Shkolnik Fig.6)
intflux1(5,0)  =  abs(intfluxn3)  ;Repeat  same  plot  one  more  time
(Shkolnik Fig.6)
intflux2(2,0)  =  abs(intfluxn4)  ;Repeat  same  plot  one  more  time
(Shkolnik Fig.6)
intflux2(3,0)  =  abs(intfluxn5)  ;Repeat  same  plot  one  more  time
(Shkolnik Fig.6)
```

```
intflux3(1,0) = abs(intfluxn7) ;Repeat same plot one more time
(Shkolnik Fig.6)

intflux1(3,1) = interrorn1 ;Repeat same plot one more time (Shkolnik
Fig.6)
intflux1(4,1) = interrorn2 ;Repeat same plot one more time (Shkolnik
Fig.6)
intflux1(5,1) = interrorn3 ;Repeat same plot one more time (Shkolnik
Fig.6)
intflux2(2,1) = interrorn4 ;Repeat same plot one more time (Shkolnik
Fig.6)
intflux2(3,1) = interrorn5 ;Repeat same plot one more time (Shkolnik
Fig.6)
intflux3(1,1) = interrorn7 ;Repeat same plot one more time (Shkolnik
Fig.6)

phase1(0) = 0.277
phase1(1) = 0.598
phase1(2) = 0.924
phase2(0) = 0.246
phase2(1) = 0.575
phase3(0) = 0.218
phase1(3) = 1.277
phase1(4) = 1.598
phase1(5) = 1.924
phase2(2) = 1.246
phase2(3) = 1.575
phase3(1) = 1.218

restore,'solid.var'
!p.font=-1
plot,wave,flux,yrange=[-
0.0025,0.045],ystyle=1,charsize=1.5,xtitle='!7u!3!Iorb!N',ytitle='Inte
grated Flux in CaII-K Core',background=255,color=0,charthick=2


restore,'dashed.var'
oplot,wave,flux,linestyle=2
phase=phase
oplot,phase1,intflux1(*,0)-min(intflux1(*,0)),psym=4
oploterr,phase1,intflux1(*,0)-min(intflux1(*,0)),intflux1(*,1),4

oplot,phase2,intflux2(*,0)-min(intflux2(*,0)),psym=5
oploterr,phase2,intflux2(*,0)-min(intflux2(*,0)),intflux2(*,1),5

oplot,phase3,intflux3(*,0)-min(intflux2(*,0)),psym=6
oploterr,phase3,intflux3(*,0)-min(intflux2(*,0)),intflux3(*,1),6

legend,['First orbit','Second orbit','Third orbit'],psym=[4,5,6]

;oplot,phase,intflux,psym=4

end
```

B 13. INTEGRAL.PRO

```
FUNCTION INTEGRAL,X,Y,XMIN,XMAX
;
;+
;                 integral
;
; Routine to perform trapezoidal integration in X,Y between limits
; xmin to xmax.
;
; CALLING SEQUENCE:
;     result = integral(x,y,xmin,xmax)
;
; INPUTS:
;     x,y - vectors to be integrated
;     xmin,xmax - vectors with lower and upper integral limits
; OUTPUTS:
;     the integrations between xmin and xmax are returned
;     as the function result
; RESTRICTIONS:
;     The values in XMIN must be greater than or equal to the minimum
;     of X. The values in XMAX must be less than or equal to the
;     maximum of X. X must be in ascending order.
;
; HISTORY:
;     Version 1,  D. Lindler  (a long time ago)
;     Version 2,  JKF/ACC     28-jan-1992 - moved to IDL V2.
;     Version 3,  DJL   17-jun-1992 - FIXED BUG AT ENDPOINTS
;     version 4,  DJL         27-Jul-1992 - fixed previous change to
;                                   work with vector inputs
;-
;-------------------------------------------------------------------
;
; COMPUTE INDEX POSITIONS OF XMIN,XMAX
;
TABINV,X,XMIN,RMIN
TABINV,X,XMAX,RMAX
n = n_elements(x)
;
; CHECK FOR VALID LIMITS
;
A=MAX(XMIN)>MAX(XMAX)
B=MIN(XMIN)<MIN(XMAX)
D=MIN(XMAX-XMIN)
IF (A GT MAX(X)) OR (B LT MIN(X)) OR (D LT 0.0) THEN $
  message,'INVALID INTEGRAL LIMITS SUPPLIED TO INTEGRAL FUNCTION'
;
; COMPUTE DIFFERENCES IN X AND Y
;
DX=SHIFT(X,-1)-X
DY=SHIFT(Y,-1)-Y
;
; COMPUTE INTEGRALS FOR EACH FULL INTERVAL IN X
```

```
;
DINT=(SHIFT(Y,-1)+Y)/2.0*DX
;
; COMPUTE FULL INTERVALS TO INTEGRATE BETWEEN
;
IMIN=FIX(RMIN)
IMAX=FIX(RMAX)
;
; COMPUTE FUNCTION VALUES AT XMIN AND XMAX
;
DXMIN=XMIN-X(IMIN)
YMIN=Y(IMIN)+DXMIN*(Y(IMIN+1)-Y(IMIN))/DX(IMIN)
DXMAX=XMAX-X(IMAX)
YMAX=Y(IMAX)+DXMAX*(Y((IMAX+1)<(n-1)) - Y(IMAX))/DX(IMAX)
;
; COMPUTE INTEGRAL FROM IMIN TO IMAX
;
NOUT=N_ELEMENTS(XMIN)
INT=FLTARR(NOUT)
FOR I=0,NOUT-1 DO BEGIN
      IF IMAX(I) NE IMIN(I) THEN INT(I)=TOTAL(DINT(IMIN(I):IMAX(I)-1))
END
;
; SUBTRACT INTEGRAL FROM IMIN TO RMIN
;
INT=INT - (Y(IMIN)+YMIN)/2.*DXMIN
;
; ADD INTEGRAL FROM IMAX TO RMAX
;
INT=INT + (Y(IMAX)+YMAX)/2.0*DXMAX
RETURN,INT
END
```

B14. CERROR.PRO

```
function cerror,wave,error,p3,p4

;**Construct list array outof input parameters
;list=strarr(n_params(0))
;list(0) = p1 ; p1 (wave) must be exist
;list(1) = p2 ; p2 (error) must be exist
;list(2) = p3 ; p3 (low_wave)
;list(3) = p4 ; p4 (high_wave)

temp=min(abs(wave-p3),count1)  ;find index value of low limit
temp=min(abs(wave-p4),count2) ;find index value of high limit

result=sqrt(total(error(count1:count2)^2))    ;    result    =    sqrt[
sigma(error^2) ]

return,result

end
```

APPENDIX C

SAMPLE REDUCED SPECTRA OF HD179949 FROM 2006 OBSERVATION RUN AT MCDONALD OBSERVATORY

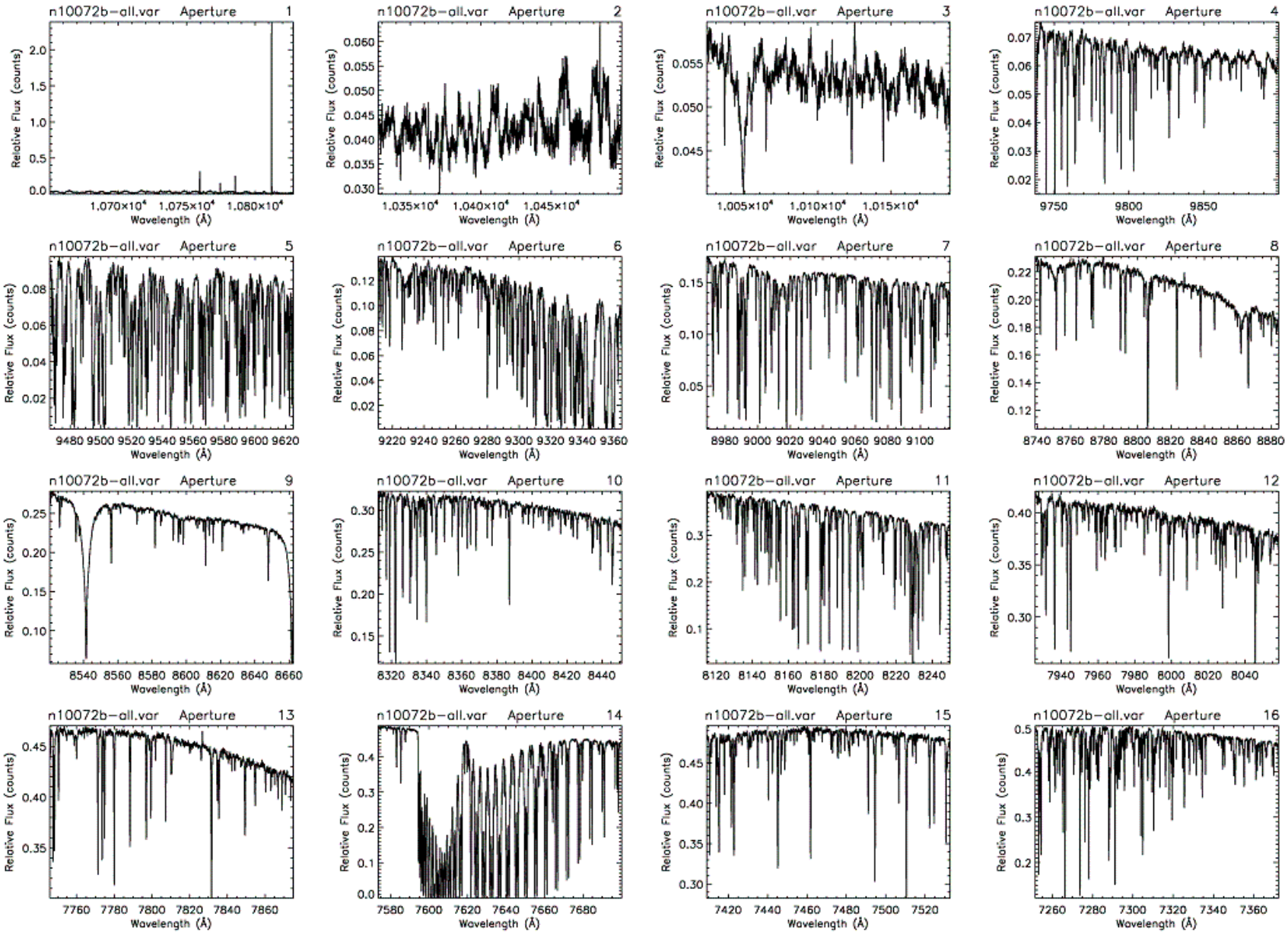
n10072b-all.var Aperture 1
Relative Flux (counts)
Wavelength (Å)
n10072b-all.var Aperture 2
Relative Flux (counts)
Wavelength (Å)
n10072b-all.var Aperture 3
Relative Flux (counts)
Wavelength (Å)
n10072b-all.var Aperture 4
Relative Flux (counts)
Wavelength (Å)
n10072b-all.var Aperture 5
Relative Flux (counts)
Wavelength (Å)
n10072b-all.var Aperture 6
Relative Flux (counts)
Wavelength (Å)
n10072b-all.var Aperture 7
Relative Flux (counts)
Wavelength (Å)
n10072b-all.var Aperture 8
Relative Flux (counts)
Wavelength (Å)
n10072b-all.var Aperture 9
Relative Flux (counts)
Wavelength (Å)
n10072b-all.var Aperture 10
Relative Flux (counts)
Wavelength (Å)
n10072b-all.var Aperture 11
Relative Flux (counts)
Wavelength (Å)
n10072b-all.var Aperture 12
Relative Flux (counts)
Wavelength (Å)
n10072b-all.var Aperture 13
Relative Flux (counts)
Wavelength (Å)
n10072b-all.var Aperture 14
Relative Flux (counts)
Wavelength (Å)
n10072b-all.var Aperture 15
Relative Flux (counts)
Wavelength (Å)
n10072b-all.var Aperture 16
Relative Flux (counts)
Wavelength (Å)

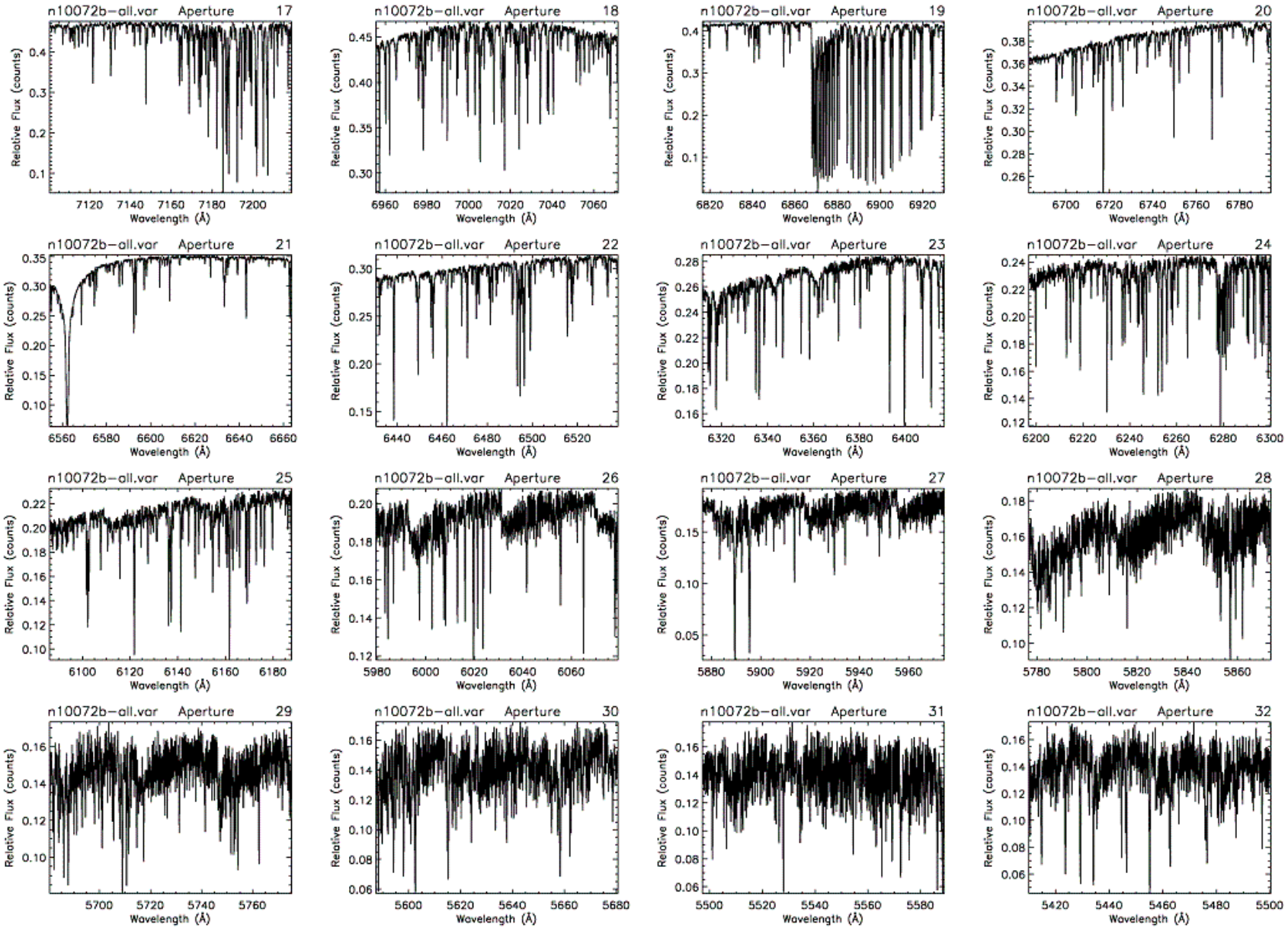
n10072b-all.var Aperture 17
Relative Flux (counts)
Wavelength (Å)
n10072b-all.var Aperture 18
Relative Flux (counts)
Wavelength (Å)
n10072b-all.var Aperture 19
Relative Flux (counts)
Wavelength (Å)
n10072b-all.var Aperture 20
Relative Flux (counts)
Wavelength (Å)
n10072b-all.var Aperture 21
Relative Flux (counts)
Wavelength (Å)
n10072b-all.var Aperture 22
Relative Flux (counts)
Wavelength (Å)
n10072b-all.var Aperture 23
Relative Flux (counts)
Wavelength (Å)
n10072b-all.var Aperture 24
Relative Flux (counts)
Wavelength (Å)
n10072b-all.var Aperture 25
Relative Flux (counts)
Wavelength (Å)
n10072b-all.var Aperture 26
Relative Flux (counts)
Wavelength (Å)
n10072b-all.var Aperture 27
Relative Flux (counts)
Wavelength (Å)
n10072b-all.var Aperture 28
Relative Flux (counts)
Wavelength (Å)
n10072b-all.var Aperture 29
Relative Flux (counts)
Wavelength (Å)
n10072b-all.var Aperture 30
Relative Flux (counts)
Wavelength (Å)
n10072b-all.var Aperture 31
Relative Flux (counts)
Wavelength (Å)
n10072b-all.var Aperture 32
Relative Flux (counts)
Wavelength (Å)

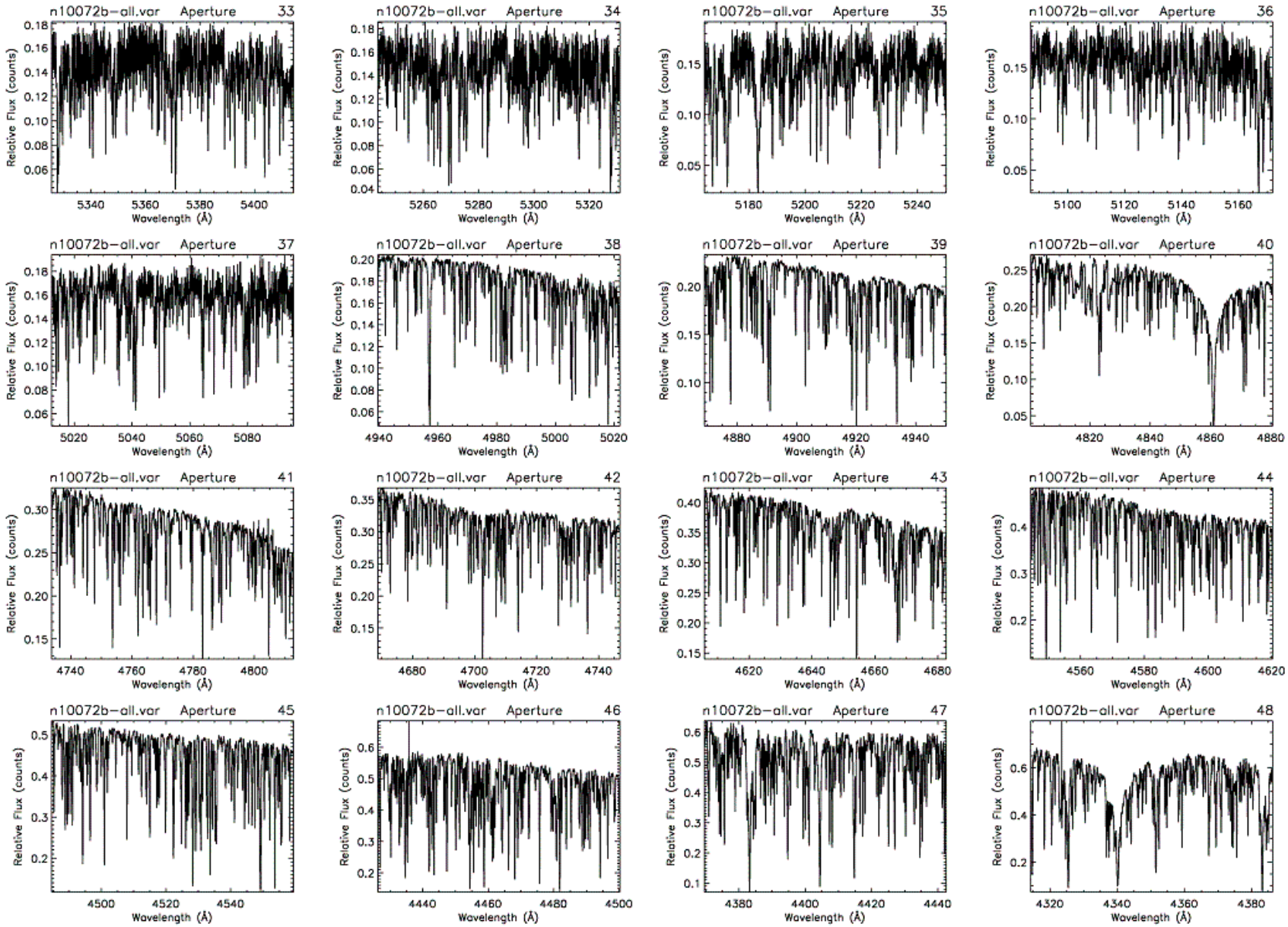
n10072b-all.var Aperture 33
n10072b-all.var Aperture 34
n10072b-all.var Aperture 35
n10072b-all.var Aperture 36
n10072b-all.var Aperture 37
n10072b-all.var Aperture 38
n10072b-all.var Aperture 39
n10072b-all.var Aperture 40
n10072b-all.var Aperture 41
n10072b-all.var Aperture 42
n10072b-all.var Aperture 43
n10072b-all.var Aperture 44
n10072b-all.var Aperture 45
n10072b-all.var Aperture 46
n10072b-all.var Aperture 47
n10072b-all.var Aperture 48
Relative Flux (counts)
Wavelength (Å)

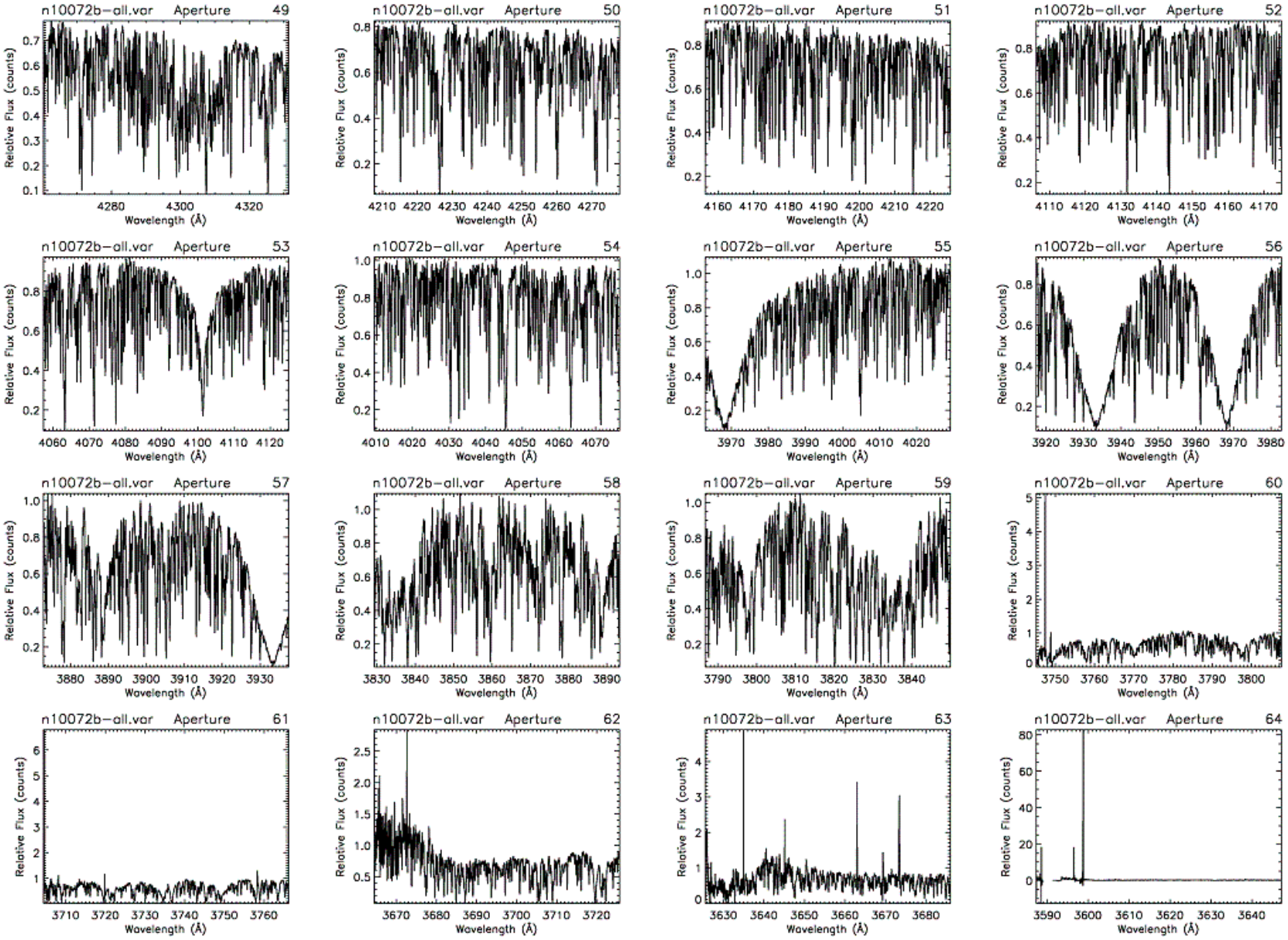
n10072b-all.var Aperture 49
n10072b-all.var Aperture 50
n10072b-all.var Aperture 51
n10072b-all.var Aperture 52
n10072b-all.var Aperture 53
n10072b-all.var Aperture 54
n10072b-all.var Aperture 55
n10072b-all.var Aperture 56
n10072b-all.var Aperture 57
n10072b-all.var Aperture 58
n10072b-all.var Aperture 59
n10072b-all.var Aperture 60
n10072b-all.var Aperture 61
n10072b-all.var Aperture 62
n10072b-all.var Aperture 63
n10072b-all.var Aperture 64
Relative Flux (counts)
Wavelength (Å)

REFERENCES

Bastian, Dulk, Leblanc, 2000, ApJ 545, 1058
Butler et al., 2006, ApJ, 646, 505
Rubenstein, Schaefer, 2000, ApJ 529, 1031
Carlos Allende Prieto, 2001, McDonald Observatory
Cohen et al., 2009, ApJ, 704, L85
Cranmer, Saar, 2007, astro-ph/0702530v1
Cuntz, Saar, Musielak, 2000, ApJ 533, L151
Cuntz, Shkolnik, 2002, Astron. Nachr, 323, 387
Donahue, 1993, Ph.D. Thesis, New Mexico State University
European Space Agency 1997, The Hipparcos and Tycho Catalogues (SP-1200) (Noordwijk: ESA)
Gonzales & Laws, 2007, MNRAS, 378, 1141
Jones B.W., International Journal of Astrobiology 7 (3&4):279-292 (2008)
Landsman, W.B., 1993, A.S.P. Conference Series, Vol. 52, ed. R. J. Hanisch, R. J. V.
Lanza, A.F., 2008, A&A, 487, 1163
McIvor et al., 2006, MNRAS, 367L, 1M
Moss, Piskunov, Sokoloff, 2002, A&A, 396, 885
Musielak, Rosner, Stein, Ulmschneider, 1994, ApJ 423, 474
Parker E.N., 1958, ApJ, 128, 664P
Ribas, Solano, Masana, Gimenez, 2003, A&A, 411, L501
Saar, Cuntz, 2001, MNRAS, 325, 55
Saar, Cuntz, Shkolnik, in IAU Symp. 219
Shkolnik, Walker, Bohlender, 2001, BAAS 33, 3.04
Shkolnik, Walker, Bohlender, 2003, ApJ 597, 1092
Shkolnik, Walker, Bohlender, Gu, Kurster, 2005, ApJ 622, 1075
Shkolnik, Bohlender, Walker, Cameron, 2008, ApJ 676, 628
Tinney, Butler, Marcy, Jones, Penny, Vogt, Apps, Henry, 2001, ApJ, 551, 207
Walker, Shkolnik, Bohlender, Yang, 2003, PASP, 115, 700
Walker et al., 2008, A&A, 482, 691
Zarka,et al., 2001, Ap&SS, 277, 293

STSDAS Help Pages, STSCI, IV. Echelle Reductions with IRAF
http://stsdas.stsci.edu/cgi-bin/gethelp.cgi?echspec
IRAF
http://iraf.noao.edu
SAOImage – DS9
http://hea-www.harvard.edu/RD/ds9/
IDL (Interactive Data Language)
http://www.ittvis.com
GHRS IDL library on public domain
http://www.astro.washington.edu/docs/idl/htmlhelp/slibrary43.html
IDL Astronomy Users Library on public domain
http://idlastro.gsfc.nasa.gov/

BIOGRAPHICAL INFORMATION

Levent Gurdemir received his degree in Astronomy and Space Sciences from the Ankara University of Turkey. He worked for the university's observatory located atop Ahlatlibel hills, where he observed binary stars and trained young astronomers on the use of research telescopes.

In 2005, Gurdemir arrived in Texas to continue his graduate study in astrophysics at the University of Texas at Arlington. In 2006, he was appointed by the Physics Chairman, Dr. James Horwitz, as the Astronomy Lab Supervisor to modernize the laboratories and improve the quality of astronomy education. Gurdemir furnished the labs with state-of-the-art computers and software. He is a co-author on the book, Practical Universe, and, furthermore, initiated construction of an on-campus observatory. He received several awards for his valuable service to the university.

In 2008, he was promoted to serve as the Planetarium Director at the University of Texas at Arlington's state-of-the-art facility to perform pivotal work for the organization and management of daily operations. Under Gurdemir's leadership, the Planetarium at the University of Texas at Arlington demonstrated excellence in education and public outreach during this time period of unprecedented growth. In 2009, the Planetarium was furnished with the state-of-the-art Digistar4 system. The Planetarium received great media coverage and record attendance.

Today, Gurdemir is working to improve prominent educational and outreach functions of the Planetarium at the University of Texas at Arlington as well as fostering community's interest in space sciences. His vision is to extend education/research/outreach functions of the Planetarium beyond astronomy. He frequently travels to Arlington area schools to offer talks, workshops and telescopic observations.

Gurdemir's professional research interests are Extra-Solar planets, habitable planets, close interacting binary stars and circumstellar disks. Besides his support for the Planetarium, Gurdemir utilizes the telescopes of the McDonald Observatory in west Texas for his active research.

Gurdemir's other interests include classic cars, rebuilding engines, computer networks, wireless communication, electronic circuits troubleshooting and diagnostics.